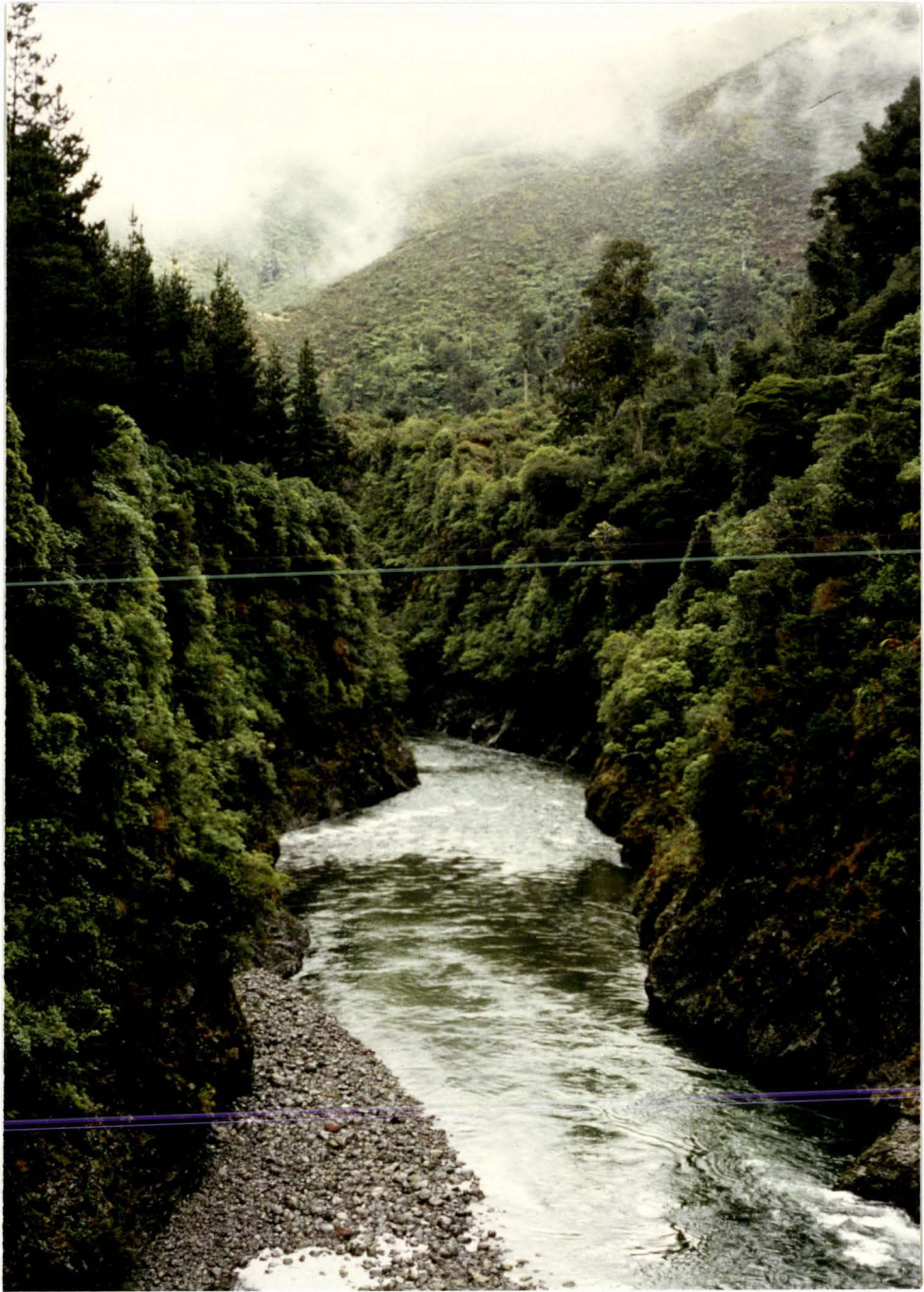


THE GEOLOGY OF THE TORLESSE SUPERGROUP,
SOUTHERN TARARUA RANGE, NORTH ISLAND
NEW ZEALAND.

THOMAS O.H. ORR

A thesis submitted in partial fulfilment of the requirements
for the degree of Master of Science with Honours in Geology,
Victoria University of Wellington. October, 1984.



FRONTISPIECE: View, looking east, of the lower Waiohine Gorge.

ABSTRACT

Basement rocks in the southern Tararua Range are part of the Torlesse Supergroup, possibly Late Triassic to Late Jurassic in age, and form two distinct associations. The sedimentary association consists mainly of quartzo-feldspathic sandstone and argillite with minor olistostrome, calcareous siltstone and microsparite. The sandstone and argillite were deposited as turbidites in a mid- to outer- submarine fan environment. The sediment was derived from a heavily dissected active continental margin that was shedding sediment of mainly plutonic and metamorphic origin.

The volcanic association consists mainly of metabasite and coloured argillite with minor chert and limestone. Geochemical data indicate that the metabasites were erupted in an oceanic intraplate environment. The nature of amygdules in amygdaloidal metabasites suggests eruption in less than 800m of water. Coloured argillites have two distinct origins, namely sediments formed by the degradation of basalt; and also pelagic material modified by metal-rich effluent either from hydrothermal systems associated with mid-ocean ridges or intraplate volcanism. The rocks of the volcanic association indicate formation in an environment similar to present day mid-ocean islands. Nowhere were rocks of the two associations observed to be conformable. Coupled with this, the nature of the two associations suggests that they were formed in separate environments.

The following structural history is proposed:

- 1) Early veining;
- 2) Isoclinal folding and development of a NNE striking cleavage;
- 3) Faulting both at low and high angles to bedding, extreme amounts of which have resulted in *mélange*;

- 4) NE-SW trending close to open folds;
- 5) E-W trending open to gentle folds;
- 6) Recent faulting, predominantly NE trending strike-slip faults.

The nature of the two associations and the deformational style and history supports an accretionary prism model for the development of the Torlesse Supergroup. Rocks of the southern Tararua Range show many similarities with, and probably represent a northward continuation of, the Esk Head Mélange of the South Island.

ACKNOWLEDGEMENTS

I would like to thank my supervisor Dr Russell Korsch both for numerous discussions and for critically reviewing this thesis. I am grateful for his continuous encouragement and prompt editing.

Constructive comments have been made on sections of this thesis by Drs B. Roser and R. Grapes.

I would also like to thank:

Claire and Peter Rumble for their hospitality and the use of their word processor;

The staff and fellow students of the Geology Department;

My family for transport to and from the field area and for putting up with my work hours.

Finally, special thanks are due to Lisa Foley whose help has been invaluable.

CONTENTS

ACKNOWLEDGEMENTS	iii
LIST OF FIGURES	vii
LIST OF TABLES	xi
CHAPTER ONE : INTRODUCTION	1
1.1: Regional geology	1
1.2: Aims	4
1.3: Field area	5
1.4: Geology of the field area	7
CHAPTER TWO : SEDIMENTARY ASSOCIATION	9
2.1: Lithofacies	9
2.1: Environment of deposition	15
2.3: Petrography	21
2.3.1 Sandstone	21
2.3.2 Argillite	27
2.3.3 Lithic sandstone	27
2.3.4 Calcareous siltstone	28
2.3.5 Microsparite	28
2.4: Geochemistry	31
2.5: Provenance and tectonic setting	39
CHAPTER THREE : VOLCANIC ASSOCIATION	48
3.1: Petrography	48
3.1.1 Metabasite	48
3.1.2 Red and green argillite	53
3.1.3 Chert	53
3.1.4 Limestone	55
3.2: Metabasite magma type and eruptive environment	57

3.3: Geochemistry of the coloured argillite and chert	68
3.3.1 Coloured argillite	68
3.3.2 Chert	72
CHAPTER FOUR : METAMORPHISM	75
4.1: Vein mineral summary	81
CHAPTER FIVE : STRUCTURE	83
5.1: Mesoscopic structure	83
5.1.1 Folds	83
5.1.2 Faults	83
5.1.3 Cleavage	86
5.1.4 Lozenge fabric and mélanges	86
5.2: Macroscopic structure	101
5.2.1 Macroscopic folds	101
5.2.2 Degree of disruption	101
5.2.3 Geometric analysis	105
5.3: Recent deformation	119
5.4: Synopsis of structure	123
5.5: Comparison with other workers	124
CHAPTER SIX : DISCUSSION	127
6.1: Summary of the sedimentary and volcanic association	127
6.1.1 Sedimentary association	127
6.1.2 Volcanic association	128
6.2: Models for the formation of the Torlesse Supergroup	129
6.2.1 Accretionary prisms	131
6.2.2 Mélange	134
6.3: Data from the field area	134
6.4: Regional correlations	136
REFERENCE LIST	141

APPENDIX I : MAPS AND AERIAL PHOTOGRAPHS	149
APPENDIX II : POINT COUNT METHODS	150
APPENDIX III : SAMPLES	151
APPENDIX IV : FELDSPAR STAIN	154
APPENDIX V : CARBONATE STAIN	155
APPENDIX VI : GEOCHEMICAL ANALYTICAL METHODS	156
APPENDIX VII : CLINOPYROXENE COMPOSITIONS	157
APPENDIX VIII : GEOCHEMICAL ANALYSES	159

LIST OF FIGURES

Figure	Page
1-1: Basement rocks of New Zealand	2
1-2: Locality map showing rocks and fossil localities of the Torlesse Supergroup	6
2-1: Sedimentary lithofacies	11
(a) Medium-bedded sandstone lithofacies	
(b) Massive argillite lithofacies	
2-2: Sedimentary lithofacies	12
(a) Chaotic lithofacies	
(b) Chaotic lithofacies	
2-3: Sedimentary lithofacies	14
(a) Oligomict, conglomerate, chaotic lithofacies	
(b) Chaotic lithofacies	
2-4: Bouma model	16
2-5: Lithofacies map of the southern Tararua Range	19
2-6: Submarine fan model	20
2-7: Microsparite	30
(a) Microsparite clasts	
(b) Microsparite clast with post-depositional structure	
2-8: Major oxide variations in sandstones and argillites from the southern Tararua Range	33
2-9: Trace element variations in sandstones and argillites from the southern Tararua Range	36
2-10: TiC_2 versus SiO_2 plot for Torlesse Supergroup sandstones and argillites from the Wellington Region	38
2-11: QFL and $QmFLt$ diagrams	41
2-12: $QmPK$ diagram	43
2-13: $LmLvLs$ and $QpLvLsm$ diagrams	44
2-14: Tectonic setting from sandstone geochemistry	46
(a) Tectonic setting of sediments using a volatile-free alkali/silica discriminant	
(b) Discriminant function diagram	

3-1: Map showing the distribution of the rocks of the volcanic association	49
3-2: Metabasite contact	51
3-3: Fault bounded red chert	54
3-4: Determination of magma type	59
(a) Y/Nb ratio	
(b) Five element discriminant function	
3-5: Harker diagrams	60
3-6: Discrimination plots for metabasite	62
3-7: Zr/Y-Zr discriminant plot	63
3-8: Ti-V discriminant plot of metabasites	65
3-9: Discriminant plots for clinopyroxenes	66
(a) TiO_2 -MgO- Na_2O diagram	
(b) Discriminant function diagram	
3-10: Mixing curves between argillite, metabasite and EPR sediment	71
3-11: SiO_2 - $\text{SiO}_2/\text{Al}_2\text{O}_3$ plot	
4-1: Al-Ti-Fe plot of sphene	77
4-2: Al-Fe-Mg plot of chlorites	78
4-3: Al-Fe-Mg plot of pumpellyites	80
5-1: Close to open folds	85
5-2: Sandstone	87
(a) Sandstone with numerous faults	
(b) Moderately disrupted sandstone	
5-3: Moderately disrupted units	89
(a) Medium bedded sandstone	
(b) Thick-bedded sandstone	
5-4: Highly disrupted units	90
(a) Sandstone lozenges and phacoids	
(b) Elongate sandstone phacoids	

5-5: Highly disrupted units	91
(a) Sandstone phacoids	
(b) Units with different phacoid sizes	
5-6: Disrupted units	92
(a) Juxtaposition of a well preserved unit and a highly disrupted unit	
(b) Juxtaposition of a highly disrupted units and a massive argillite unit	
5-7: Detailed map of olistostones and mélanges at G.R. S26C/ 0255 1340, Tauherenikau Gorge	94
5-8: Map of the confluence of "Campsite Creek" and the Tauherenikau River	95
5-9: Highly disrupted units	97
5-10: Rock units	99
(a) Fault contact between unit I and J	
(b) Unit J	
5-11: Map of the Lower Marchant Creek	102
5-12: Map showing the degree of disruption	103
5-13: Comparison of bedding and shear foliation orientations from Domain 2	106
5-14: Map of the field area showing structural "domains" with bedding and shear foliation orientations for each domain .	107
5-15: Synoptic net showing π axis for each domain	108
5-16: Possible methods by which pattern seen in the synoptic net (Fig 5-15) can be produced	110
(a) Alternative 1	
(b) Alternative 2	
5-17: Cleavage traces	111
5-18: Mesocropic folds	113
(a) Axial surface orientations	
(b) Fold axis from field area	
5-19: Macroscopic fold axes	115
5-20: High-angle fault orientation data for each domain	116

5-21: Net showing great-circle girdles which contain the π axis of π So and π Sf for the domains 1, 4, and 8	117
5-22: Map showing air photograph lineaments, crush zones and recent faults	120
5-23: Recent faults plotted as planes on a Wulff net	121
6-1: Cross-section of a typical island arc system, showing tectonic units	132
6-2: Speculative models of deformation of accreted material in a subduction zone	135
6-3: Map showing the Esk Head Mélange and possible North Island continuation	139

LIST OF TABLES

Table	(f = facing page)	Page
2-1: Correlation of the submarine fan facies of Mutti and Ricci Lucchi (1972) and the lithofacies of this study . . .		17
2-2: Association of facies and relative environments of sedimentation, after Mutti and Ricci Lucchi (1972)		18
2-3: Modal analyses of 15 fine-grained sandstones		22
2-4: Microprobe analyses of various detrital minerals from sandstone sample 17211		25
2-5: Geochemical analyses of sediments		32
2-6: Correlation matrix for sandstones and argillites from the southern Tararua Range		34
3-1: Analysis of metabasites from the Tararua Range		58
3-2: Representative clinopyroxene analyses	f64	
3-3: Comparison of average metabasite and black argillite compositions with that of red argillite		69
3-4: Analyses of chert from the Tararua Range	f73	
4-1: Microprobe analyses of sphene	f77	
4-2: Microprobe analyses of chlorites	f78	
4-3: Microprobe analyses of pumpellyites	f80	
5-1: Mesoscopic fold data		84
5-2: Comparison of deformation seen in other areas within the Torlesse Supergroup		125

CHAPTER ONE

INTRODUCTION

This thesis represents the results of a geological study on basement rocks in the south-eastern Tararua Range, of the southern North Island.

1.1 REGIONAL SETTING

New Zealand's basement rocks are divided into Western and Eastern Provinces, separated in part by a tectonically complex zone referred to as the Median Tectonic Line (Landis & Coombs 1967) and in part by the younger and still active Alpine Fault (Wellman & Willet 1942) (Fig.1-1).

The Western Province contains Paleozoic and Mesozoic sediments and a wide variety of crystalline rocks of Precambrian to Cretaceous age (Coombs et al. 1976) and is considered to have formed as part of the Gondwana continental margin (eg. Cooper 1975; Howell 1980). The Eastern Province is made up of several subparallel belts each characterised by distinctive details of sedimentation, petrography, metamorphism and structural style (Carter et al. 1978). From west to east these are:

- 1) Brook Street (Permian tholeiitic arc) and Drumduan (Jurassic calc-alkaline arc) groups;
- 2) Maitai-Murihiku fore-arc basin, Late Permian to Late Jurassic;
- 3) Dun Mountain Ophiolite, Late Paleozoic;
- 4) Caples-Pelorus-Waipapa groups, Permian to Jurassic;
- 5) Haast Schist (low- to medium-grade schist), which is the metamorphic equivalent of belts 4 and 6;
- 6) Torlesse Supergroup, Permian to Early Cretaceous (Carter

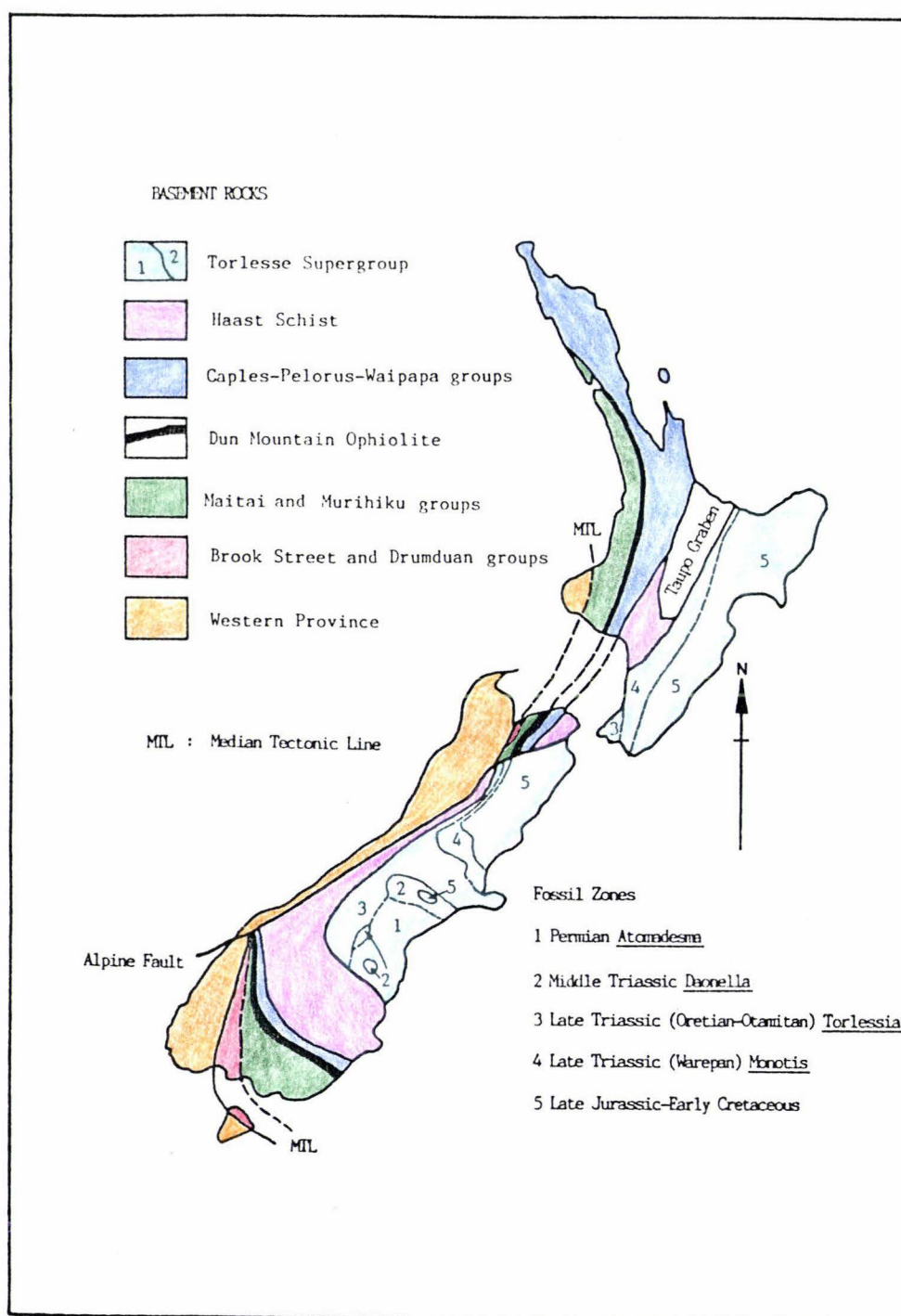


Figure 1-1: Basement rocks of New Zealand modified after Spörli (1978) with Torlesse Supergroup fossil zones from Landis & Bishop (1972), Speden (1976) and MacKinnon (1981).

et al. 1978; Bradshaw et al. 1980).

The belts of the Eastern Province, often referred to as terranes, are considered by many to represent an arc-trench-ocean basin system which was active from the ? Carboniferous to Mid-Cretaceous (eg. Carter et al. 1978; Spörli 1978; Korsch & Wellman in press).

Two compositionally-discrete facies associations occur in the Eastern Province. Belts 1, 2 and 4 form the dominantly volcanoclastic Hokonui Association (Wellman 1952), while the more extensive and mainly deep water Torlesse belt constitutes the strongly deformed quartzo-feldspathic Alpine Association.

The contact between the two associations lies within the Haast Schist, although its exact location and nature have not been determined. Recent workers have emphasised that it is inconceivable that the two associations were derived from a common source. Recently, an unknown source terrane to the east (Coombs et al. 1976; Howell 1980), large scale strike-slip faulting (Bradshaw et al. 1980; MacKinnon 1983) and long distance sediment transport (Spörli 1978; Dickinson 1982; Korsch & Wellman in press) have been invoked to explain their juxtaposition.

The Torlesse Supergroup (Suggate 1961; Suggate et al. 1978) consists of sparsely fossiliferous, quartzo-feldspathic sandstone (commonly referred to as greywacke) and argillite along with minor amounts of basalt, chert, coloured argillite, conglomerate and limestone. The Supergroup has undergone intense deformation and low grade metamorphism (prehnite-pumpellyite to pumpellyite-actinolite). Most of the known fossil occurrences can be grouped into five major zones. These are: 1) Atomadesma, Permian; 2) Daonella, Mid

Triassic; 3) Torlessia, Late Triassic (Oretian-Otamitan); 4) Monotis, Late Triassic (Warepan); 5) Late Jurassic to Early Cretaceous, (Campbell & Warren 1965; Bradshaw 1973; Andrews et al. 1976; Speden 1976; MacKinnon 1983). With few exceptions the zones become progressively younger eastward, and within each zone the dominant younging direction is westward. This agrees well with the accretionary prism model supported by many authors (eg. Spörli 1978; Carter et al. 1978; Korsch & Wellman in press).

In the Southern part of the North Island, fossils of the Torlessia zone (several localities in the Wellington area), Monotis zone (four localities adjacent to the Otaki River) and the Late Jurassic to Early Cretaceous zone (only one locality near Eketahuna) have been found (Grant-Taylor & Waterhouse 1963; Speden 1976).

Several studies have been conducted in the Torlesse rocks of the Wellington Region, eg. petrographic (Reed 1957a; Rowe 1980), sedimentological and structural (Brodie 1953; Webby 1959a & b; Lauder 1962; Barnes 1979; Cranney 1979; Keall 1980; Webster 1982; Rattenbury 1983; MacKenzie 1983), and geochemical (Reed 1957a; Rowe 1980; Roser 1983). L. Foley is working concurrently in an area to the east of this study (see below).

1.2 AIMS

The aims of this study on basement rocks of the Tauherenikau Valley part of the Tararua Range are:

- 1) to produce geologic maps showing lithologies, lithofacies associations and structural domains for the field area;
- 2) to map areas of specific interest in detail;

3) to investigate petrographically and geochemically the various lithologies, and their interrelationships and origins;

4) relate the field area to the geology of the Torlesse Supergroup and discuss the implications of this study for recent models that have been proposed for the origin of the supergroup.

1.3 FIELD AREA

Field work was undertaken in a seventeen by seven kilometre block of rugged, densely forested hill country, 55 kilometres northeast of Wellington, in the south-eastern Tararua Range (Fig. 1-2).

The topography of the study area exhibits two dominant trends. In the central and southern portions, the middle Tauherenikau River and associated Marchant Ridge and Mt Tauherenikau-Mt Reeves Ridge define a northeast-southwest trend. To the north, the Waiohine River and its associated ridge system show alignment in a north-south direction. A maximum relief of 828 metres occurs between Mt Omega (1118m) on Marchant Ridge and the Tauherenikau River bed below (290m).

Access to most of the field area is only by foot. Easy access is possible by two routes, one in the south via the Smith Creek Walking Track, and the other in the north-east along the Waiohine Gorge Road and then the lower Waiohine track. Several good Forest Service tracks serve the field area in the north and west. In the south east, access was gained along the Tauherenikau Gorge during "low water", and by "bush bashing" along the Mt Reeves-Mt Tauherenikau Ridge.

Most of the outcrops occur in stream and river beds (mainly in those of the Tauherenikau and Waiohine) with only minor amounts cropping out on slips, tracks and ridges. Forest over most of the area obscures what little outcrop occurs away from these areas.

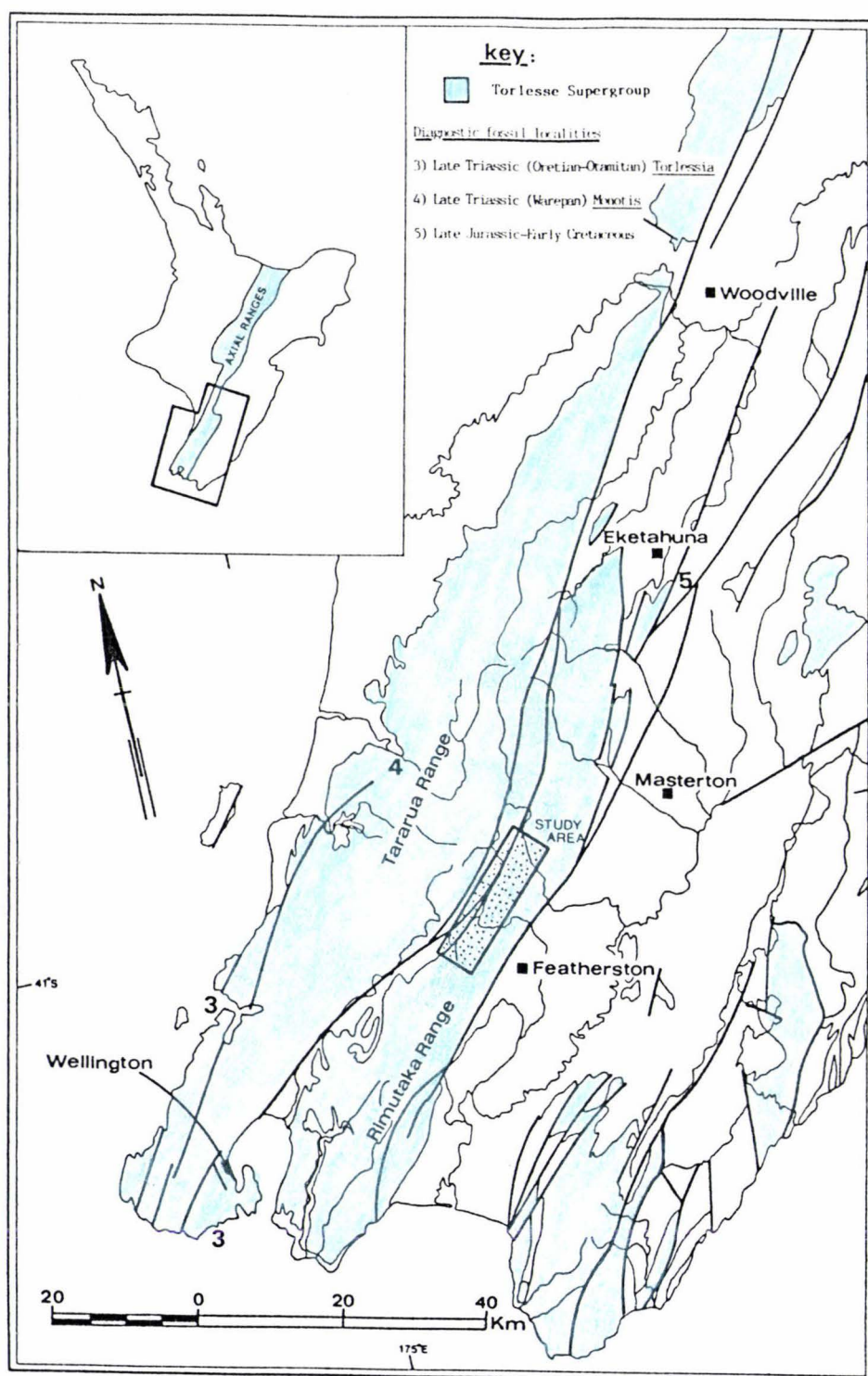


Figure 1-2: Locality map showing rocks and fossil localities of the Torlesse Supergroup, after Kingma (1967) and Speden (1976).

1.4 GEOLOGY OF THE FIELD AREA

The only recorded previous works in the Torlesse of the study area are those of McKay (1888a & b) and Kingma (1967). McKay produced a geological sketch map and brief description of the area between the Waiohine and Tauherenikau Rivers. Basement rocks were grouped into four units, these being:

- 1) Sandstones and breccia beds;
- 2) Diabasic greenstones, hematites and cherts;
- 3) Drossy shales and quartz;
- 4) Plant sandstones, slates and conglomerate.

According to Kingma, the study area straddles a contact between Late Jurassic (Heterian to Ohauan) and Latest Jurassic (Puarooan) units, in the form of the Tauherenikau Fault. Speden (1976) places the field area within the Late Triassic Monotis zone. The units are described as consisting of alternating argillite and sandstone, massive greywacke sandstone, conglomerate, spilitic lava intrusions, pink limestone and jasperoid chert. In addition to the rock types described by McKay and Kingma, I recognise major *mélange* zones and numerous occurrences of red and green argillite.

For the purposes of this study, basement rock types mapped in the field area are grouped into two associations. The redeposited and associated deep marine sediments (ie. sandstone, argillite, olistostrome, microsparite and calcareous siltstone) make up the "Sedimentary Association" which is described in Chapter Two. The remaining lithologies (eg. metabasite, red and green argillite, limestone and chert) constitute the "Volcanic Association" which is dealt with in Chapter Three. Aspects of the metamorphism and structure of the rocks are covered in chapters Four and Five respectively.

Maps produced during this study are based on the NZMS 260
1:50,000 scale topographical series (see Appendix I)

CHAPTER TWO

SEDIMENTARY ASSOCIATION

This chapter describes and discusses the rocks of the sedimentary association. Initially the rocks are divided into five lithofacies which are used to provide an interpretation of the depositional environment. Subsequent sections outline the sedimentary petrography, geochemistry and provenance.

2.1 LITHOFACIES

Beds of the sedimentary association which show little internal deformation can be divided into five lithofacies based on bed thickness, sandstone to argillite ratio and sedimentary structures.

1) Thick-bedded sandstone lithofacies.

The thick-bedded sandstone lithofacies consists of sandstone-dominated sequences, with bed thicknesses generally between 20cm and 1.2m, the sandstone being mainly medium-grained. Argillite occurs commonly as the graded tops of sandstone beds, generally between 1cm and 5cm thick. Sandstone to argillite ratios are generally in excess of 4:1 and less than 9:1. Amalgamated sandstone beds are not uncommon and sometimes reach thicknesses of several tens of metres. Basal contacts of beds are generally sharp. Graded bedding was observed only rarely.

2) Medium-bedded sandstone-dominated lithofacies.

This lithofacies is characterised by sandstone to argillite ratios that range from 4:1 to 1:1. Sandstones are generally fine- to medium-grained, and usually less than 20cm thick, whereas argillites are usually less than 10cm thick and commonly sheared. Graded bedding is not uncommon and parallel laminations and cross-bedding were observed at several localities. This lithofacies is particularly well

developed in the lower section of Marchant Creek (S26C/ 0150 1578; Fig. 2-1a).

3) Medium- to thin-bedded argillite-dominated lithofacies

This lithofacies consists of sandstone (mainly fine-grained) and argillite beds that are generally between 2cm and 10cm in thickness. Sandstone to argillite ratios are generally between 1:1 and 1:3 with most being close to 1:1. Sedimentary structures are the same as those seen in lithofacies 2. Both bioturbated, calcareous siltstone (see section 2.3.3) and fossiliferous microsparite (see section 2.3.4) lenses occur in this lithofacies.

4) Massive argillite lithofacies.

The massive argillite lithofacies consists of argillite-dominated sequences with minor interbeds of very fine-grained sandstone. Argillite, where not sheared, commonly shows fine laminations and occasionally occurs as medium-bedded sequences. Several sparsely-fossiliferous microsparite (see section 2.3.4) lenses were noted in rocks of this lithofacies at G.R. S26C/ 0255 1337 (Fig. 2-1b).

5) Chaotic lithofacies.

In the Tauherenikau Gorge (G.R. S26C/ 0256 1340) two types of this lithofacies were recognised.

Type A consists mainly of angular to subangular sandstone clasts and occasional well-rounded microsparite clasts, set in a matrix (45% to 75%) of very fine-grained sandstone or argillite. Clasts are poorly sorted and range in size from a few millimetres to several metres. Microsparite clasts have an average size that is three to four times that of the sandstone clasts (Fig. 2-2a). Boulder-sized clasts of both fossiliferous microsparite (Fig. 2-2b) thin-bedded, fine-grained sandstone occur. A small, inversely- to normally-graded,

Figure 2-1a: Medium-bedded sandstone
dominated lithofacies showing well
preserved bedding.
Marchant Creek S26C/ 0150 1578,
geological hammer 31cm long.

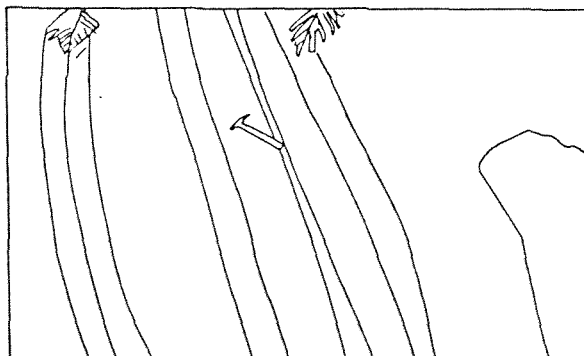


Figure 2-1b: Massive argillite lithofacies.
Note microsparite lenses (R).
Tauherenikau Gorge S26C/ 0255 1337,
geological hammer 31cm long.

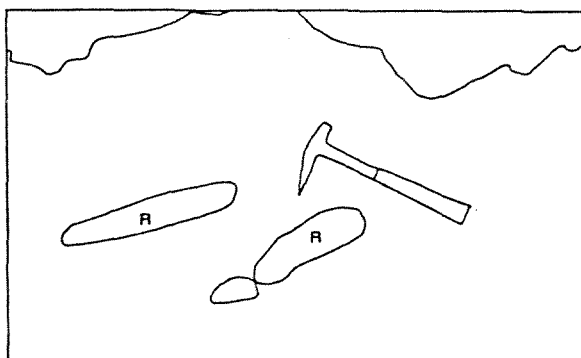




Figure 2-2a: Chaotic lithofacies, Type A.

Clasts are mainly angular sandstone (S) of various grain sizes, with minor microsparite clasts (R), set in a black argillite matrix. Note roundness of the microsparite clasts compared with the sandstone clasts.

Tauherenikau Gorge S26C/ 0250 1340,
pen 15cm long.

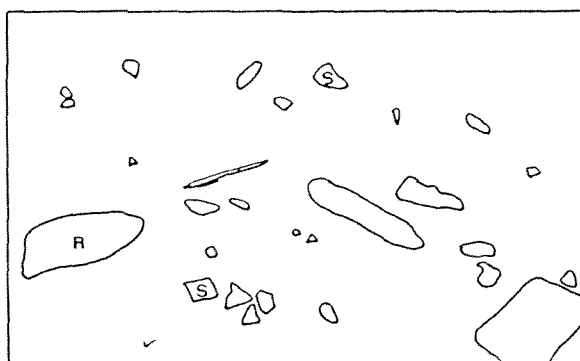
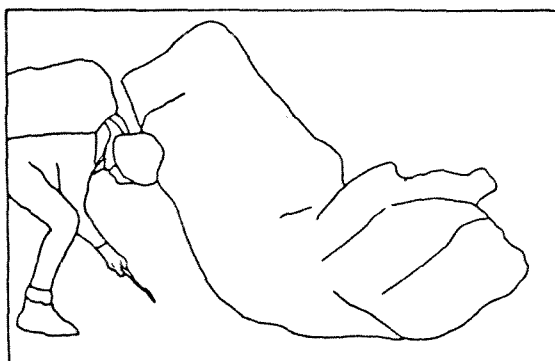
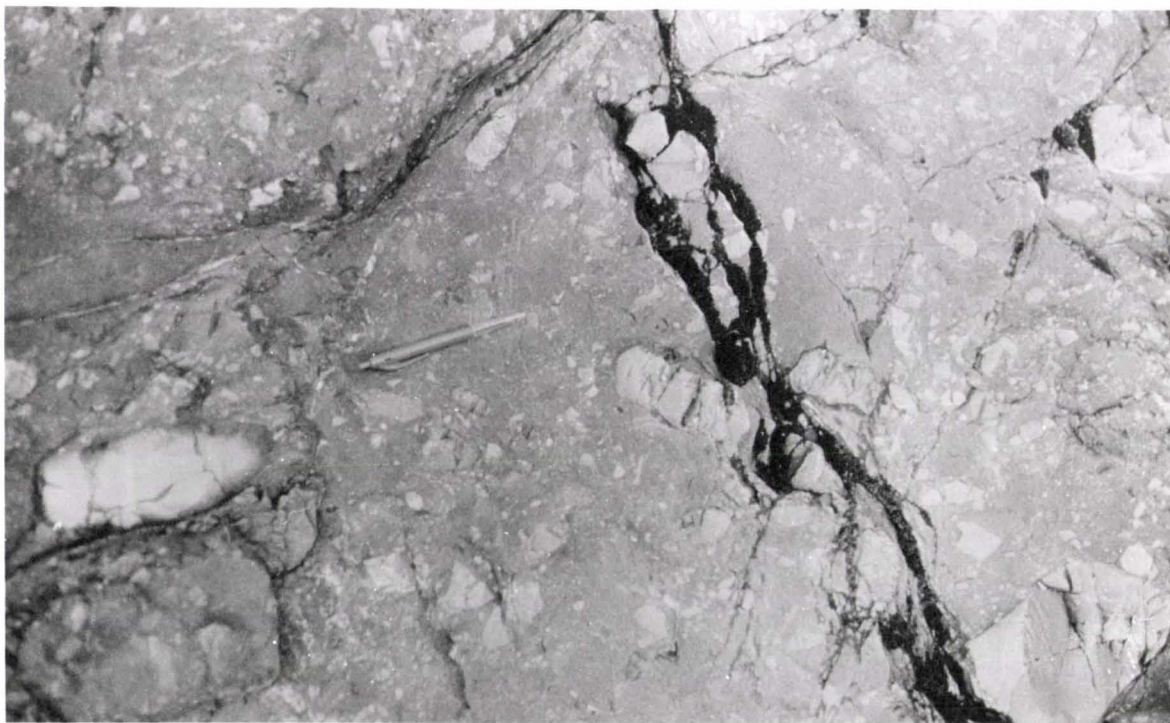


Figure 2-2b: Chaotic lithofacies, Type A.

Large boulder of fossiliferous microsparite (17261) set in an argillite matrix.

Approximately 20 metres down stream from
outcrop shown in Fig. 2-2a.





clast-supported, oligomict conglomerate (the only recorded occurrence of conglomerate in the study area) occurs within a boulder-sized clast of fine-grained sandstone (Fig. 2-3a).

Type B is very similar texturally to type A but differs in that it contains significant amounts of clasts of the volcanic association (Fig. 2-3b). Clast lithologies include red and white chert, red and green metabasites (as well as amygdaloidal types) and red and green argillite. The largest clast observed (2m by 1.5m) was a red argillite. Approximately 20% of clasts were of the sedimentary association (fine-grained to medium-grained sandstone, argillite and rare microsparite clasts). The matrix is generally coarser than observed in type A. Crude bedding defined by alignment of clasts was observed.

A sequence which contains both type A and B is described further in Chapter 5. Rocks of this lithofacies also occur in the Waiohine River and above the gorge in the Tauherenikau River (see below).

Figure 2-3a: Oligomict conglomerate within
a block in chaotic lithofacies, Type A.

Conglomerate consists of subangular to
angular clasts of sandstone of various grain
sizes. Note erosional base (B) and normal
grading.

Tauherenikau Gorge S26C/ 0223 1338,
pen 15 cm long

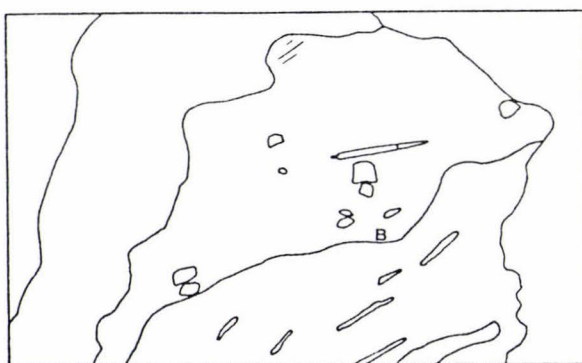
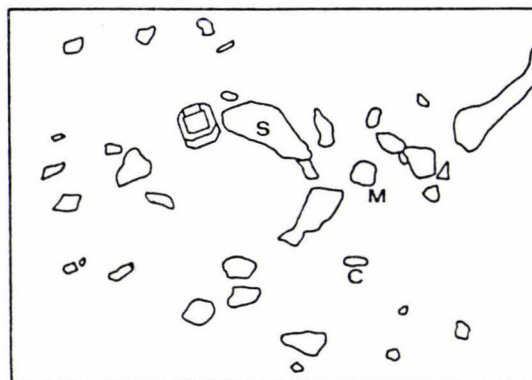
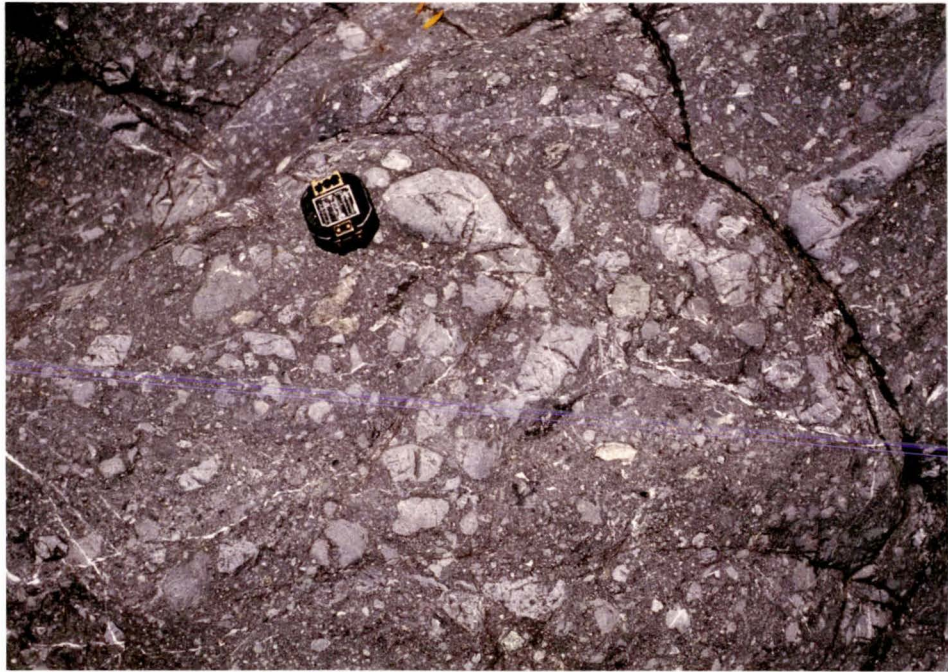


Figure 2-3b: Chaotic lithofacies, Type B.

Clasts are sandstone (S), metabasite (M)
and chert (C).

Tauherenikau Gorge S26C/ 0253 1347,
Brunton compass 7 cm across.





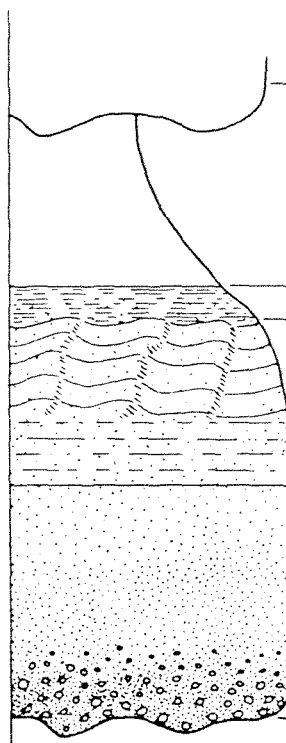
2.2 ENVIRONMENT OF DEPOSITION

The monotonous sequences of sandstone and argillite that dominate the basement geology of the field area exhibit many of the features typical of turbidite sequences eg. vertical grading, ripple laminations, rip up clasts of both argillite and plant material, sandstone beds (with sharp erosional bases) that grade upwards to siltstones.

Using sedimentary structures Bouma (1962) was able to produce a model that divided sandy and silty turbidites (often referred to as classical turbidites) into five divisions, A-E, which occur in a fixed sequence (Fig. 2-4). Lithofacies 2 and 3 of this study (see previous section) can be described in terms of the Bouma sequence. Divisions C and D were observed rarely and beds commonly consist of divisions A and E and, less commonly A, B and E. Division E consists of calcareous siltstone at one outcrop and microsparite at several other outcrops (see section 2.3).

Mutti and Ricci Lucchi (1972), based on work in the Appennines, classified submarine fan facies into seven categories. Two facies included in this list are not strictly turbidite, these being facies F and G. Table 2-1 shows the possible correlation between the submarine fan facies of Mutti and Ricci Lucchi (1972) and lithofacies described in this study. The submarine fan facies of Mutti and Ricci Lucchi (1972) can be grouped into 3 facies associations, which are listed together with a brief description and characteristic facies types in Table 2-2.

Two lithofacies associations occur in the field area (Fig. 2-5). The eastern facies association consists mainly of facies B with minor C, D and F. This facies association seems most likely to have formed in



The diagram illustrates a cross-section of a turbidite bed. The bed is divided into five horizontal layers, labeled A through E from bottom to top. The grain size decreases upwards: Division A is sand (to granule at base), Division B is sand, Division C is sand-silt, Division D is silt, and Division E is mud. The layers show different internal structures: A is massive and graded; B consists of plane parallel laminae; C shows ripples, wavy, or convoluted laminae; D shows upper parallel laminae; and E is a pelite. The interpretation for each layer is provided in the adjacent column.

Grain Size		Bouma (1962) Divisions	Interpretation
Mud	E	Pelite	Pelagic sedimentation or fine grained, low density turbidity current deposition
	D	Upper parallel laminae	? ? ?
Sand-Silt	C	Ripples, wavy or convoluted laminae	Lower part of Lower Flow Regime
Sand	B	Plane parallel laminae	Upper Flow Regime Plane Bed
Sand (to granule at base)	A	Massive, graded	? Upper Flow Regime Rapid deposition and Quick bed (?)

Figure 2-4: Bouma model (from Middleton and Hampton 1973).

Table 2-1: Correlation of the submarine fan facies of Mutti and Ricci Lucchi (1972) and the lithofacies of this study.

Mutti and Ricci Lucchi (1972)	This study
* A. Arenaceous-conglomeratic facies	
* B. Arenaceous facies	1). Thick-bedded sandstone lithofacies
C. Arenaceous-pelitic facies	2). Medium-bedded sandstone-dominated lithofacies
D. Pelitic-arenaceous facies I	3). Medium to thin bedded argillite dominated lithofacies
E. Pelitic-arenaceous facies II	
* F. Chaotic facies	5). Chaotic lithofacies
* G. Hemipelagic and pelagic facies	4). Massive argillite lithofacies

* Bouma sequence not applicable

Table 2-2: Association of facies and relative environments of sedimentation, after Mutti and Ricci Lucchi (1972).

Facies types	General characteristics	Environment	
G A E F (B,C,D)	Massive or plane-parallel stratified pelites; can include channelized sandstone bodies (A); thin shaly or sandy turbidites (D,E) and thick graded turbidites (C).	Slope	
A,B G E,D (C,F)	Sandstones and conglomerates (A,B) limited to submarine valleys incised in pelites (G); thin channel and overbank turbidites (E,D).	Fan or proximal basin	inner
A,B D (C,E,F)	Coarse-grained filling of large submarine valleys (A,B) cut into facies D turbidites.		middle
C (D,E,F)	Arenaceous-pelitic turbidites (C) in lenticular bodies enclosed in pelitic arenaceous turbidites (D).		outer
D G (C) (F)	Alternation of pelitic-arenaceous (D) turbidites with hemipelagics (G); with sporadic intercalations of thick arenaceous-pelitic turbidites (C); sometimes totally hemipelagic pelites (G).	Submarine plain or distal basin	

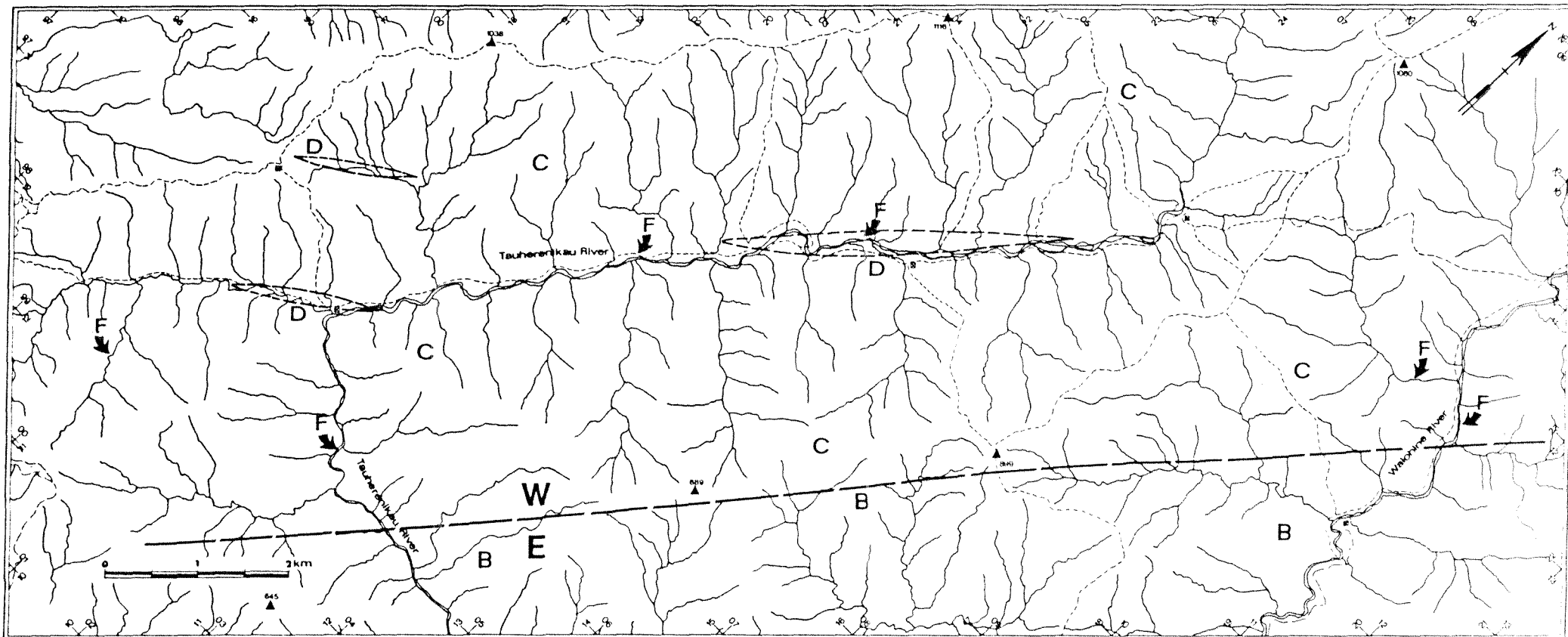


Figure 2-5: Lithofacies map of the southern Tararua Range.

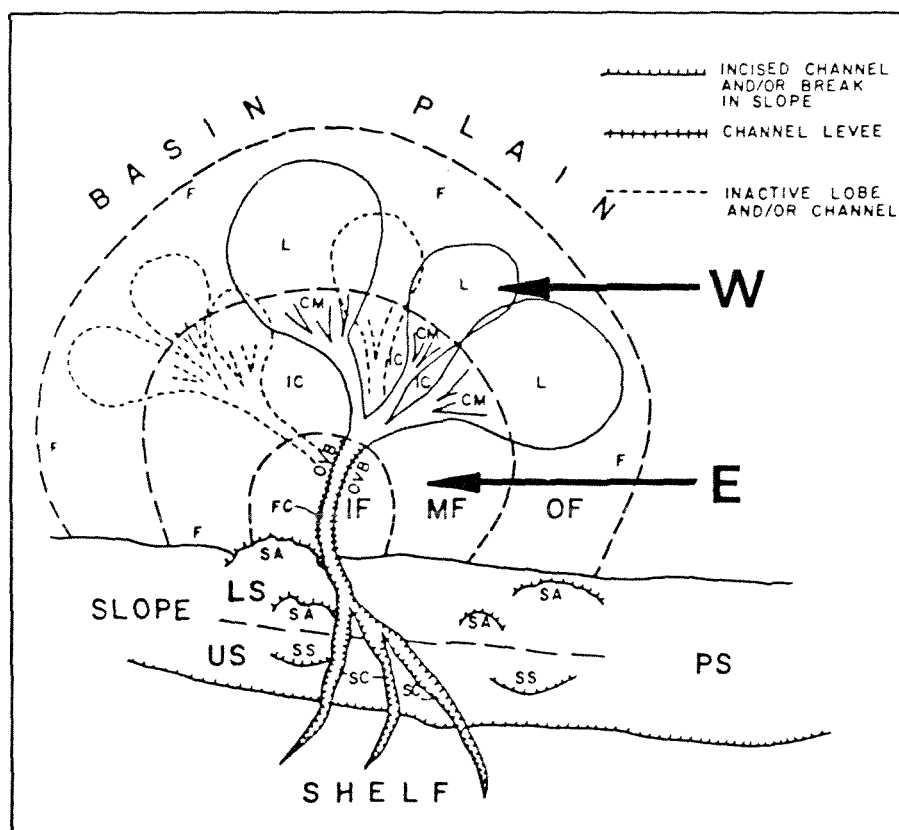
Refer to Table 2-1 for lithofacies types.

W = Western facies association which consists mainly of
facies C and D with minor G, B and F.
(outer-fan environment)

E = Eastern facies association which consists mainly of
facies B with minor C, D and F.
(mid-fan environment)

a mid-fan environment. The western facies association consists mainly of facies C and D with minor G, B and F. This association would be best explained as being deposited in an outer-fan environment. Figure 2-6 shows the postulated environment of deposition for these two facies associations.

Figure 2-6: Submarine fan model after Ingersoll (1978) showing the site of deposition of the western (W) and eastern (E) lithofacies associations.



CM = Channelized Midfan, F = Fan Fringe, FC = Fan Channel, IC = Interchannel Area, IF = Inner Fan, L = Depositional Lobe, LS = Lower Slope, MF = Midfan, OF = Outer Fan, OVB = Overbank Area, PS = Passive or Prograding Slope, SA = Slump Accumulation, SC = Slope Channel, SS = Slump Scar, US = Upper Slope.

2.3 PETROGRAPHY

Petrographic data was supplemented with electron microprobe analyses to provide information on the chemistry and composition of minerals.

2.3.1 Sandstone

In the study area, sandstone is generally fine-to medium-grained, well-indurated and when fresh ranges in colour from medium- to dark-grey.

Twenty eight sandstones were examined in thin section, of which 14 were selected for point-counting to determine modal proportions of grain type and size (Table 2-3; see appendix II for point-count methods). The grain size of point-counted sections ranged from 0.13mm to 0.19mm and average 0.17mm. During point-counting, material smaller than 0.02mm was regarded as matrix.

Descriptions of metamorphic minerals are included in Chapter 4. The following presents descriptions of detrital components only.

Quartz (20.2-39.6%)

Quartz occurs generally as monocrystalline, angular to subrounded, inclusion-free grains. Moderate to strong undulose extinction is common. Grain boundaries are sometimes sutured (17219*) and in detail are often irregular (17212). Replacement of quartz by calcite was noted in several sections (eg. 17257). Polycrystalline quartz is less common, comprising 0.4% to 8.0% of the total rock. Rare inclusions of rutile (17257,17210,17209), white mica (17215,17222), apatite (17222) and sphene (17217) were observed. Myrmekitic intergrowths were found in several samples (eg. 17257,17213,17215).

* Numbers refer to specimens housed in the petrology collection, Geology Department, Victoria University of Wellington. All specimens, with grid references and short descriptions are listed in Appendix III.

Table 2-3: Modal analyses of fifteen fine grained sandstones.

Sample number	17209	17210	17211	17212	17222
Grain size (mm)	0.16	0.17	0.18	0.13	0.17
Monocrystalline Quartz	27.0	31.4	37.0	22.6	26.8
Polycrystalline Quartz	8.0	4.2	1.4	0.4	1.6
Chert	0.8	1.2	0.4	0.8	0.2
Plagioclase	37.6	30.2	27.0	27.8	31.4
Alkali Feldspar	2.2	2.0	0.8	0.8	1.6
Fe-Mg Minerals	0.6	0.0	1.6	0.6	0.6
Lithic Fragments	11.8	16.6	8.4	11.0	10.0
Other	2.2	3.2	5.2	2.4	2.8
Matrix	9.8	11.2	18.2	33.6	25.0
Lithic Fragments:					
Volcanic	43.5	62.2	64.2	58.0	54.0
Sedimentary	42.0	31.1	25.0	26.0	38.0
Metavolcanic	5.5	2.7	5.8	7.7	1.3
Metasedimentary	9.0	4.0	5.0	8.3	6.7
Sample number	17213	17214	17215	17216	17217
Grain size (mm)	0.17	0.19	0.19	0.18	0.17
Monocrystalline Quartz	33.0	24.8	31.6	20.2	39.6
Polycrystalline Quartz	0.6	2.2	1.2	2.4	2.2
Chert	0.2	0.2	0.4	1.0	0.4
Plagioclase	36.6	25.2	28.2	31.0	34.0
Alkali Feldspar	1.0	1.4	2.0	0.8	1.2
Fe-Mg Minerals	0.6	2.0	0.2	0.6	0.2
Lithic Fragments	8.2	9.2	15.8	9.2	4.0
Other	2.8	2.6	2.2	2.6	0.8
Matrix	17.0	32.4	18.4	32.2	17.6
Lithic Fragments:					
Volcanic	76.5	73.8	73.3	69.0	63.3
Sedimentary	17.9	22.0	22.7	20.0	28.3
Metavolcanic	1.4	0.7	1.6	4.1	1.6
Metasedimentary	4.2	3.5	2.4	6.9	6.8
Sample number	17218	17219	17220	17221	17223 ¹
Grain size (mm)	0.17	0.15	0.14	0.13	-
Monocrystalline Quartz	31.6	35.8	28.4	39.2	5.0
Polycrystalline Quartz	2.2	3.0	1.6	2.6	5.0
Chert	0.2	0.2	0.2	0.4	3.0
Plagioclase	33.8	31.4	36.6	29.8	2.8
Alkali Feldspar	1.0	2.4	2.0	2.2	0.0
Fe-Mg Minerals	0.4	0.2	0.6	0.0	0.0
Lithic Fragments	10.8	6.8	11.8	6.8	69.6
Other	3.0	1.4	3.8	0.8	0.8
Matrix	17.0	18.8	15.0	18.2	13.8
Lithic Fragments:					
Volcanic	62.5	60.7	67.5	56.3	12.9
Sedimentary	27.8	34.0	21.9	35.5	61.5
Metavolcanic	3.2	2.2	2.5	2.2	3.0
Metasedimentary	6.5	3.1	8.1	6.0	22.6

¹ lithic sandstone

Plagioclase (25.2-37.6%)

Plagioclase occurs as elongate to equant grains with larger crystals tending to be more rounded. Compositions, determined by the Michel-Levy method, range from albite to labradorite with most being albite or oligoclase. Microprobe analyses of four plagioclase from sample 17211 showed a range in composition of $An_{3.5} Ab_{95.3} Or_{1.2}$ to $An_{29.7} Ab_{69.5} Or_{0.8}$ (see Chapter 4 for discussion). Approximately 25% of the grains were twinned, with most being combined Albite-Carlsbad type. Kinked, and more rarely, slightly-bent twins occurred (17221). Intergrowths with alkali feldspar, (mainly perthitic) occurred in several samples (eg. 17209, 17222). Chessboard texture was seen in an antiperthitic intergrowth of orthoclase and albite in sample 17211 (confirmed by microprobe).

The intensity of sericitic alteration varied considerably but most grains have been affected. Less common replacement by calcite (17257, 17259, 17260) and epidote (17211) occurred. Inclusions of zircon (17215), opaques (17215) and minerals of indeterminate nature (17220) were not uncommon.

Alkali feldspar (0.8-2.4%)

Staining with sodium cobaltinitrite (see Appendix IV) was only partly successful. As untwinned and unstained grains were counted as either quartz or plagioclase, the modal values for alkali feldspar should be treated as minimum values. Grains were generally equant and angular to subangular, with alteration occurring in minor amounts. Two orthoclase grains probed in sample 17211 had values of Or_{85} and Or_{95} .

Micas (0-1.6%)

Biotite and, less commonly, muscovite both occur as elongate grains which show weak alignment in some samples (17211). Biotite often

occurs as highly deformed brown flakes (17214) which commonly show alteration to green chlorite (17211,17218). Three brown biotites in sample 17211 were probed, all of which were found to be in various stages of oxidation (see Table 2-4).

Muscovite grains are generally less deformed and sometimes occur as relatively large grains (eg. 0.75 mm by 0.02mm in sample 17214, average grain size 0.19mm). Muscovite probe analyses from sample 17214 are shown in Table 2-4.

Chlorite

Rare detrital brown chlorite was observed (17211), and probed grains were found to have high TiO_2 content relative to authigenic chlorite (see Chapter 4).

Accessory Minerals

Epidote is the most common accessory mineral and generally occurs as small, fractured and sometimes euhedral grains. Electron microscope examination of one grain (17211) with a pistacite ratio of .21 (see Table 2-4 for analyses) showed a network of SrO enriched cracks. Similar grains have been reported from greywacke in the Wellington area by MacKenzie (1983).

Other common accessory minerals, in order of decreasing abundance, are opaque minerals (eg. 17257,17214,17216), apatite (17258,17218), zircon (17211,17215), hornblende (17213) and sphene (17211, see Table 2-4 for probe analysis).

Lithic Fragments

Three types of lithic fragments occur, making up 6.6-22% of samples:

Volcanic lithic fragments (2.4-11%) are usually rounded to subrounded and can be divided into two types; acid and basic, with the

Table 2-4: Microprobe analyses of various detrital minerals from
sandstone sample 17211.

	BIOTITE				MUSCOVITE		EPIDOTE	SPHENE
SiO ₂	37.02	32.34	29.46	35.40	48.38	47.41	37.90	29.80
Al ₂ O ₃	20.02	19.07	13.54	18.89	32.66	33.40	25.47	1.39
TiO ₂	1.92	2.97	2.18	1.84	1.03	0.18		36.90
FeO	21.36	20.70	23.71	22.69	3.54	2.24		
Fe ₂ O ₃							10.77	1.99
MnO	0.31	0.34	0.34	0.30		0.11	0.49	0.19
MgO	5.80	7.46	8.33	6.45	0.89	0.64	0.05	
CaO	0.12	0.11	0.13	0.14			23.15	26.95
Na ₂ O		0.10			0.38	0.24		
K ₂ O	4.98	3.56	2.29	4.50	9.09	10.40		
Total	91.53	86.65	79.98	90.21	95.97	94.62	97.83	97.22

former accounting for approximately 70% of the total.

Acid lithic fragments are mostly devitrified. When fresh, they show rare microphenocrysts of quartz and feldspar surrounded by a dark cryptocrystalline groundmass which sometimes displays flow texture.

Basic lithic fragments appear to be mainly basaltic with mainly doleritic, and less commonly, variolitic texture.

Sedimentary lithic fragments (1.4-6.2%) are generally rounded, and sometimes appear to be squashed between larger grains (17219). Most fragments consist of sediments that range in size from fine silt to fine sand, which commonly have a "dirty" brown clay matrix that is often oxide speckled (17210); they are considered to be intrabasinal in origin (Reed 1957a; Rowe 1980).

Chert occurs in all samples (0.2-1.2%) generally as rounded to subangular fragments. It is possible that a small number of devitrified volcanic lithics were mistaken for chert, and vice versa, during point-counting.

Metamorphic lithic fragments were generally small, subrounded to rounded and rare (0-1.8%). Fragments of phyllite, and metaquartzite were observed.

Matrix (9.8-33.6%)

Most detrital minerals seen in this section also occur in the matrix size range. In Wellington greywacke, Rowe (1980) noted that biotite, hornblende and some accessory minerals may not occur in the matrix.

The large range in matrix content from samples of similar grain size may be due to one or more of the following: 1) depositional processes, ie. turbidity currents; 2) bottom water contour currents, winnowing out of fine-grained material (Rupke 1978); 3) differential

compaction; 4) diagenetic and metamorphic effects.

2.3.2 Argillite

In outcrop, argillite is generally well indurated, often sheared, and ranges in colour from grey to black (those of darker colour being finer grained). Graded bedding (eg. 17235) and less common cross bedding were observed.

Samples examined in thin section (17262, 17263, 17264, 17265, 17266) range in average grain size from 0.055mm to 0.035mm, and show a texture similar to that of the sandstone described above.

In general, detrital grains are equant, angular to subrounded, fresh and monocrystalline. In order of decreasing abundance, detrital minerals are quartz, feldspar (plagioclases range from An₃ to An₃₃ (Michel-Levy method)), biotite, white mica and heavy minerals (mainly epidote group minerals). Perthitic (17263, 17265) and less common myrmekitic (17265) intergrowths were noted. Minor amounts of rock fragments (approximately equal amounts of sedimentary and igneous) and opaque minerals (often concentrated along stylolites eg. 17262) occur.

The matrix, which accounts for approximately 1/2 to 2/3 of the total rock, is dominated by quartz, opaque minerals and chlorite.

2.3.3 Lithic sandstone

A sliver of lithic sandstone approximately 1.8m thick and at least 5m in length was found at G.R. S26A/ 1055 2350 and occurs in fault contact with a sliver of red metabasite of similar dimensions. Both slivers occur within a faulted sequence consisting mainly of sheared beds of sandstone and argillite.

The rock was point-counted (see Table 2-1, sample 17223) and analysed for major and trace elements (see following section). The rock is dominated by large, well-rounded, lithic fragments accounting for

73% of the total volume, 84% of these being sedimentary in origin. The average grain size of the sample was that of a very coarse sand with rock fragments being up to 2mm in size.

Equal amounts of subangular to angular, monocrystalline and polycrystalline quartz grains constitute 10% of the sample. Strongly sericitized plagioclase grains (2.8%), detrital heavy minerals (<1%), micaceous minerals (<1%), and matrix (13.8%), make up the remainder of the sample. Prehnite was noted as a detrital grain.

2.3.4 Calcareous siltstone

Calcareous siltstone occurs in Smiths Creek (G.R. S26C/ 0081 1408) as a lens two metres in length and seven centimetres thick in a sequence of medium-bedded alternating fine-grained sand and argillite. Thin section examination (T.S. 17267) reveals signs of bioturbation (several burrows, average diameter 0.5mm) but no trace of biogenic material.

2.3.5 Microsparite

Autochthonous microsparite occurs in three outcrops in the Middle Tauherenikau Gorge. Several lenses of microsparite (Fig. 2-1b, average size 30cm in length by 5cm thick) occur at G.R. S26C/ 0255 1337, in an outcrop of finely-laminated argillite. Fine pryite disseminations were common throughout the outcrop, and occasionally formed lens-shaped bodies, one being 0.5cm thick by 30cm long. A thin section (17268) of one microsparite lens showed occasional oxide-coated shell fragments (largest 3mm by 1.5mm), and many ?radiolarian ghosts (infilled with sparry calcite and, less commonly, opaque oxide grains) set in calcite microsparite (carbonate determination by staining with Alizarin Red S and Potassium ferri-cyanide, see Appendix V).

At G.R S26A/ 0255 1340 microsparite occurs as rounded clasts in

sheared argillite (Fig. 2-7a). In thin section the clasts (17269) contain several shell fragments (largest was 3mm by 0.4mm), most of which were almost totally replaced by opaque minerals. Calcite filled ?radiolarian ghosts were common with several possible Nassellariina being observed. A post-depositional structure of unknown origin was observed in one of the microsparite clasts (Fig. 2-7b).

Across the river from the above outcrop a 13cm thick by 90cm long lens of microsparite occurred in a medium-bedded sequence of argillite with minor interbeds of fine sandstone.

Figure 2-7a: Rounded sparsely fossiliferous
microsparite clasts (R; 17269) in black
argillite. Note the remnants of bedding.
Tauherenikau Gorge S26C/ 0255 1340,
geological hammer 31 cm long.

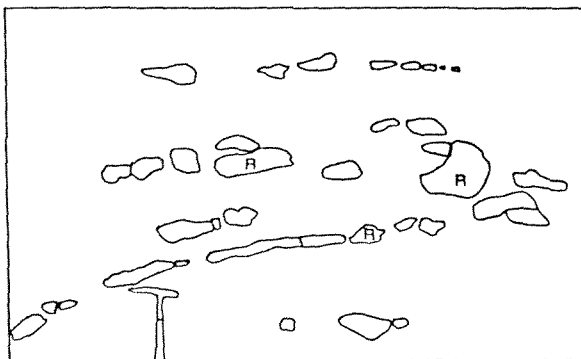
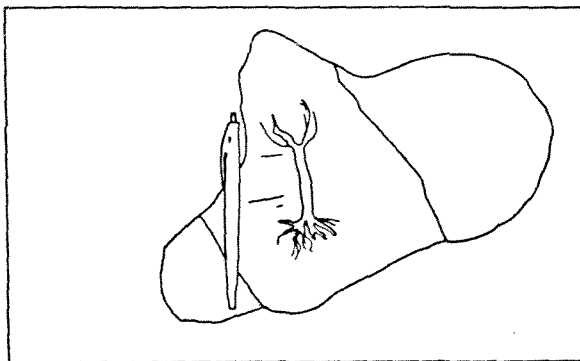


Figure 2-7b: Microsparite clast with
post-depositional structure of unknown
origin. Sequence is younging upwards.
From the same locality as outcrop
in Fig. 2-7a.
Pen 15 cm long.





2.4 GEOCHEMISTRY

In order to determine the chemical composition and nature of chemical variations within the sandstone-argillite rocks of the field area, ten sandstones (including the lithic sandstone) and seven argillites were sampled and analysed for major oxides and trace elements. Geochemical analyses are listed in Table 2-5 and analytical methods are described in Appendix VI.

During sample collection, which was conducted in various parts of the field area, an attempt was made to select samples that would adequately represent the range of grain sizes present.

Major oxide variations:

Sandstone and argillite are chemically distinct in terms of weight percent abundances for SiO_2 , TiO_2 , Al_2O_3 , FeO , MgO and K_2O while minimal overlap occurs in Na_2O , P_2O_5 and loss on ignition values (Loss). Relative to argillite the sandstones are depleted in all major element oxides except for SiO_2 and Na_2O ; while similar amounts of Fe_2O_3 and CaO occur in both.

From plots of anhydrous oxide data versus SiO_2 (Fig. 2-8) it can be seen that Al_2O_3 , TiO_2 , FeO , MnO , MgO , K_2O and P_2O_5 all tend to decrease with increasing SiO_2 . TiO_2 , Al_2O_3 , FeO , MgO and K_2O all have correlation coefficients that are significant at the 95% level of confidence (Table 2-6).

Na_2O is the only major oxide that increases with increasing SiO_2 , this correlation however is not significant at the 95% level of confidence. CaO , Fe_2O_3 and MnO show no significant correlation with SiO_2 or any other major oxide.

The major oxide trends observed in this study are similar to those found in the greywacke and argillite from the Wellington area by

Table 2-5: Geochemical analyses of argillite (1-7), sandstone (9-17)
and lithic sandstone (8) from the Tararua Range.

Analysis	(1)	(2)	(3)	(4)	(5)	(6)
Sample No.	17237	17229	17232	17233	17224	17234
Major Oxides (wt.%)						
SiO ₂	49.40	55.95	56.55	56.56	56.90	61.10
TiO ₂	1.02	0.90	0.97	0.95	0.92	0.82
Al ₂ O ₃	22.06	19.72	19.91	20.21	20.16	18.01
Fe ₂ O ₃	0.89	1.02	0.73	0.93	0.24	0.33
FeO	6.84	5.68	5.62	5.10	5.81	4.79
MnO	0.06	0.06	0.06	0.05	0.06	0.05
MgO	2.29	2.22	2.49	2.37	2.24	1.98
CaO	2.44	1.36	1.05	1.13	0.76	1.15
Na ₂ O	1.50	1.82	1.98	2.07	1.67	2.44
K ₂ O	5.20	4.48	4.65	4.78	4.95	4.01
P ₂ O ₅	1.40	0.55	0.20	0.18	0.31	0.18
Loss	6.69	5.75	5.62	5.49	5.60	4.96
TOTAL	99.80	99.51	99.82	99.82	99.61	99.82
Trace Elements (ppm)						
Ba	492	535	420	476	511	455
Ce	91	82	79	77	78	73
Cr	101	86	85	85	98	71
Cu	33	26	28	28	33	19
Ga	32	27	28	26	28	23
La	50	41	41	42	36	36
Nb	18	16	16	16	18	13
Ni	29	30	23	23	36	20
Pb	22	27	25	25	28	25
Rb	245	244	232	231	241	195
Sc	21	18	16	16	17	14
Sr	163	110	183	243	108	200
Th	19	18	18	17	18	16
U	3	3	3	3	3	4
V	198	164	165	164	175	132
Y	46	43	35	37	37	34
Zn	156	142	125	133	135	109
Zr	183	154	175	175	168	220

Table 2-5 (continued): Geochemical analyses of argillite (1-7),
sandstone (9-17) and lithic sandstone (8) from the
Tararua Range.

Analysis	(7)	(8)	(9)	(10)	(11)	(12)
Sample No.	17238	17223	17227	17235	17230	17293
<hr/>						
Major Oxides (wt.%)						
SiO ₂	61.10	66.94	68.75	70.50	71.26	72.08
TiO ₂	0.85	0.76	0.51	0.55	0.53	0.47
Al ₂ O ₃	18.82	13.15	14.86	13.95	13.51	13.36
Fe ₂ O ₃	0.26	0.56	0.45	0.39	1.55	0.42
FeO	4.60	3.77	3.26	3.13	2.68	2.33
MnO	0.04	0.08	0.04	0.03	0.03	0.05
MgO	1.88	1.42	1.17	1.18	1.17	0.92
CaO	0.64	2.76	1.23	0.93	0.62	1.56
Na ₂ O	2.73	3.06	2.89	3.28	3.44	3.96
K ₂ O	3.81	2.27	2.74	2.64	2.45	2.45
P ₂ O ₅	0.16	0.20	0.13	0.12	0.13	0.11
Loss	4.93	4.85	3.84	3.02	2.97	2.05
	-----	-----	-----	-----	-----	-----
TOTAL	99.83	99.82	99.88	99.72	100.34	99.76
 Trace Elements (ppm)						
Ba	402	333	514	503	623	628
Ce	63	47	65	49	60	57
Cr	72	56	36	42	40	47
Cu	16	14	8	8	9	6
Ga	27	17	21	20	14	14
La	33	22	30	27	29	28
Nb	14	12	12	9	8	7
Ni	21	24	11	8	15	9
Pb	20	19	25	20	24	16
Rb	176	92	121	108	98	80
Sc	13	13	8	8	9	7
Sr	164	162	293	245	216	259
Th	16	11	14	12	11	11
U	3	3	3	2	2	3
V	140	98	67	75	70	60
Y	32	25	30	22	23	24
Zn	110	78	78	65	78	46
Zr	229	135	232	272	248	293

Table 2-5 (continued): Geochemical analyses of argillite (1-7),
sandstone (9-17) and lithic sandstone (8) from the
Tararua Range.

Analysis	(13)	(14)	(15)	(16)	(17)
Sample No.	17236	17231	17225	17226	17228
Major Oxides (wt.%)					
SiO ₂	72.15	72.45	73.58	75.21	76.42
TiO ₂	0.50	0.52	0.42	0.36	0.33
Al ₂ O ₃	12.57	13.44	13.44	11.99	11.67
Fe ₂ O ₃	0.75	0.73	0.20	0.53	0.16
FeO	3.57	2.56	1.75	1.97	1.82
MnO	0.05	0.03	0.02	0.03	0.03
MgO	1.25	1.02	0.66	0.76	0.70
CaO	0.91	0.68	1.08	0.54	1.05
Na ₂ O	2.72	3.29	4.75	3.46	3.78
K ₂ O	2.32	2.39	1.49	2.80	1.62
P ₂ O ₅	0.11	0.12	0.07	0.05	0.06
Loss	2.94	2.42	2.27	2.01	2.15
TOTAL	99.84	99.65	99.73	99.71	99.80
Trace Elements (ppm)					
Ba	477	538	366	600	384
Ce	38	49	61	45	39
Cr	40	38	31	30	24
Cu	8	6	3	4	<2
Ga	13	15	15	13	14
La	19	28	30	21	18
Nb	8	8	8	8	6
Ni	13	11	7	4	4
Pb	25	18	21	21	19
Rb	96	95	64	101	64
Sc	8	7	8	5	4
Sr	209	223	284	191	248
Th	10	11	11	11	10
U	<2	2	4	2	<2
V	67	59	50	45	38
Y	20	25	20	17	18
Zn	73	68	46	44	44
Zr	199	269	258	172	182

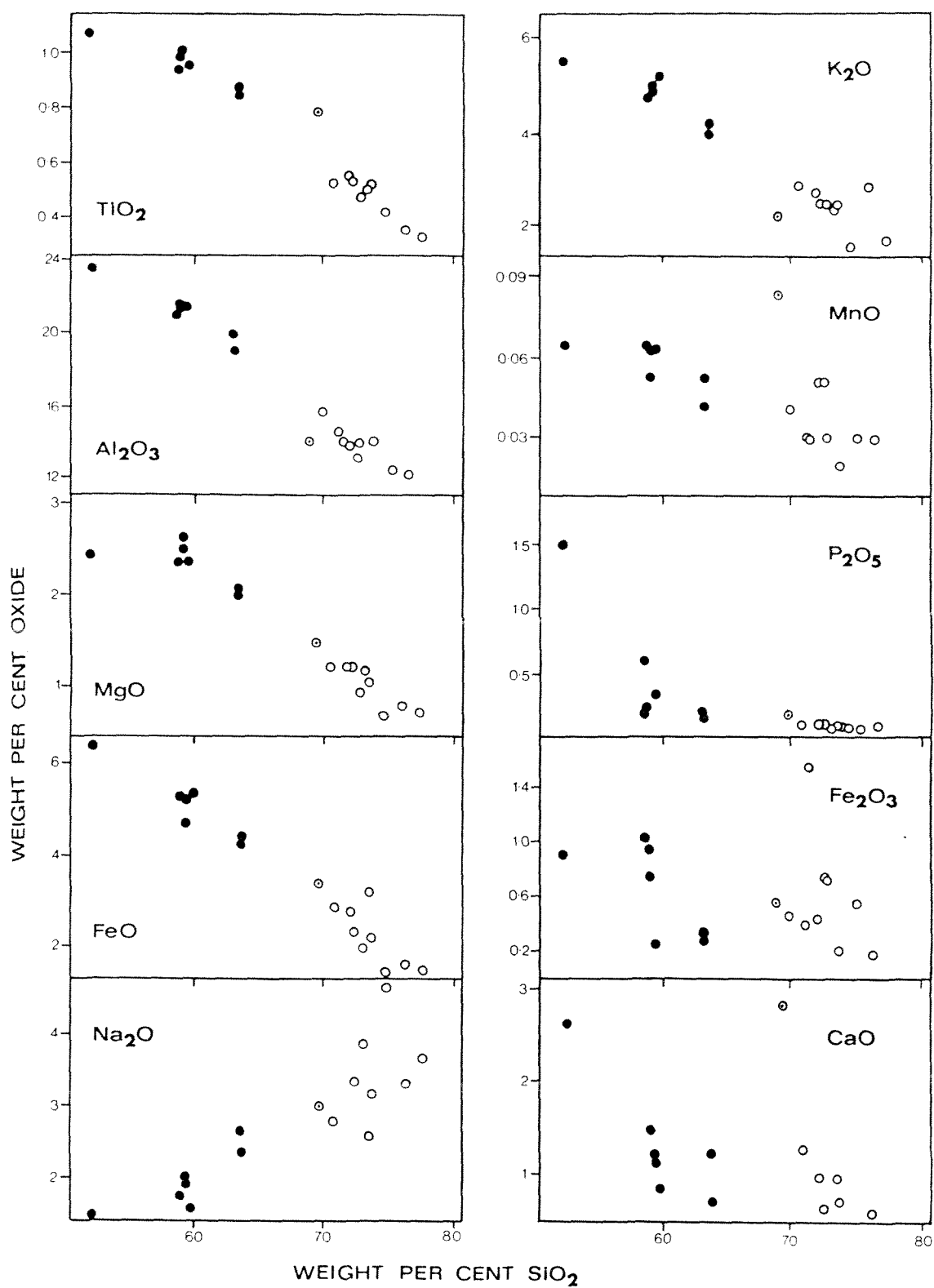


Figure 2-8: Major oxide variations in sandstones and argillites from the southern Tararua Range.

Symbols

● Argillite

○ Sandstone

⊙ Lithic sandstone

Data from Table 2-5.

	SI02	TI02	AL203	FE203	FEO	MNO	MGO	CAO	NA2O	K2O	P2O5	BA	CE	CR	CU	GA	LA	NB	NI	PB	RB	SC	SR	TH	U	V	Y	ZN	ZR
SI02	1.00000																												
TI02	-0.97021	1.00000																											
AL203	-0.98538	0.94720	1.00000																										
FE203	-0.27180	0.25340	0.19621	1.00000																									
FEO	-0.97529	0.96435	0.94771	0.25636	1.00000																								
MNO	-0.65445	0.73052	0.55217	0.16778	0.72743	1.00000																							
MGO	-0.96201	0.97776	0.95160	0.28405	0.96751	0.69070	1.00000																						
CAO	-0.35477	0.36957	0.22528	0.07758	0.35883	0.69178	0.24170	1.00000																					
NA2O	0.87929	-0.86550	-0.85142	-0.32831	-0.94067	-0.68471	-0.91465	-0.21621	1.00000																				
K2O	-0.95855	0.92036	0.96219	0.24914	0.94220	0.58541	0.95119	0.16485	-0.91702	1.00000																			
P2O5	-0.71589	0.59892	0.64801	0.31659	0.69874	0.45217	0.53852	0.58897	-0.60686	0.61514	1.00000																		
BA	0.09770	-0.20815	-0.09873	0.44910	-0.12885	-0.21994	-0.13506	-0.33128	-0.02843	0.06140	0.03267	1.00000																	
CE	-0.91083	0.83019	0.92515	0.27433	0.82782	0.44669	0.82926	0.25051	-0.70063	0.86833	0.64978	0.04946	1.00000																
CR	-0.97710	0.97197	0.96170	0.21506	0.96565	0.71074	0.96200	0.32520	-0.87431	0.95511	0.64531	-0.08341	0.86126	1.00000															
CU	-0.97068	0.96065	0.95181	0.27194	0.96779	0.70569	0.96747	0.31087	-0.90809	0.95881	0.64123	-0.08322	0.86181	0.98330	1.00000														
GA	-0.95503	0.92153	0.97224	0.08696	0.93103	0.53735	0.91656	0.25458	-0.83560	0.92433	0.64261	-0.18015	0.87696	0.91880	0.91078	1.00000													
LA	-0.92174	0.84413	0.93200	0.32508	0.83221	0.40249	0.83445	0.25824	-0.70165	0.86993	0.69714	0.03866	0.97124	0.85897	0.85128	0.88324	1.00000												
NB	-0.96117	0.95352	0.95611	0.16501	0.95561	0.68082	0.94532	0.32049	-0.88537	0.93866	0.61339	-0.16974	0.86850	0.95005	0.96211	0.95418	0.84344	1.00000											
NI	-0.88717	0.92188	0.85210	0.27353	0.91541	0.78659	0.89450	0.36779	-0.84606	0.83861	0.57724	-0.12981	0.75789	0.93105	0.93008	0.81284	0.71457	0.91185	1.00000										
PB	-0.53985	0.50864	0.56127	0.31409	0.59692	0.31337	0.62297	-0.16884	-0.66987	0.59731	0.18395	0.05313	0.56354	0.52304	0.61445	0.51137	0.45994	0.61682	0.59126	1.00000									
RB	-0.96167	0.92841	0.97168	0.24789	0.94916	0.57901	0.96585	0.14660	-0.91617	0.98709	0.58776	-0.00984	0.88322	0.45170	0.96092	0.93592	0.87564	0.94929	0.85580	0.66360	1.00000								
SC	-0.97607	0.97266	0.94088	0.30417	0.96516	0.72851	0.94179	0.44480	-0.84742	0.90309	0.71354	-0.16628	0.87520	0.96788	0.96312	0.93346	0.87301	0.94910	0.93820	0.55016	0.91755	1.00000							
SR	0.60719	-0.65551	-0.56351	-0.20102	-0.68314	-0.63791	-0.63776	-0.17283	0.69001	-0.63298	-0.45060	0.02249	-0.40571	-0.69413	-0.67316	-0.54172	-0.36262	-0.63708	-0.75990	-0.40208	-0.64077	-0.67290	1.00000						
TH	-0.96251	0.91432	0.98480	0.15097	0.92910	0.53448	0.93423	0.18415	-0.85590	0.96242	0.60987	-0.06596	0.92897	0.93259	0.93201	0.97471	0.91241	0.95749	0.82292	0.60742	0.97744	0.90761	-0.56150	1.00000					
U	-0.45190	0.44908	0.47892	-0.29287	0.36818	0.31505	0.38532	0.34241	-0.12103	0.33378	0.18261	-0.39320	0.59609	0.43449	0.38014	0.44297	0.51709	0.46439	0.38710	0.23098	0.37764	0.48805	-0.04222	0.47983	1.00000				
V	-0.99027	0.98375	0.97772	0.23905	0.97964	0.67998	0.97735	0.31506	-0.89015	0.95979	0.65823	-0.13805	0.86984	0.99079	0.98346	0.94744	0.87494	0.95640	0.91948	0.55647	0.96522	0.47689	-0.67407	0.95158	0.42611	1.00000			
Y	-0.96649	0.91515	0.95711	0.28360	0.93587	0.61951	0.90811	0.36260	-0.85777	0.91769	0.72689	-0.01639	0.92631	0.92715	0.91806	0.93033	0.92455	0.93037	0.86173	0.53776	0.93334	0.93741	-0.55886	0.95022	0.46625	0.93821	1.00000		
ZN	-0.97687	0.95851	0.96451	0.35266	0.97766	0.63770	0.96850	0.26706	-0.92711	0.94730	0.67186	-0.07691	0.86823	0.95570	0.96560	0.92920	0.87365	0.95437	0.91581	0.64474	0.96521	0.96237	-0.65677	0.94270	0.35603	0.97741	0.95678	1.00000	
ZR	0.50545	-0.50488	-0.47062	-0.15538	-0.56592	-0.54732	-0.56112	-0.20321	0.65077	-0.55148	-0.34271	0.25497	-0.33154	-0.51508	-0.59506	-0.45570	-0.26962	-0.58560	-0.55368	-0.57665	-0.58493	-0.52814	0.63303	-0.50466	-0.02973	-0.54583	-0.44326	-0.55722	1.00000

Table 2-6: Correlation matrix for sandstones and argillites from the southern Tararua Range.

Rowe (1980) who showed the variation to be a function of grain size. The separation of sandstone and argillite data seen in Fig. 2-8 is a result of this effect.

Rowe (1980) demonstrated that with the transition from sandstone to argillite (decreasing grain size) the matrix content increased (see also section 2.3). Higher matrix content in argillite is also indicated by appreciably higher losses on ignition. Matrix consists predominantly of clay minerals which are rich in those major oxides that decrease in abundance with increasing SiO_2 . The weak correlation of P_2O_5 is probably due to the presence of detrital apatite.

Most Na_2O in the sandstones and argillites occurs in albitized plagioclase grains (see section 2.3). The effect of increased matrix content is to decrease the plagioclase content and hence Na_2O .

The poor correlation of CaO with other major element oxides is probably due to small amounts of calcite veining and replacement (see section 2.2).

As the abundance of Fe_2O_3 is related to weathering processes, either pre- or post sedimentation, no interelement correlation is expected and none is observed.

Trace element variation:

Of the 18 trace elements analysed Ce, Cr, Cu, Ga, La, Nb, Ni, Pb, Sc, Th, V, Y and Zn show a systematic decrease in abundance with increasing SiO_2 (Fig. 2-9). This trend is weakly developed for Pb which is intermediate in size between Ca^{2+} and K^+ and therefore may be expected to occur in both feldspar and mica (Taylor 1965). Other trace elements listed are thought to be abundant in matrix (Pettijohn 1963) and therefore controlled to a large extent by its variation.

Both Sr and Zr show a weak positive correlation with SiO_2 . Sr

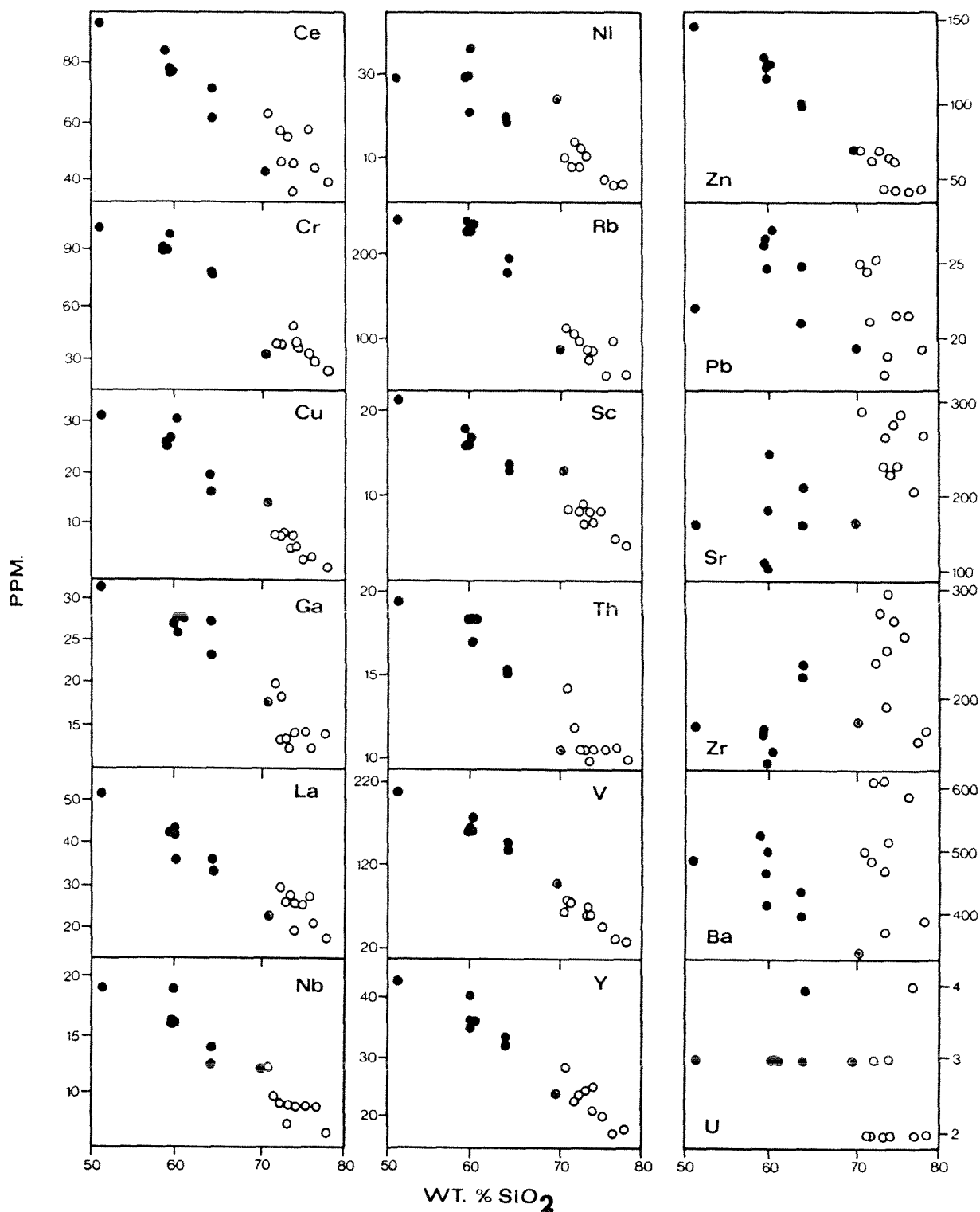


Figure 2-9: Trace element variations in sandstones and argillites from the southern Tararua Range.

Symbols

- Argillite
- Sandstone
- ⊙ Lithic sandstone

Data from Table 2-5.

can substitute for Ca^{2+} and K^{+} in feldspar but not in mica (Taylor 1965); the effect of increased grain size is to increase feldspar content and hence Sr. The abundance of Zr is related to the heavy detrital mineral zircon. Due to its high density, zircon and hence Zr would tend to be more abundant in coarser sediments; such a trend is observed.

Ba and U show no correlation with SiO_2 and hence grain size. Ba, which shows greater variations in the sandstones, can substitute for K^{+} in both mica and feldspar with substitution occurring more readily in the latter (Taylor 1965). The poor correlation of Ba with SiO_2 is most probably due to a lack of dominance of either substitution type.

Very low abundances combined with a lack of analytical precision for U makes it difficult to determine the occurrence of any systematic variation. Taylor (1965) lists sphene, allanite and zircon as being important hosts for U, in which case a positive correlation with SiO_2 would be expected.

The variations in major oxides and trace elements described above suggests the sandstones and argillites, although chemically distinct (which may be a function of sampling method), are part of a chemical continuum rather than distinct end members and that the major control of element distribution is matrix content.

For comparison, data from this study and that of Rowe (1980) and Foley (1984) are shown in Fig. 2-10. While these studies show variation trends that are similar, differences occur as a result of differences in mineral composition and abundance which are primarily controlled by source composition.

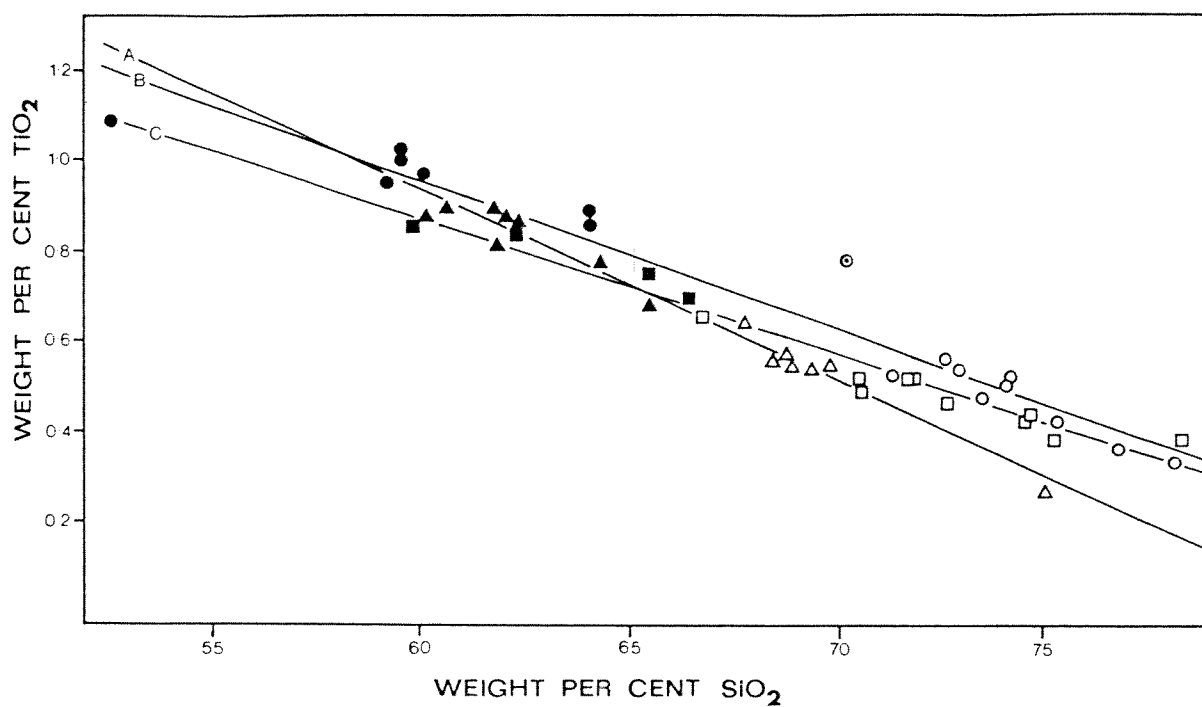


Figure 2-10: TiO_2 versus SiO_2 plot for Torlesse Supergroup sandstones and argillites from the Wellington Region.

Symbols

$\Delta \square \circ$ Sandstone

$\blacktriangle \blacksquare \bullet$ Argillite

\odot Lithic sandstone

\bullet This study, regression line B. (lithic sandstone not included in the calculation of the regression line).

\blacktriangle Data from Rowe (1980), excluding data east of the Wellington Fault and Te Rewarewa Point, regression line A.

\blacksquare Data from Foley (1984), regression line C.

Note that the lithic sandstone from this study plots well off the trend of the "normal" sandstones and argillites.

2.5. PROVENANCE AND TECTONIC SETTING

The composition of terrigenous sandstones are influenced by the nature of the sedimentary provenance and the processes affecting sedimentation, both of which are primarily dependant on plate tectonic setting. In this study both petrographic and geochemical data are used to interpret the provenance and the plate tectonic setting of the depositional site of the sandstones and argillites. The following can be concluded from petrographic examination of sandstone from the study area (see section 2.3):

- 1) Textural and compositional immaturity of the sandstone is probably due to most of the sediments being subjected to only a single cycle of sedimentation;

- 2) The dominant detrital mineral assemblage is quartz (undulose extinction is common and rutile inclusions are frequent), alkali-rich feldspar and biotite. Perthitic and myrmekitic intergrowths are not uncommon. The detrital heavy mineral assemblage consists of euhedral zircon, sphene, apatite and epidote group minerals. Rock fragments of quartzite and phyllite occur. Hence a significant proportion of the source region consisted of plutonic and associated metamorphic rocks.

- 3) Rock fragments consisting of chert, acid volcanics and basic volcanics were common and hence the source region also contained volcanic and sedimentary rocks.

Because the character and amount of matrix in a rock such as a greywacke is partly the result of diagenetic processes, petrographic studies of the provenance of such rocks has focused on the detrital framework grains (Dickinson 1970). Significant compositional variation among terrigenous sandstones traditionally has been displayed on triangular diagrams where the apices represent recalculated proportions

of detrital framework grains determined by modal point-counts.

On Q-F-L and Qm-F-Lt plots sandstones from this study (Fig. 2-11a & b), with the exception of the lithic sandstone, form a field that overlaps both the dissected magmatic arc and basement uplift provenance fields of Dickinson et al. (1983). The dissected magmatic arc field represents sands derived from magmatic arcs where erosion has exposed batholiths beneath the volcanic cover. Sands with a basement uplift provenance are derived from continental blocks where intraplate deformation has occurred (eg. rifting, thrusting and transcurrent faulting). Such tectonism may expose granite and gneiss from which a sand could be derived that would be petrographically indistinguishable from similar sands derived mainly from the plutons of a magmatic arc. Because all sands in the study area obviously from the same source region they are interpreted as being derived from a deeply eroded magmatic arc.

The lithic sandstone (sample 17223) plots in different fields on the Q-F-L (undissected arc) and Qm-F-Lt (lithic recycled) diagrams to those of the "normal" sandstones (Fig. 2-11a & b).

Sands with an undissected magmatic arc provenance are derived mainly from the volcanic capping of undissected magmatic arcs. Such sands would be expected to contain significant amounts of volcanic lithic fragments. However, sixty-five percent of the lithic sandstone is made up of sedimentary lithic fragments and as such is unlikely to have been derived from an undissected magmatic arc.

Sands with a recycled orogenic provenance are derived from orogenic belts where sediment sources are sedimentary strata and subordinate volcanic rocks which are in part metamorphosed. Sands of this provenance are generally low in feldspar as igneous rocks are not

Figure 2-11a: Q-F-L diagram with provenance categories from

Dickinson et al. (1983).

Q = Total quartzose grains, including polycrystalline lithic fragments such as chert and quartzite.

F = Monocrystalline feldspar grains.

L = Unstable polycrystalline lithic fragments of either igneous or sedimentary origin, including metamorphic origin.

Symbols

● Sandstone

■ Lithic sandstone

Figure 2-11b: Qm-F-Lt diagram with provenance categories from

Dickinson et al. (1983).

Qm = Quartz grains that are exclusively monocrystalline.

F = Monocrystalline feldspar grains.

Lt = Total polycrystalline grains (including quartzose varieties).

Symbols

● Sandstone

■ Lithic sandstone

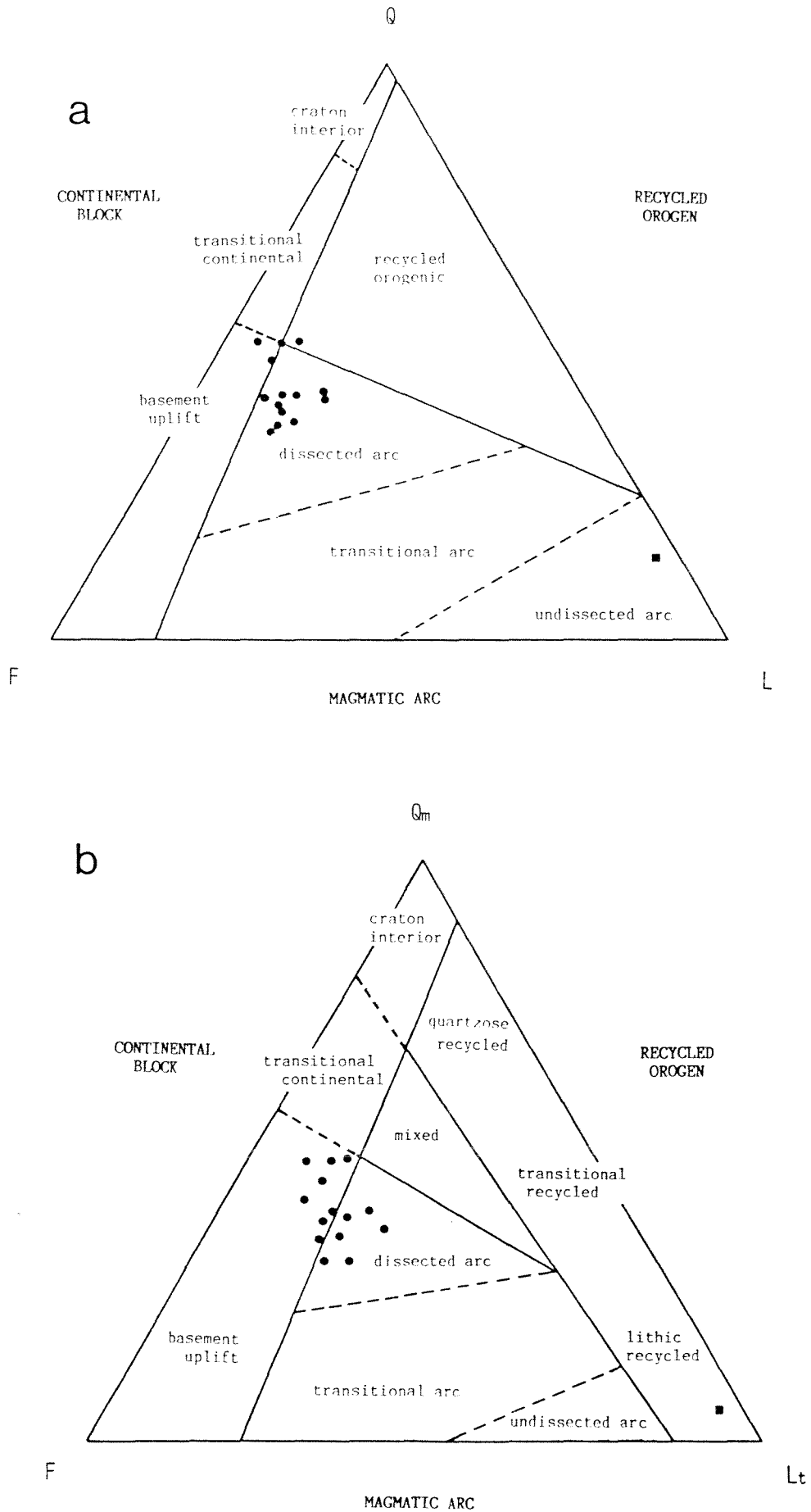


Figure 2-11

prime sources. Possible tectonic settings of depositional basins include subduction complexes, highlands along collision belts and foreland fold and thrust belts. The high percentage of sedimentary lithic rock fragments and the low percentage of feldspar (2.8%) relative to quartz (10%) in the lithic sandstone (sample 17233) is consistent with a recycled orogen provenance.

Figure 2-12 shows the sandstones plotted on a Qm-P-K diagram with field boundaries based on the data of Dickinson and Suczek (1979). The "normal" sandstones spread across the transitional and dissected magmatic arc fields whereas the lithic sandstone plots within the dissected magmatic arc field closer to the field of continental block and recycled orogen provenances.

Ingersoll and Suczek (1979) used two triangular diagrams (Lm-Lv-Ls and Qp-Lvm-Lsm) which utilize modal proportions of lithic fragments to distinguish sandstone provenance. On both diagrams the "normal" sandstones plot mainly within the provenance field of mixed magmatic arcs and rifted continental margins (Fig. 2-13a & b) which is consistent with a magmatic arc provenance.

The lithic sandstone plots within the suture belts field on both Lm-Lv-Ls and Qp-Lvm-Lsm diagrams (Fig. 2-13a & b). On the Lm-Lv-Ls diagram the lithic sandstone plots where three fields overlap, these being: suture belts, mixed magmatic arcs and subduction complexes, and rifted continental margins. On the Qp-Lvm-Lsm diagram these fields show little overlap. Suture belts, which are included in the recycled orogen provenance of Dickinson et al. (1983), lack significant volcanics and primarily consist of uplifted sedimentary and metasedimentary rocks.

Recently, sedimentary geochemical data have been used, with some

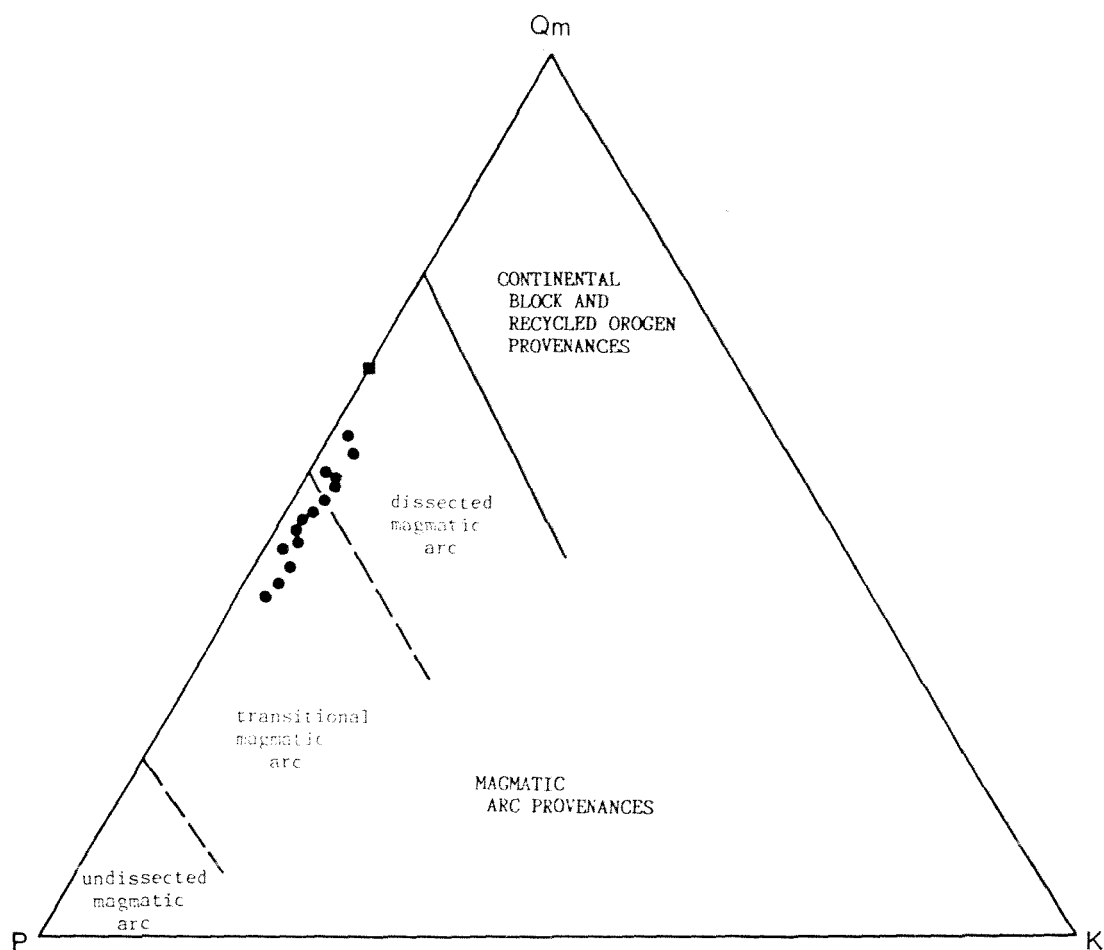


Figure 2-12: Qm-P-K diagram showing sandstone from the Tararua Range.

Field boundaries are interpreted from the data of Dickinson & Suczek (1979).

Qm = Quartz grains that are exclusively monocrystalline.

P = Plagioclase grains.

K = Alkali feldspar grains.

Symbols

● sandstone

■ lithic sandstone

Figure 2-13a: Lm-Lv-Ls diagram showing sandstone from the Tararua Range with provenance fields from Ingersoll & Suczek (1979).

Lm = Metamorphic lithic fragments.

Lv = Volcanic lithic fragments.

Ls = Sedimentary lithic fragments.

Symbols

● Sandstone

■ Lithic sandstone

Figure 2-13b: Qp-Lvm-Lsm diagram showing sandstone from the Tararua Range with provenance fields from Ingersoll & Suczek (1979).

Qp = Polycrystalline quartz including chert and quartzite.

Lvm = Volcanic and metavolcanic lithic fragments.

Lsm = Sedimentary and metasedimentary lithic fragments.

Symbols

● Sandstone

■ Lithic sandstone

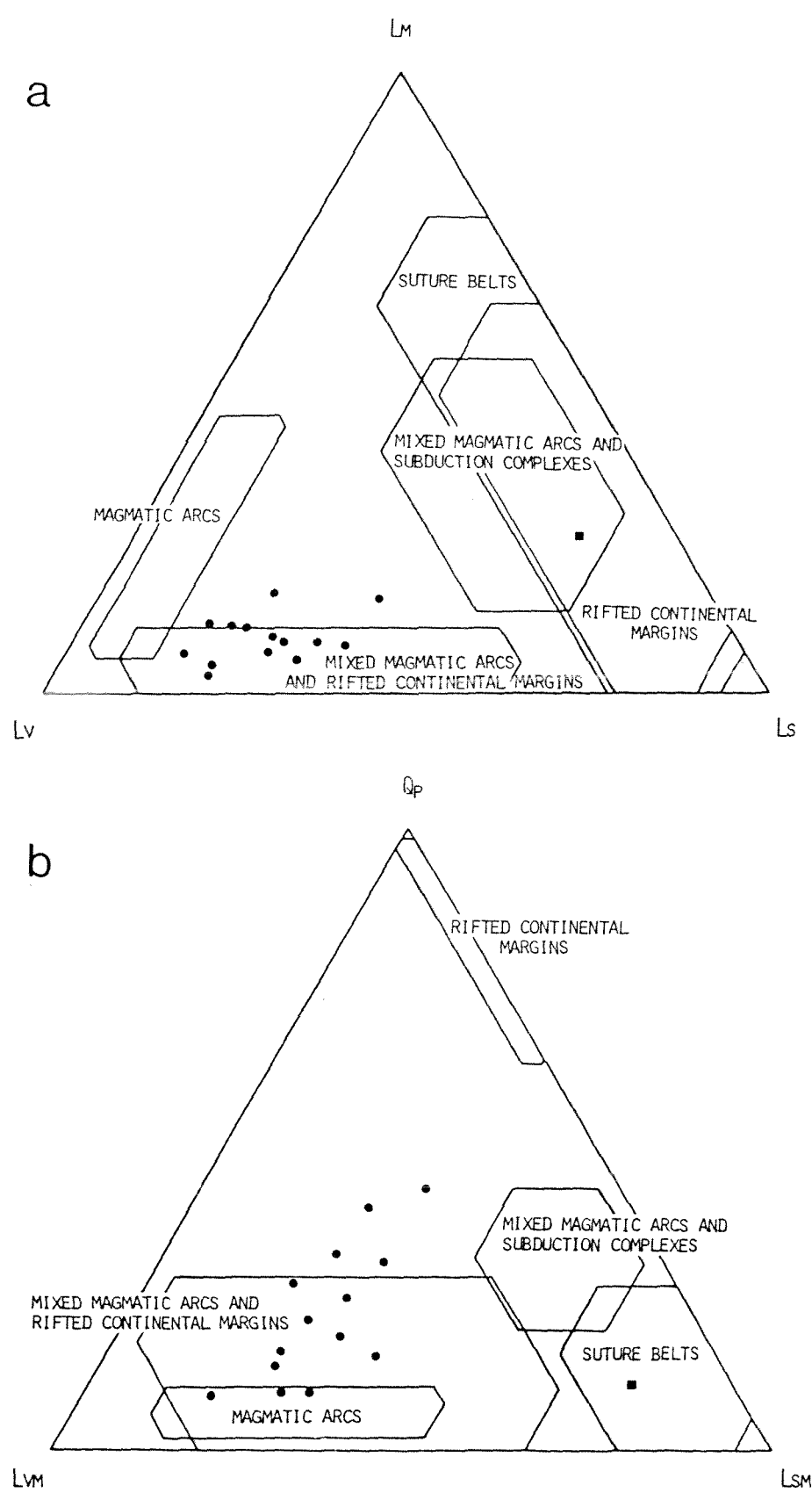


Figure 2-13

success, to discriminate the tectonic setting of sandstone depositional environments. Roser (1983) utilized a binary SiO_2 versus $\text{K}_2\text{O}/\text{Na}_2\text{O}$ discriminant plot, which represents an extension of a scheme originally proposed by Crook (1974). Three major tectonic settings are differentiated, these being:

- 1) Passive continental margins where sediment accumulated in plate interiors and at passive continental margins;
- 2) Tectonically-active continental margins where detritus is supplied from tectonically-active continental crust, and deposited at subducting plate margins;
- 3) Oceanic island arcs where sedimentation occurs in trenches off active volcanic island arcs in both fore-arc and back-arc settings.

Both sandstone and argillite data from this study plot almost entirely within the active continental margin field with minimal spread into the passive margin field (Fig. 2-14a). The trend shown by the sandstone and argillite data parallels that expected for sediments derived from a tectonically-active continental margin (Roser 1983).

Bhatia (1983) attempted to discriminate the tectonic setting of sandstone sedimentation using two discriminant functions which utilize 11 major element oxides as variables.

Both sandstone and argillite are plotted on Figure 2-14b. The sandstones form a field that overlaps both the active continental margin and continental island arc fields with equal amounts of data falling in each field. The continental island arc setting is transitional between active continental margin and oceanic island arc settings (ie. an island arc formed on well developed continental crust).

The spread in data seen in both the plots of Roser and Bhatia is

Figure 2-14a: Tectonic setting of sediments using a volatile-free alkali/silica discriminant (after Roser 1983).

Symbols

- Argillite
- Sandstone
- ⊙ Lithic sandstone

Figure 2-14b: Discriminant Function I versus Discriminant Function II for sandstone and argillite from the southern Tararua Range (after Bhatia 1983).

$$\begin{aligned} \text{DFI} = & -0.0447\text{SiO}_2 - 0.972\text{TiO}_2 + 0.008\text{Al}_2\text{O}_3 - 0.267\text{Fe}_2\text{O}_3 + 0.208\text{FeO} \\ & - 3.082\text{MnO} + 0.140\text{MgO} + 0.195\text{CaO} + 0.719\text{Na}_2\text{O} - 0.032\text{K}_2\text{O} \\ & + 7.510\text{P}_2\text{O}_5 + 0.303. \end{aligned}$$

$$\begin{aligned} \text{DFII} = & -0.421\text{SiO}_2 + 1.988\text{TiO}_2 - 0.526\text{Al}_2\text{O}_3 - 0.551\text{Fe}_2\text{O}_3 - 1.610\text{FeO} \\ & + 2.720\text{MnO} + 0.881\text{MgO} - 0.907\text{CaO} - 0.177\text{Na}_2\text{O} - 1.840\text{K}_2\text{O} \\ & + 7.244\text{P}_2\text{O}_5 + 43.57. \end{aligned}$$

Note sandstones are used to determine provenance.

One argillite plots off the diagram.

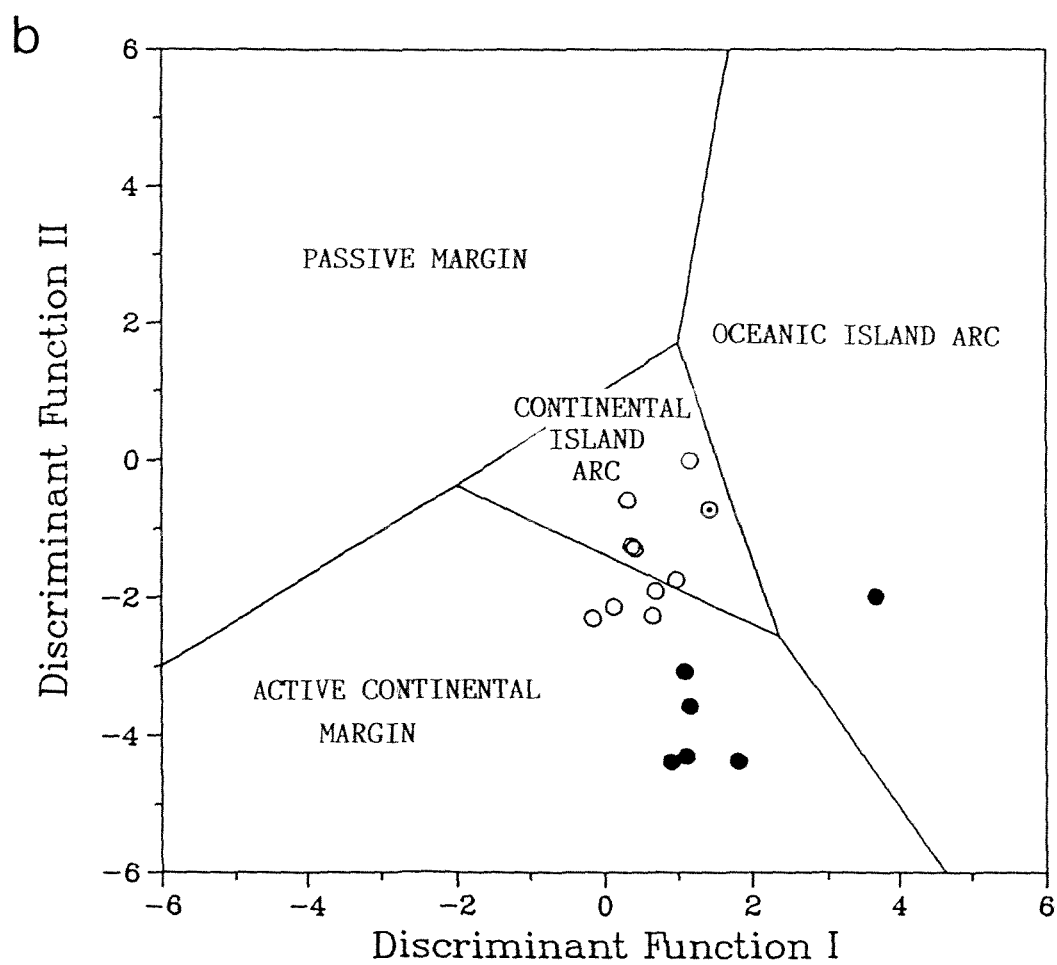
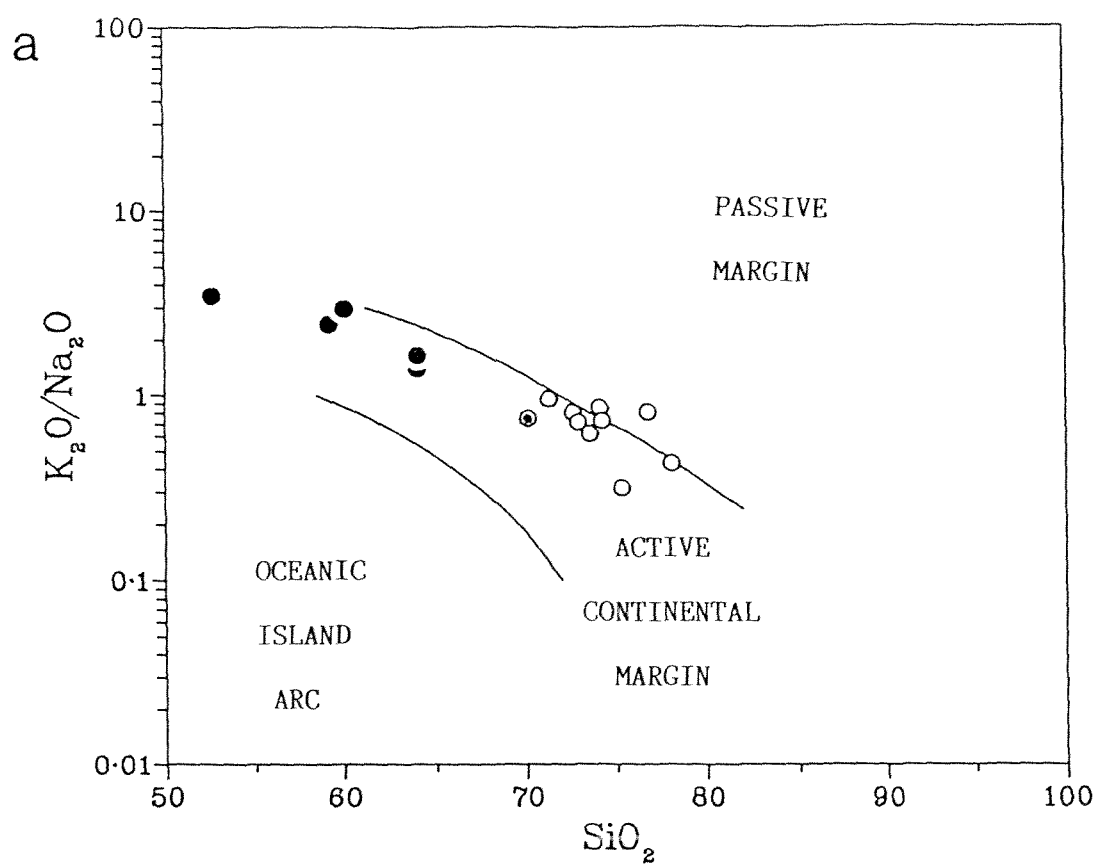


Figure 2-14

clearly a result of the effect of grain size. As samples analysed were no coarser than medium sand, the spread of data would be increased with the inclusion of coarser sandstones. On the plot of Bhatia this increase in spread would be likely to cause further discriminant fields to be covered although this would be unlikely to occur on the Roser plot because the data trend parallel to the closest field boundary.

In conclusion, analysis of both the petrographic and geochemical data obtained in this study indicate an active continental margin tectonic setting. A magmatic arc provenance is suggested for the "normal" sandstones while a recycled orogen provenance is indicated for the lithic sandstone.

CHAPTER THREE

VOLCANIC ASSOCIATION

This chapter describes the petrography and geochemistry of rocks of the volcanic association, that is, metabasite, chert, coloured argillite and limestone. Initially, the field occurrence and petrography of the various lithologies will be described, and then geochemical data are used to provide an interpretation of the eruptive and depositional environment.

3.1 PETROGRAPHY

This section includes data obtained from field observations, thin section examination and microprobe analyses. The lithologies are described in order of decreasing abundance. Metamorphic minerals will be described in Chapter Four.

3.1.1 Metabasite

Red, green and blue-black metabasites occur usually as relatively small slivers, blocks or phacoids, of which red metabasite is the most common. Figure 3-1 shows the mapped occurrence of metabasite and the other lithologies of the volcanic association, and from this figure it is obvious that, although not volumetrically significant (probably less than 5%), the rocks of volcanic association occur at many locations throughout the field area.

Both red and green amygdaloidal metabasite were observed and these make up approximately one third to half of the metabasites. Pillow metabasite was observed in only a few outcrops (eg. G.R. S26C/0283 1310, average pillow size 60cm by 35cm by 35cm). The pillows were either poorly developed or exposed and could not be used to determine facing.

One of the largest outcrops of metabasite occurs in the

Figure 3-1: Map showing the distribution of the rocks of the volcanic association.

KEY



Metabasite



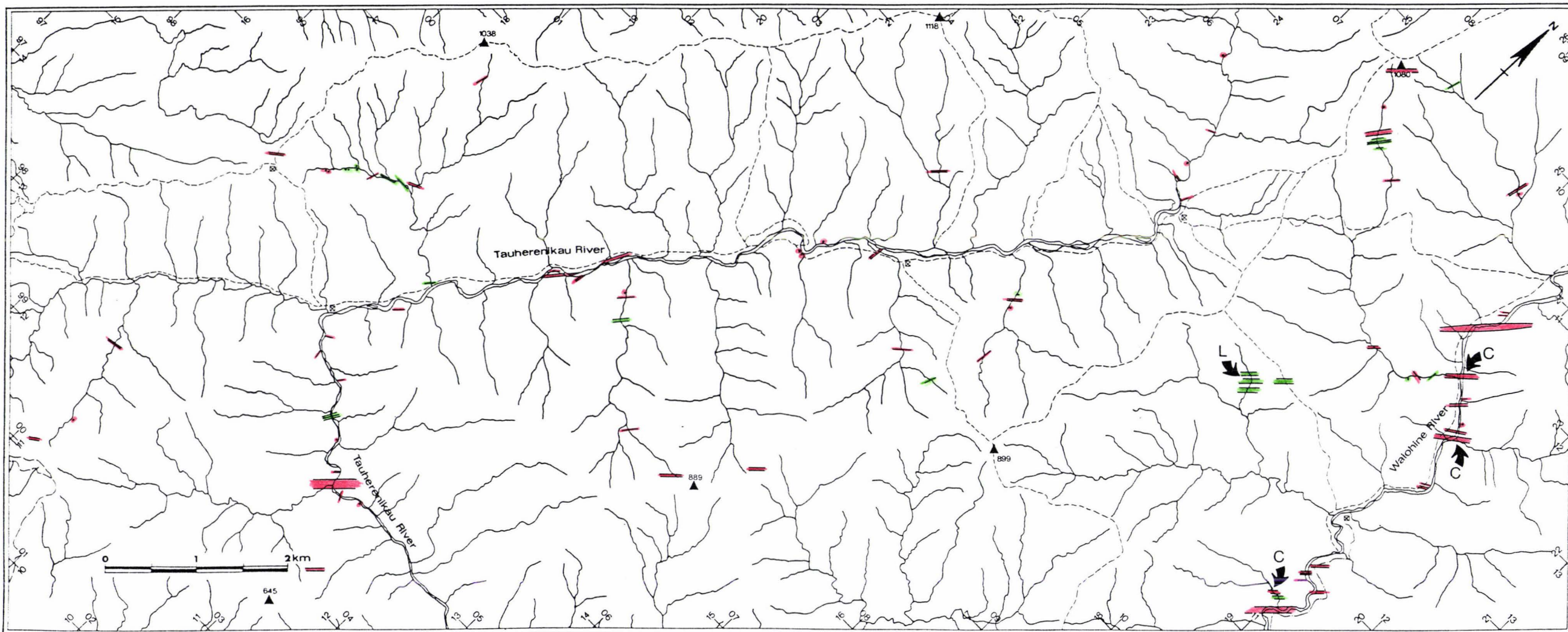
Coloured argillite

C

Chert

L

Limestone



Tauherenikau Gorge at G.R. S26C/ 0283 1310. This outcrop was mapped in detail (see section 5.1.4), and consists of at least three fault-bounded slivers of red and green amygdaloidal metabasite (Fig. 3-2)

As well as metabasite lavas, outcrops consisting of metabasite and chert clasts within a coloured argillite matrix, and metabasite pillows(?) in coloured argillite were observed.

Elsewhere in the field area, where contacts between rocks of the sedimentary and volcanic association could be observed, faults separate the two associations. That is, nowhere were rocks of the two associations observed to be conformable.

In thin section, metabasites exhibit mainly variolitic and subophitic textures. Subophitic types have a primary mineralogy which consists mainly of plagioclase ($\approx 55\%$), clinopyroxene ($\approx 5\%$) and oxide minerals ($\approx 10\%$), set in a fine grained mesostasis ($\approx 30\%$).

Plagioclase grains, which are commonly simply twinned and full of inclusions, vary from acicular (average size 0.3mm by 0.04mm) in variolitic lavas to tabular (average size 0.3mm by 0.2mm) in subophitic lavas. Plagioclase compositions determined by the Michel-Levy method were either albite or andesine. Acicular plagioclase grains were often bent (eg. 17278, 17288) and occasionally glomerocrysts of tabular plagioclase grains occur in the rare porphyritic lavas (17255, 17274).

Clinopyroxene grains occur mainly in the subophitic lavas and were generally small (average size 0.1mm by 0.15mm) and anhedral. Zoning was observed in only one grain (17255). Microprobe analyses of clinopyroxenes (Appendix VII) indicate that the compositions are augite and salite. Clinopyroxene composition is used below to determine magma type.

Opaque minerals are common in most of the metabasites, making up



Figure 3-2: Faulted contact between red amygdaloidal metabasite and a disrupted unit of fine sand and argillite.

Tauherenikau Gorge S26C/ 0283 1310, geological hammer 31 cm long.

as much as 15% of the thin-section (17243) and are commonly acicular and, less commonly, euhedral equant grains. Acicular grains commonly show alignment with nearby grains (17280). Microprobe analyses of the opaque grains indicate that they are titaniferous magnetite (20.1% TiO_2) and ilmenite.

Amygdules occur in several thin sections (17242, 17252, 17254, 17257, 17288) and in T.S. 17242 they constitute approximately 15% of the thin section (average size 0.6mm by 0.6mm), of which 70% were calcite filled and 30% were chlorite filled. The volume percent and average diameter of amygdules in this sample suggest extrusion at a water depth of approximately 800 metres (Moore 1965). A sample of red amygdaloidal metabasite from the Tauherenikau Gorge (17285) was slabbed and point counted (400 counts) and contains calcite-filled amygdules with an average diameter of 1.7mm which made up 34% of the rock, suggesting extrusion at a water depth of less than 500 metres. Other samples have average amygdule sizes that fall between those of samples 17285 and 17242. Many calcite-filled amygdules are rimmed with opaque minerals. In T.S. 17267 the amygdules are filled with colloform chlorite with occasional opaque mineral grains.

Interpillow and selvage material in samples 17250 and 17249 were collected from a single metabasite outcrop in the middle Tauherenikau River (G.R. S26C/ 0325 1700). T.S. 17250 consists in part of subangular fragments (average size 0.5mm by 0.3mm) of devitrified spherulites set in a matrix of fine grained material, and in part of a finely-laminated clay to silt-sized material with occasional fine sand-sized fragments of feldspar, epidote and fine grained metabasite. T.S. 17249 consists of angular to subangular fragments of fine grained (largest feldspar 0.25mm by 0.02mm) and altered "glassy" metabasite set in a hematitic

clay matrix (approximately 35%). Clast size ranges from 0.1mm by 0.1mm to 0.75mm by 0.6mm and averages approximately 0.5mm by 0.4mm.

3.1.2 Red and green argillite

Red and, less commonly, green argillite occur as fault-bounded slivers in many parts of the field area but are most common in the southern arm of Coal Stream (G.R. S26C/ 0070 1575; Fig. 3-1). The slivers are generally two to three metres wide and rarely exceed five metres in width. Coloured argillite is found associated with metabasite (eg. at G.R. S26C/ 0283 1310 metabasite pillows(?) are found "floating" in a red argillite matrix, see Fig. 5-10a), and slivers are commonly faulted against intensely sheared argillite and sandstone units of the sedimentary association. The only lithologies in conformable contact with coloured argillite are metabasite, limestone and chert.

Coloured argillites examined in thin section consist mainly of clay size material, sometimes with minor amounts of very fine sand and silt grains. Identifiable grains consist mainly of plagioclase (eg. 17272, 17275, 17253) and less commonly very fine grained metabasite (17251, 17275, 17277). Chert was observed as "patches" and lenses (average 0.25mm thick) in several samples (eg. 17272) and as fragments in the more intensely sheared argillites (17282, 17292, 17251). Alternating lenses of hematite-rich, hematite-poor and opaque mineral rich material were observed in sample 17239.

3.1.3 Chert

Chert of variable colour, but most commonly red and white, generally occurs as small slivers, phacoids and clasts within chaotic units. The largest occurrence was recorded in the middle Waiohine River (G.R. S26D/ 1110 2210, Fig. 3-3) where a wedge-shaped sliver (maximum width of 4 metres) of massive red chert occurs in a disrupted sequence



Figure 3-3: Large fault bounded sliver of massive red chert.

Waiohine Gorge S26D/ 1110 2210.

that consists of metabasite and thinly-bedded sandstone and argillite (geochemistry sample 17247, see following section). Chert is common as angular fragments in the type B chaotic facies described in Chapter Two, and as phacoids or slivers in the disrupted volcanic rich units (Type Cii) that will be described in section 5.2.2.

Cherts examined in thin section (17247,17258,17279,17286,17290) are all very similar with the major difference being the amount of granular hematite present. Each chert consists of subequal amounts of microcrystalline, sutured quartz grains (with an average grain size of around 0.01mm) and somewhat coarser crystalline quartz which form a vein-like network (average grain size 0.06mm). Granular hematite is abundant in red cherts (eg. 17247) and absent in white cherts (eg. 17279). In sample 17258, granular hematite is abundant (40% of total thin section) giving the rock an argillitic appearance in parts. This sample probably represents a transitional type in a compositional continuum that appears to exist between chert and coloured argillite. Rare euhedral pyrite cubes were observed in sample 17279.

Rare radiolarian ghosts occur in thin sections from large chert outcrops (17279,17286) and chert fragments in chaotic sedimentary units (ie. T.S. 17281, Type B chaotic facies, middle Tauherenikau Gorge). A sample of red chert (T.S. 17289) from an intensely sheared zone from the Tauherenikau Gorge (G.R. S26C/ 0280 1322) contained abundant sponge(?) spicules as well as many radiolarian skeletons. Only one chert was found to contain well preserved radiolaria (17289) and an attempt to extract radiolaria from this sample was unsuccessful.

3.1.4 Limestone

A limestone block (56cm wide and at least 1.3m long) was found in Coal Creek (G.R. S26C/ 0915 2094) at a contact between red argillite

(which extended at least 10m downstream, T.S. 17220) and thin bedded sandstone and argillite units. The red argillite-limestone contact appears to be conformable while the contact between the limestone and the sandstone-argillite unit is clearly faulted. Poorly-defined bedding in the limestone is approximately parallel to the long axis of the limestone block which itself was aligned along the faulted contact. In thin-section (T.S. 17276) the limestone is highly recrystallized, moderately sheared and contains several stylolites. Laminations of alternating light and dark calcite (on average 0.06mm thick) were observed in several parts of the slide. Recrystallized bivalve shells with micritized rims were noted in this sample. Two generations of compaction are evident (Harmsen pers. com. 1984).

Several small limestone clasts (eg. 23cm by 15cm) were found in an intensely-sheared, volcanic-rich chaotic unit in the lower Tauherenikau Gorge (G.R. S26C/ 0317 1315). One clast, a silty, recrystallized limestone, examined in thin-section contains two generations of stylolites which are at a low angle to each other and are cut by calcite veins (17291). The margin of the clast is intensely sheared and fragments of limestone have been sliced off and incorporated into the surrounding green argillite matrix.

3.2 METABASITE MAGMA TYPE AND ERUPTIVE ENVIRONMENT

In order to determine the magma type and eruptive environment of metabasites from the field area, both trace element data (determined by whole rock XRF analysis; Table 3-1) and clinopyroxene composition (determined by electron microprobe; Appendix VII) are utilized. Only ten metabasites that show good igneous texture are used in this section, that is, analysis of rocks that show signs of brecciation have not been used here (see below).

The magma types of the metabasites have been determined by two methods. Pearce and Cann (1973) used the Y/Nb ratios to divide metabasites into tholeiitic, transitional and alkaline types. The Y/Nb ratios of the metabasites from the Tararua Range are plotted on Figure 3-4a together with a selection of basalt data from known tectonic settings. This method classified two as tholeiitic, seven as transitional and one as alkaline.

The second method is a five element (Ti,P,Nb,Y and Zr) discriminant function developed by Grapes and Palmer (1984). Due to the inclusion of Ti, P, and Zr data this method gives better separation of the two petrological types than Y/Nb ratios and shows the majority of metabasites from this study to be tholeiitic (Fig. 3-4b). Magma types determined by this method are shown on relevant graphs in this section.

Y, Ti, P, Nb, V and Sr are plotted against Zr (Fig. 3-5) because Zr varies systematically with such processes as fractional crystallisation and is relatively immobile with respect to such processes as metamorphism and hydrothermal alteration. P, Y, Nb, Ti, and V all increase with increasing Zr. This systematic variation with Zr indicates that these elements have not undergone significant mobilization. Sr shows no systematic variation with Zr suggesting that

Table 3-1: Analyses of metabasites from the Tararua Range.

Analysis	(1)	(2)	(3)	(4)	(5)	(6)	(7)	(8)	(9)	(10)
Sample	17242	17241	17248	17254	17252	17243	17245	17246	17244	17255
Major oxides (wt%)										
SiO ₂	33.15	49.11	56.42	39.35	40.52	43.65	44.59	44.89	45.17	47.05
TiO ₂	1.91	2.83	2.98	3.06	2.05	2.30	2.81	4.56	3.43	2.53
Al ₂ O ₃	9.15	17.51	13.35	14.04	13.21	16.45	15.60	13.90	13.62	15.59
Fe ₂ O ₃	5.82	11.91	7.42	6.89	9.65	2.63	4.15	5.42	1.77	2.94
FeO	1.24	0.91	2.76	4.79	1.60	5.66	7.26	9.14	9.22	7.88
MnO	0.09	0.11	0.50	0.16	0.17	0.14	0.13	0.24	0.18	0.12
MgO	2.55	1.42	2.02	3.69	2.14	2.69	6.03	5.60	4.48	4.64
CaO	22.79	2.42	4.50	12.92	13.08	12.44	9.24	5.38	9.22	8.33
Na ₂ O	3.89	5.21	5.99	3.94	5.07	4.07	3.72	4.53	3.84	4.37
K ₂ O	0.45	2.68	0.04	0.46	1.26	0.62	0.25	0.06	0.06	0.04
P ₂ O ₅	0.47	1.01	0.65	0.29	0.31	0.42	0.26	0.51	0.38	0.22
Loss	18.39	4.66	3.21	10.13	11.03	8.71	5.76	5.44	8.24	5.74
Total	99.90	99.78	99.84	99.72	100.09	99.78	99.80	99.67	99.76	99.45
Fe ₂ O ₃ ^T	7.20	12.93	10.49	12.22	11.43	8.92	12.22	15.58	12.19	11.70
Trace elements (ppm)										
Ba	111	697	57	103	211	125	111	139	153	89
Ce	39	49	70	38	39	42	37	67	39	29
Cr	134	51	84	90	31	199	61	10	73	163
Cu	37	52	23	58	18	28	36	59	33	68
Ga	8	27	15	23	16	22	22	29	24	22
La	13	25	23	25	9	15	12	27	14	7
Nb	20	31	45	19	15	32	18	39	23	12
Ni	69	60	59	96	39	80	90	26	47	62
Pb	<2	2	13	3	<2	<2	<2	<2	<2	3
Rb	14	105	<2	17	44	23	3	<2	<2	<2
Sc	21	35	19	28	34	33	25	32	29	34
Sr	400	721	201	365	565	215	334	221	264	228
Th	2	4	5	<2	<2	3	<2	3	<2	<2
U	<2	<2	<2	<2	<2	<2	<2	<2	<2	<2
V	164	208	220	275	257	285	245	379	341	299
Y	21	57	35	36	32	40	33	43	42	30
Zn	79	215	147	121	107	116	88	118	132	106
Zr	156	201	329	204	139	198	186	285	245	156

1-3 alkaline

4-10 tholeiitic

Figure 3-4a: Determination of magma type using Y/Nb ratio

(after Pearce & Cann 1973).

$Y/Nb < 1$ = alkaline

Y/Nb 1-2 = transitional

$Y/Nb > 2$ = tholeiitic

O.I.B = Ocean Island Basalt

O.F.B = Ocean Floor Basalt

Figure 3-4b: Determination of magma type, of metabasites from the
Tararua Range, using a five element discriminant function
(Ti, P, Nb, Y and Zr) from Grapes and Palmer (1984).

$$Df = -0.2163TiO_2 + 7.2431P_2O_5 + 0.0196Nb - 0.1047Y + 0.0019Zr - 0.8983$$

Df positive = alkaline

Df negative = tholeiitic

No transitional magma type by definition.

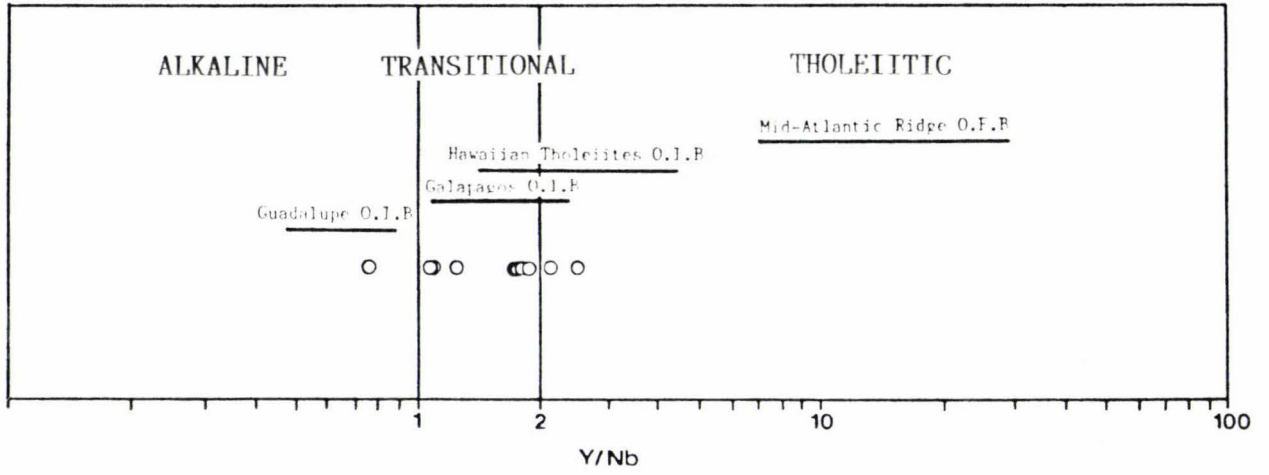
Colours represent magma type determined by the Y/Nb ratio.

● alkaline

● transitional

● tholeiitic

a



b

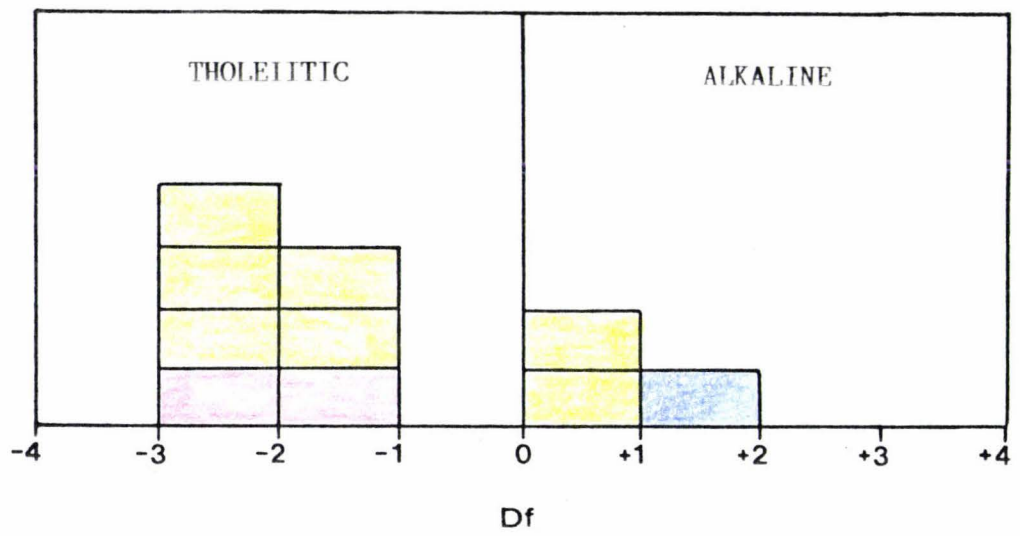


Figure 3-4

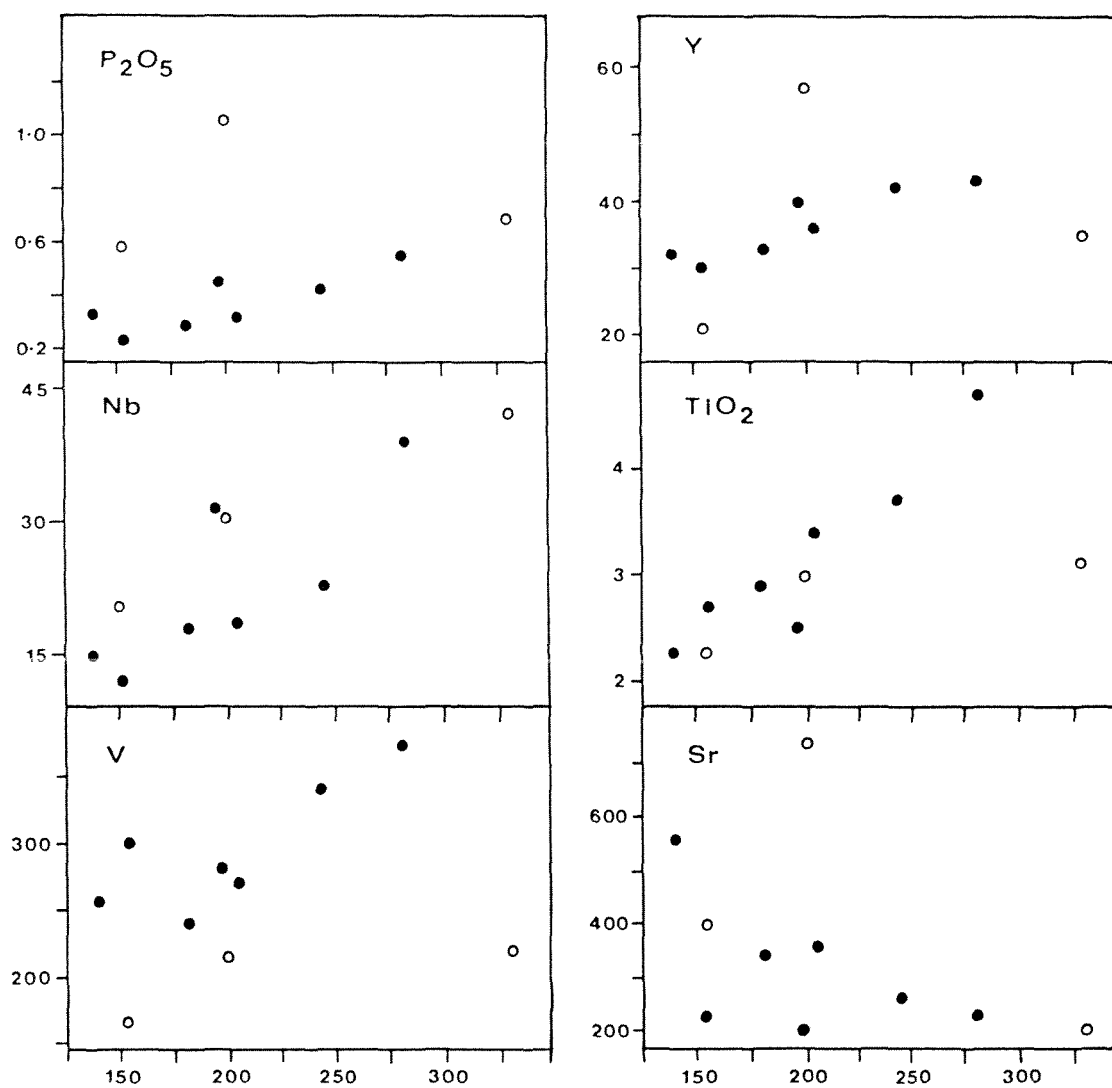


Figure 3-5: Harker diagrams with Tararua Range metabasites plotted.

Symbols

● tholeiitic basalts

○ alkaline basalts

Data from Table 3-1

significant mobilization of this element possibly has occurred. On most plots in Figure 3-5 the alkaline basalts do not fall on the trend defined by the tholeiitic basalts and correlations are enhanced by their removal. This feature is also evident in the data of Roser (1983) where the Torlesse alkaline basalts from the Wellington region plot consistently off the tholeiitic trend.

On a Ti-Zr-Y diagram, Pearce and Cann (1973) discriminate the following magma types or tectonic settings: intra-plate basalts (IPB); ocean-floor basalts (OFB = mid-ocean ridge basalts); island arc low-potassium tholeiites (LKT); and calc-alkaline basalts (CAB). Most of the Tararua Range metabasites plot in the IPB field with minimal scatter into the CAB and OFB fields (Fig. 3-6a). The Ti-Sr-Zr discriminant, also used by Pearce and Cann (1973), is not used in this study as Sr mobilization is indicated in Figure 3-5.

On a Ti-Zr plot (Fig. 3-6b) none of the Tararua Range metabasites plot within the discriminant fields of Pearce and Cann (1973) which supports an intra-plate eruptive environment. On a Zr/Y-Zr diagram the following discriminant fields were defined by Pearce and Norry (1979): intra-plate basalts (IPB); mid-ocean ridge basalts (MORB = OFB); and island arc basalts. Metabasites from the Tararua Range plot almost exclusively within the IPB field (Fig. 3-7). Only one metabasite (17241), an alkaline basalt, plots within the discriminant fields of OFB on both Ti-Zr-Y and Zr/Y-Zr diagrams. On both plots, this sample falls close to the field boundary between OFB and IPB, and as indicated by high Ti and Zr values has a strong affinity with IPB's.

Ti-V ratios (Shervais 1982) can be used to characterise certain types of basaltic magma and hence their tectonic setting. Both MORB and continental flood basalts have Ti-V ratios of about 20-50 whereas

Figure 3-6a: Ti-Zr-Y discriminant plot after Pearce and Cann (1973).

Discriminant fields

Fields A + B = low K tholeiites (LKT)

Field B = ocean floor basalts (OFB)

Fields B + C = calc-alkaline basalts (CAB)

Field D = intraplate basalts (IPB)

Symbols

● alkaline basalts

● tholeiitic basalts

Figure 3-6b: Ti-Zr discriminant plot, after Pearce and Cann (1973).

Discriminant Fields

A + B = low-potassium tholeiites (LKT)

B + C = calc-alkaline basalts (CAB)

B + D = ocean floor basalts (OFB)

Symbols

● alkaline basalts

● tholeiitic basalts

Note, three metabasites plot off this diagram.

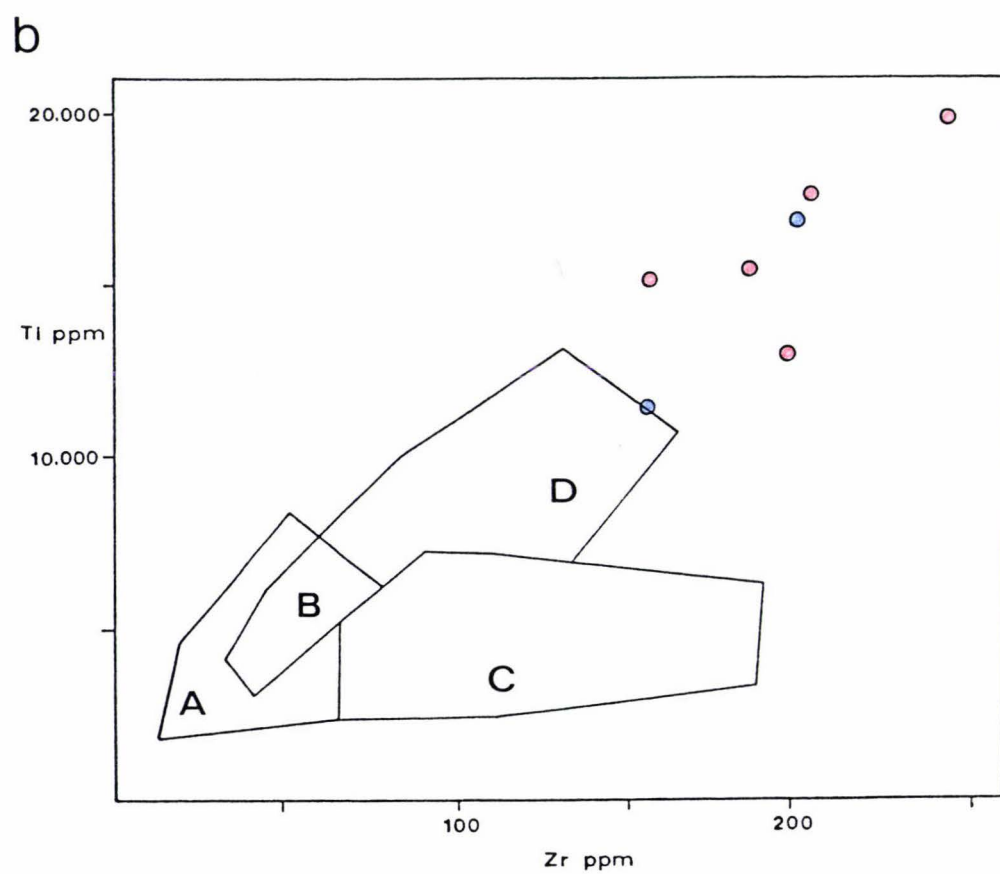
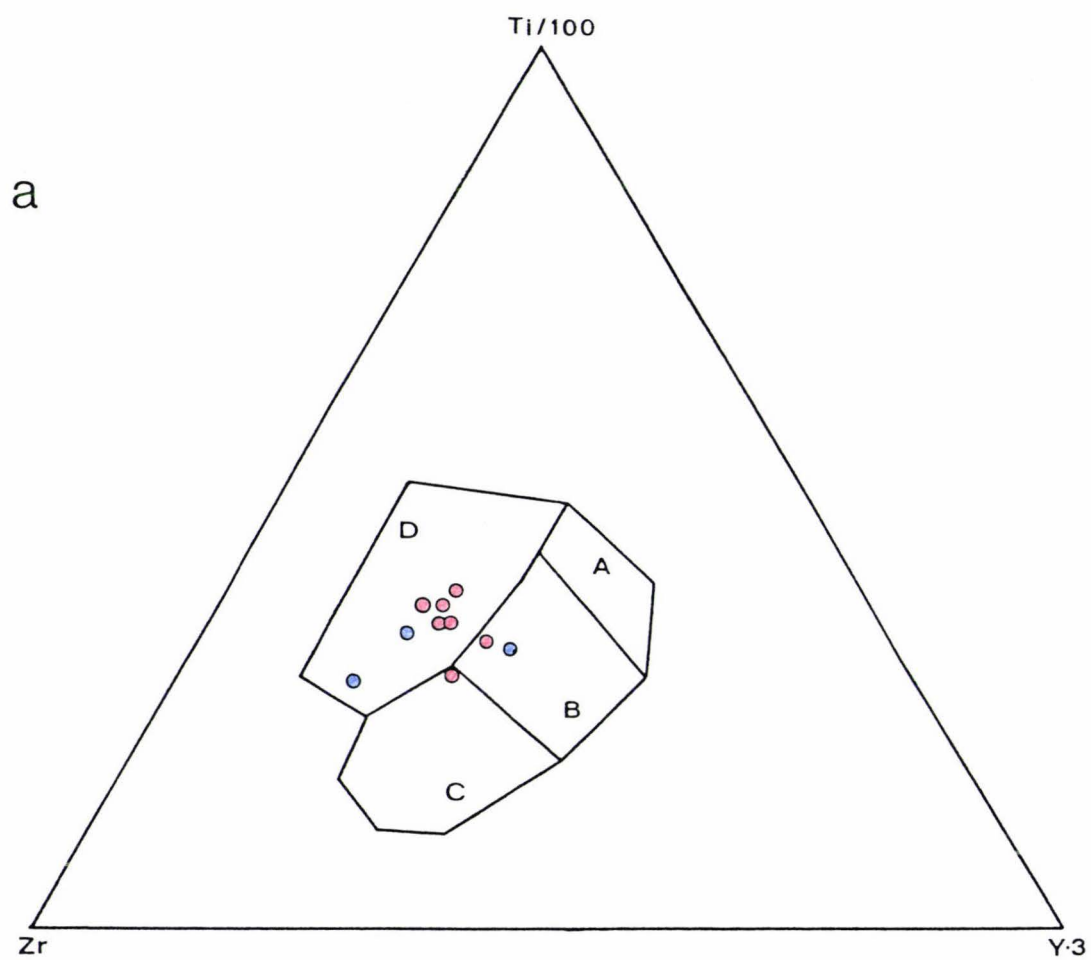


Figure 3-6

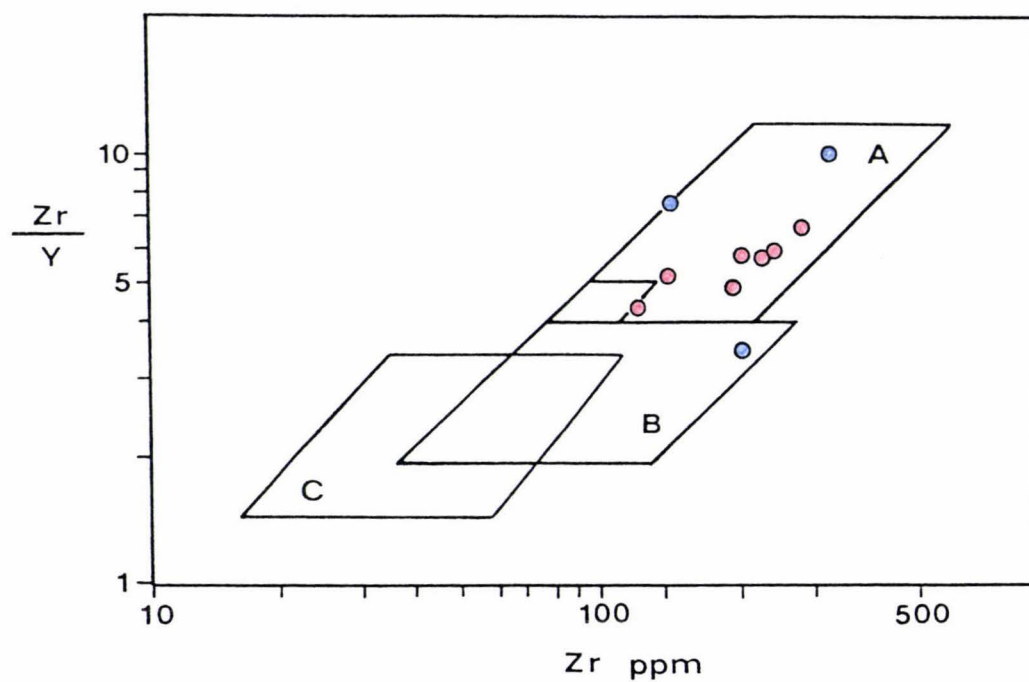


Figure 3-7: Zr/Y - Zr discriminant plot, after Pearce and Norry (1979).

A = intraplate basalts

B = mid-ocean ridge basalts

C = island arc basalts

Symbols

● alkaline basalts

● tholeiitic basalts

Table 3-2: Representative clinopyroxene analyses.

	17246	17255	17256	17270
SiO ₂	49.17	50.79	42.56	49.39
Al ₂ O ₃	3.65	2.62	7.93	3.35
TiO ₂	1.73	0.91	4.97	1.70
*FeO	8.30	7.59	10.30	10.07
MnO	0.13	0.20	0.15	0.30
MgO	14.28	15.88	10.65	14.20
CaO	21.28	21.26	21.77	20.54
Na ₂ O	0.36	0.26	0.59	0.40
Cr ₂ O ₃		0.22		
Total	98.90	99.73	99.15	99.95

* Total Fe as FeO

alkaline basalts have Ti/V generally greater than 50. Tararua Range tholeiites (Fig. 3-8) have Ti/V that range from 44 to 67 while the alkaline basalts have Ti/V ratios between 67 and 80.

Clinopyroxene composition has been shown to be a successful tool in the discrimination of basaltic magma types and as such provides a useful adjunct to the trace element discriminants used above (Nisbet & Pearce 1977). Only three metabasite outcrops were found to contain clinopyroxenes suitable for microprobe analysis. Samples from these outcrops were analysed for major and trace elements and determined to be tholeiitic, and they plot within IPB fields on the discriminant plots used above. Clinopyroxene compositions in samples 17255 (bulk chemistry sample 17255) and 17256 (bulk chemistry sample 17252) were determined from two different metabasites in the Tauherenikau Gorge (G.R. S26C/ 0283 1308), and samples 17270 and 17246 from a single outcrop in the Waiohine River (G.R. S26D/ 1132 2153, bulk chemistry sample 17246). Representative clinopyroxene analyses are listed in Table 3-2.

Clinopyroxene data from the Tararua metabasites have been plotted on a ternary $\text{TiO}_2\text{-MnO-Na}_2\text{O}$ diagram (Fig. 3-9a) and a discriminant F1-F2 plot (Fig. 3-9b), from Nisbet and Pearce (1977). Magma types differentiated on these plots are: ocean-floor basalts (OFB = MORB), volcanic arc basalts (VAB = LKT+CAB), within-plate tholeiitic basalts (WPT) and within-plate alkaline basalts (WPA; WPT+WPA = IPB).

While data from sample 17255 are inconclusive, data from sample 17256 plot exclusively as WPA in both plots which supports the intraplate setting determined from trace element data. Data from the Waiohine samples are inconclusive and form a field that approximates to

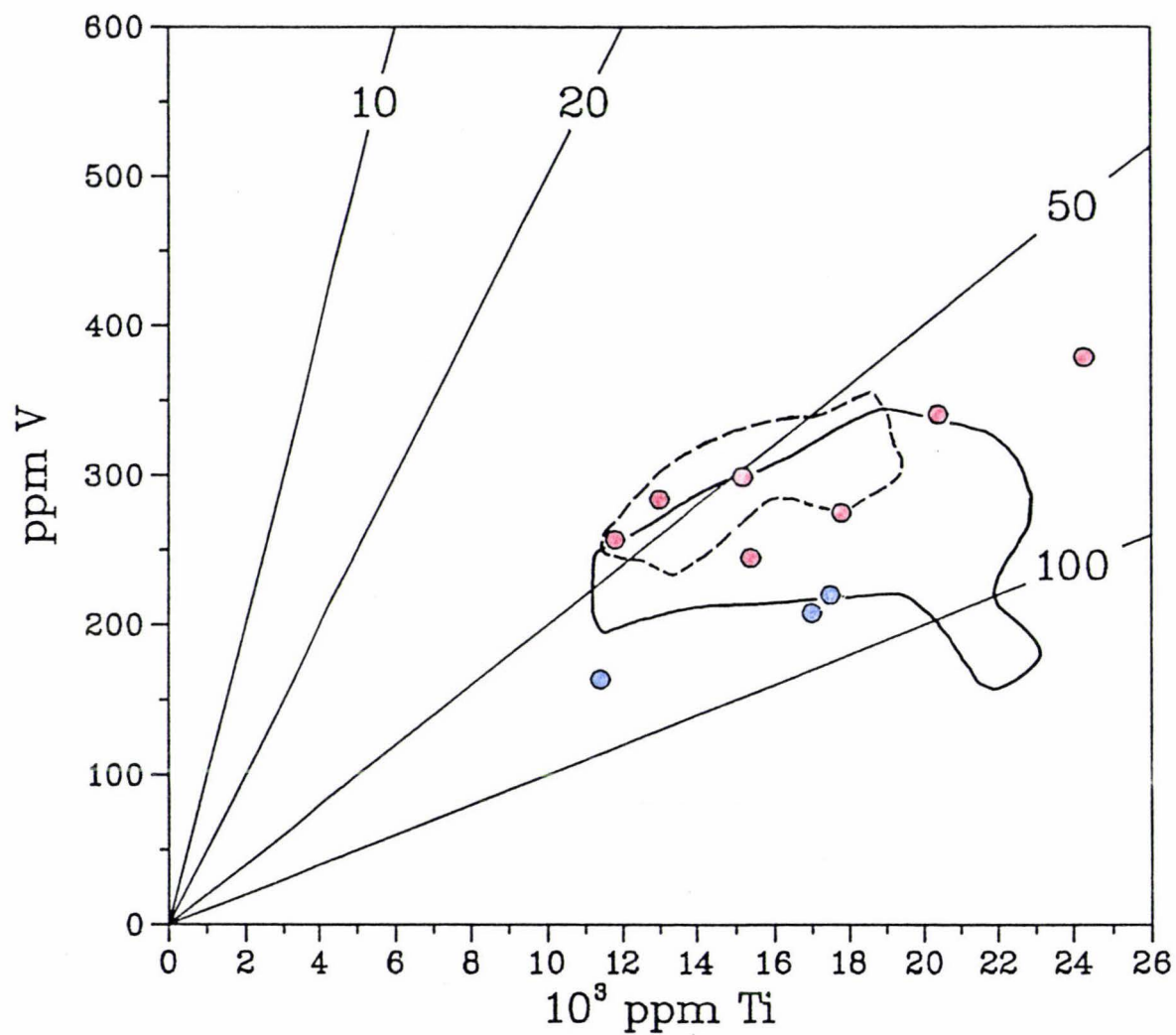




Figure 3-8: Ti-V discriminant plot of metabasites from the Tararua Range
(after Shervais 1982).

Trend lines 10, 20, 50 and 100 are Ti/V ratios

Fields

-  Hawaiian tholeiitic basalts
-  Hawaiian alkaline basalts

Symbols



-  alkaline basalts
-  tholeiitic basalts

Figure 3-9a: TiO_2 - MnO - Na_2O diagram with discriminant fields from Nisbet & Pearce (1977) and Tararua Range data plotted.

Key to fields

A = VAB

B = OFB

C = WPA

D = ALL

E = VAB + WPT + WPA

F = VAB + WPA

G = WPA

Symbols

- | | | |
|---|--------------|----------------------|
| ● | sample 17256 |] Tauherenikau Gorge |
| ○ | sample 17255 | |
| □ | sample 17270 |] Waiohine River |
| ■ | sample 17246 | |

Figure 3-9b: Plot of discriminant functions, F1 against F2 for clinopyroxene analysis from Tararua Range metabasites, after Nisbet and Pearce (1977).

- - - Field boundary of WPT data from Nisbet and Pearce (1977).

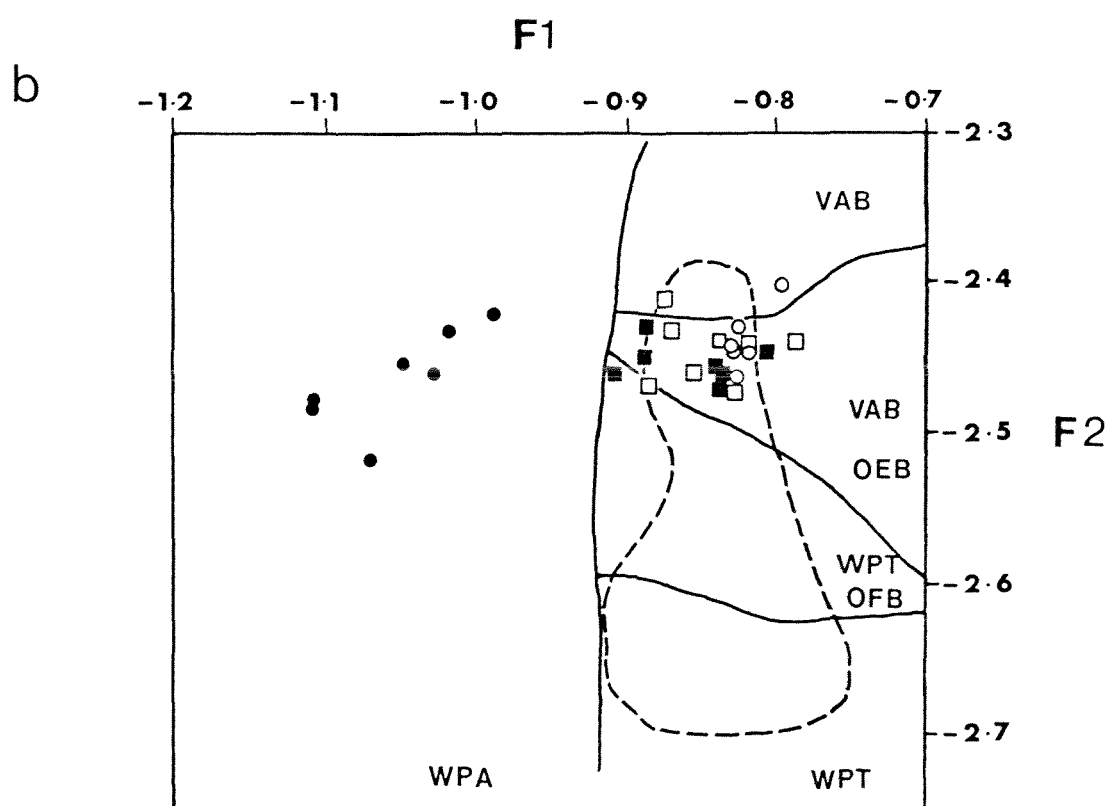
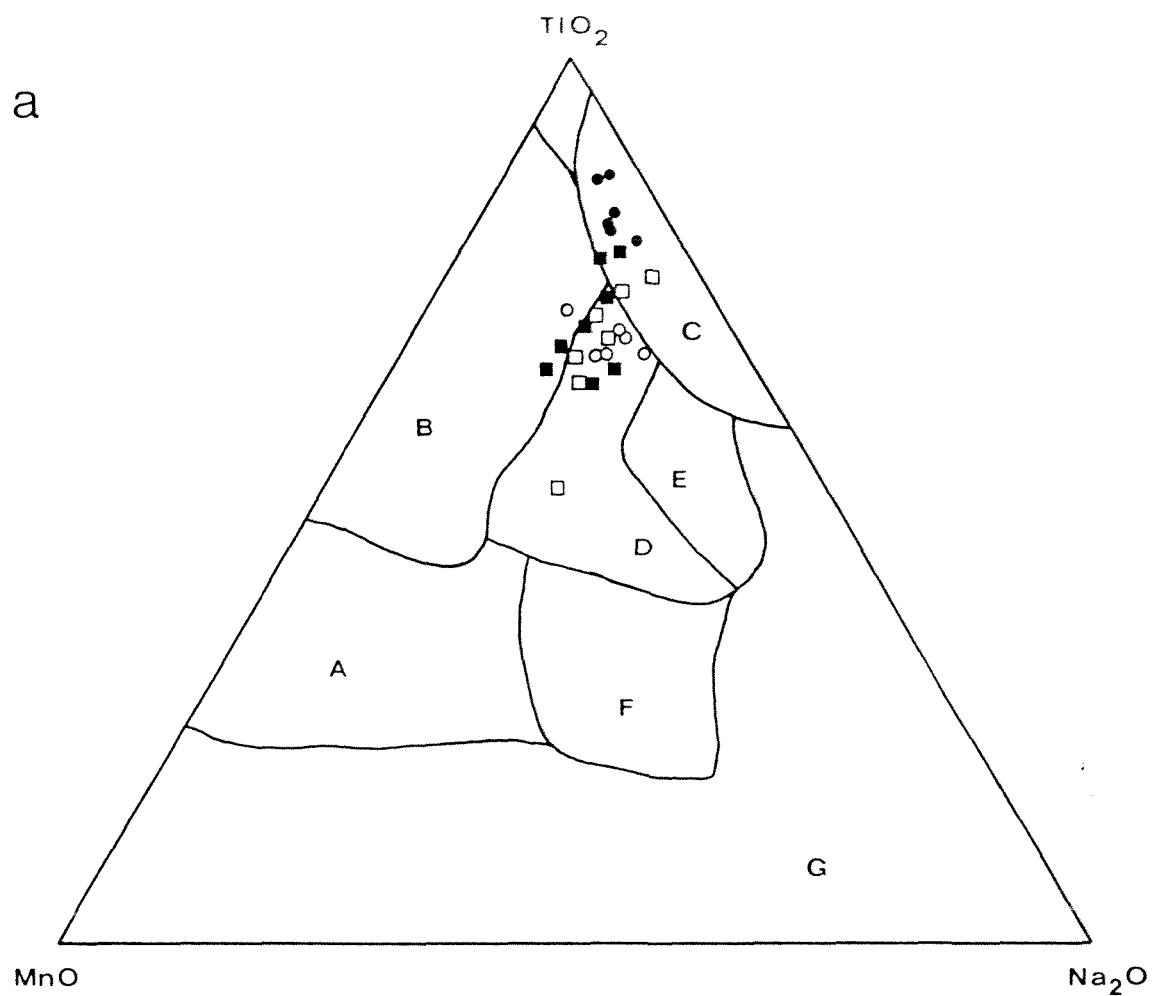


Figure 3-9

that of sample 17255. In conclusion all the metabasites used in this section have affinities with intraplate basalts and most are tholeiitic in composition.

3.3 GEOCHEMISTRY OF THE COLOURED ARGILLITE AND CHERT

The aim of this section is to compare the geochemistry of the red argillites and cherts with that of metabasites and black argillites, and to provide an interpretation of both their origin and environment of deposition.

3.3.1 Coloured Argillite

Three red argillites from the Tararua Range, two of which contained clasts of metabasite (17253,17251), were analysed for major oxides and trace elements (17239,17253,17251; Table 3-3). The three samples have significant differences in chemistry but have similarly high Fe-oxidation ratios (17239 52%; 17251 92%; 17253 69%) when compared with those of the black argillites (ie. from 4% to 14%).

Sample 17239 is very similar geochemically to the average composition of black argillite from the Tararua Range (Table 3-3), with only small discrepancies occurring between some major oxides ie. sample 17239 is relatively depleted in P_2O_5 , CaO, MgO and enriched in MnO. Samples 17251 and 17253 however are significantly enriched in TiO_2 , MnO, Na_2O , Fe_2O_3 , Ba, Ce, Cu, Nb, Ni, Zn and depleted in Al_2O_3 , K_2O , P_2O_5 , Cr, Rb and V. Values for TiO_2 , K_2O , Na_2O and Nb lie between those of the average black argillite and average metabasite from the Tararua Range.

The presence of calcite veining in sample 17253 makes direct comparisons of element abundance difficult but the geochemistry is more similar to that of sample 17251 than sample 17239.

Both the geochemistry and the presence of basalt fragments suggests samples 17253 and 17251 contain a significant basaltic component. To give an indication of the basaltic component present, models using the parameters Fe/Ti and $Al/(Al + Fe + Mn)$ (Bostrom 1970,

Table 3-3: Comparison of average metabasite and black argillite compositions with that of red argillite.

	Average black argillite	Red argillite			Average metabasite
		17239	17251	17253	
Major oxides (wt%)					
SiO ₂	56.79	59.41	61.36	42.76	47.97
TiO ₂	0.92	0.83	1.21	2.84	3.07
Al ₂ O ₃	19.84	18.80	15.61	12.43	15.39
Fe ₂ O ₃	0.63	3.72	7.51	12.72	5.86
FeO	5.49	3.00	0.57	5.10	5.06
MnO	0.05	0.07	0.39	0.40	0.19
MgO	2.21	1.95	1.63	3.81	3.81
CaO	1.21	0.61	1.56	8.06	11.18
Na ₂ O	2.03	2.10	3.01	4.04	4.84
K ₂ O	4.55	4.37	3.33	0.15	0.64
P ₂ O ₅	0.43	0.20	0.23	0.34	0.48
Loss	5.58	4.45	3.55	7.05	8.13
	-----	-----	-----	-----	-----
Total	99.74	99.51	99.96	99.70	99.78
Fe ₂ O ₃ T	6.73	7.05	8.14	18.39	12.40
Trace elements (ppm)					
Ba	470	477	855	210	179
Ce	77	67	120	49	45
Cr	85	74	41	44	90
Cu	26	28	47	77	41
Ga	27	25	26	22	21
La	39	32	49	9	17
Nb	15	14	24	12	25
Ni	26	26	86	60	63
Pb	24	15	30	<2	3
Rb	223	240	167	3	21
Sc	16	16	19	46	29
Sr	167	167	170	254	351
Th	17	17	15	<2	3
U	3	2	3	<2	2
V	162	163	139	520	267
Y	37	33	47	85	37
Zn	130	125	178	205	123
Zr	186	140	216	202	210

1973) are used. The ratios used by Bostrom were based on the assumption that Al and Ti in pelagic sediments is primarily of detrital origin, whereas Fe and Mn may be enriched from various oceanic sources. On a Bostrom plot (Fig. 3-10) sample 17251 falls between the average basalt and average black argillite compositions at a point that indicates a 20 weight percent basaltic contribution to the mix. Sample 17251 also plots marginally towards the EPR end member which suggests the possibility that all three end members have contributed. Sample 17253 plots on the curve generated by the mixing of EPR sediment and the average metabasite (20% EPR; 80% metabasite).

Red, green and blue coloured argillites with similar compositions to samples 17251 and 17253 have been described mantling the Pacific Line Islands seamounts (Jenkyns & Hardy 1976). Like samples 17253 and 17251, these sediments are enriched in the elements that are considered to reflect a basaltic influence (eg. TiO_2 , Fe_2O_3). Jenkyns and Hardy interpret the Line Island coloured argillite as mainly the result of halmyrolic degradation of basalt. The geochemistry of metabasite from the Tararua Range suggest a seamount setting, that is, an intraplate setting. Samples 17251 and 17253 have a similar lithology and geochemistry to the Line Island argillites and therefore possibly the same setting.

Sample 17239 plots close to the average black argillite and slightly along a mixing curve between the average black argillite and the Al-Ti poor sediments from the East Pacific Rise. The Al-Ti poor sediments are enriched in Fe, Mn and many trace elements, and are precipitates of elements leached by hydrothermal circulation at spreading ridges. Besides forming metalliferous accumulations at ridge crests, much of this material is dispersed by ocean currents. This

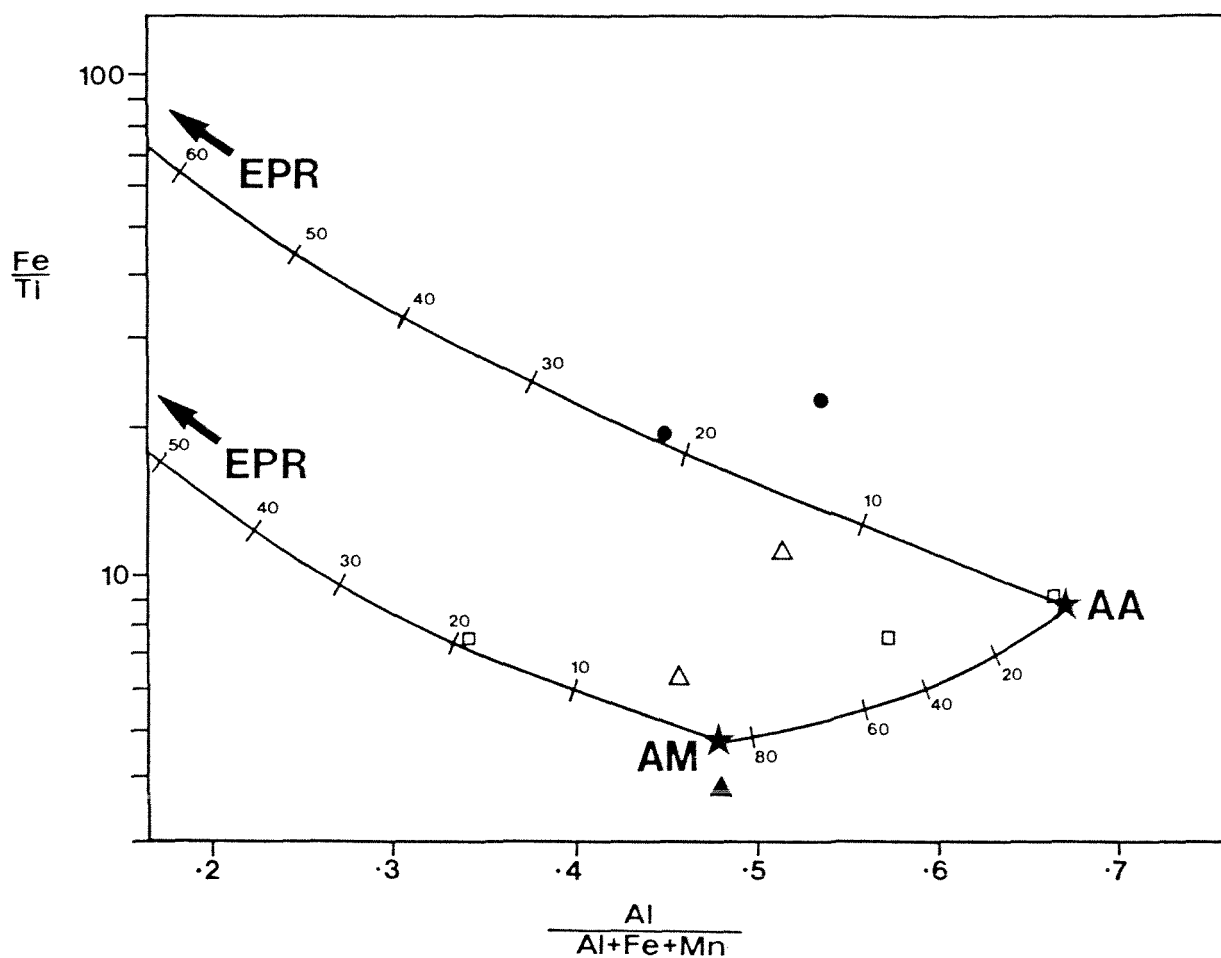


Figure 3-10: Mixing curves between average Tararua black argillite (AA), average Tararua metabasite (AM) and active spreading ridge sediment (EPR from Bostrom 1973). Numbers refer to weight percent contribution to the mix.

Symbols

- red argillite (Table 3-3)
- chert (Table 3-4)
- △ interpillow material (Appendix VIII)
- ▲ intensely sheared metabasite (Appendix VIII)

End Members

- AA average argillite (from Table 2-5, analyses 1-7)
- AM average metabasite (from Table 3-1)
- EPR from Bostrom (1973)

material has been identified as a component in modern pelagic sediments several thousand kilometres away from active spreading ridges (eg. Bostrom et al., 1969). Such a source may account for the slight modification of sample 17239 from an original black argillite composition and the EPR component noted for sample 17253. A second possible source of the Fe and Mn in these samples is hydrothermal systems associated with submarine volcanoes. Submarine hydrothermal spring deposits that, like the Al-Ti poor EPR sediments, are enriched in iron, manganese and various trace metals have been described from submarine volcanoes in the South Pacific (eg. Malahoff et al., 1982).

3.3.2 Chert

The presence of radiolaria skeletons and clay-sized detritus in thin section indicates a hemipelagic depositional environment for cherts from the Tararua Range. Contributions from terrigenous, biogenic, hydrothermal and volcanic sediment sources may be reflected in the geochemistry of these cherts.

The geochemistry of two cherts from the Tararua Range (17247, 17271) was obtained by XRF analysis (Table 3-4). Fe oxidation ratios of the cherts are high (76% and 79%) and are comparable to those of the red argillite described above. On a Bostrom plot the cherts plot near the mixing curve between the average black argillite and the Al-Ti poor EPR sediments (Fig. 3-10). A 15 to 22 weight percent contribution by EPR sediments is indicated, which is significantly more than indicated for the red argillites.

An $\text{SiO}_2\text{-SiO}_2/\text{Al}_2\text{O}_3$ plot (after Cressman 1962) shows that the chert samples plot on a mixing curve generated by adding pure SiO_2 to the average black argillite (Fig. 3-11). This and the presence of

Table 3-4: Analyses of chert from the Tararua Range.

	17247	17271
Major oxides (wt%)		
SiO ₂	93.31	88.61
TiO ₂	0.06	0.18
Al ₂ O ₃	2.07	3.54
Fe ₂ O ₃	0.92	2.43
FeO	0.25	0.57
MnO	0.17	0.16
MgO	0.32	0.39
CaO	0.77	0.89
Na ₂ O	0.07	0.75
K ₂ O	0.34	0.61
P ₂ O ₅	0.00	0.02
Loss	1.51	1.53
Total	99.79	99.68
Fe ₂ O ₃ T	1.20	3.07
Trace elements (ppm)		
Ba	1005	115
Ce	29	18
Cr	3	8
Cu	48	19
Ga	4	5
La	6	10
Nb	<2	<2
Ni	41	7
Pb	13	13
Rb	15	30
Sc	4	6
Sr	69	50
Th	2	5
U	<2	<2
V	18	24
Y	7	11
Zn	43	28
Zr	19	46

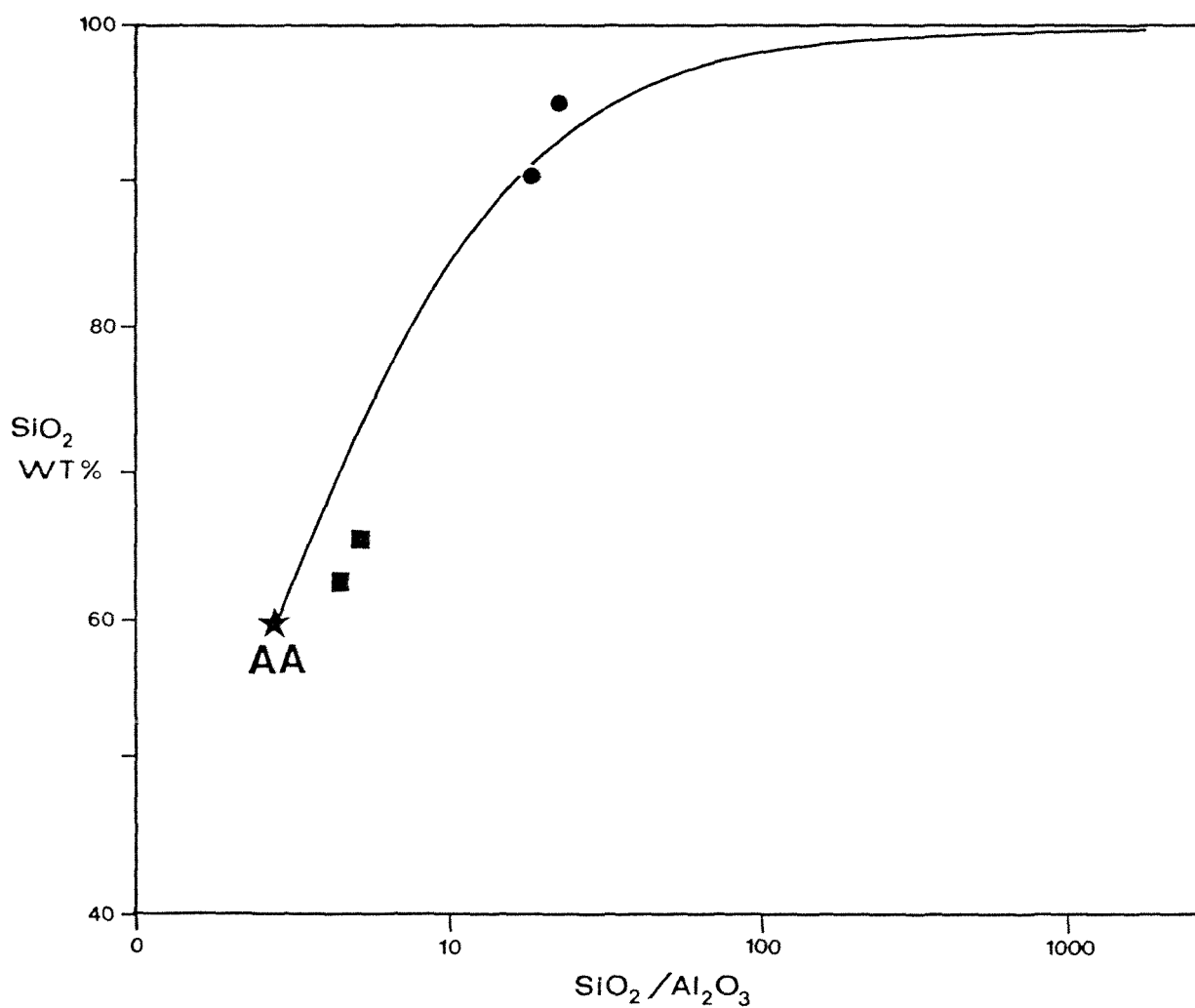


Figure 3-11: SiO₂ - SiO₂/Al₂O₃ plot (after Cressman 1962).

The curve from AA describes the compositional change produced by addition of SiO₂ to average black argillite from the Tararua Range.

Symbols

- chert
- red argillite

Data from Table 2-5. Note sample 17253 is not plotted due to the presence of calcite veining.

radiolaria suggests a mostly biogenous source for the excess SiO_2 . In the case of a substantial hydrothermal input, significant displacements from this curve will occur (Roser 1983). The red argillites also plot close to this curve which indicates a similar source for their excess SiO_2 and gives further support to the concept of a compositional continuum between the coloured argillites and cherts (as indicated by petrographic data, see section 3.1.3).

CHAPTER FOUR

METAMORPHISM

In this chapter the metamorphic minerals that occur in rocks of both the volcanic and sedimentary associations are described and an interpretation of the metamorphic grade is provided. The following metamorphic minerals are recognised in the various rock types: quartz, albite, chlorite, pumpellyite, sphene, epidote and sericite.

Quartz

Quartz occurs most commonly as a vein mineral in rocks of both associations. Veins are generally between 0.5mm and 1.6mm thick and consist of polycrystalline quartz with a grain size that ranges from 0.04mm to 0.3mm. In rocks where quartz veining is intense, patches of relatively fine grained (generally around 0.04mm or less) polycrystalline quartz are common in areas close to quartz veins (eg. 17216).

Calcite

Calcite occurs in rocks of both associations, typically as a vein mineral. Vein calcite is often associated with quartz and is commonly the earlier phase (ie. calcite occurs within quartz). Complex veining was observed in several samples with as many as three generations being apparent (see below). In more intensely veined sandstones, calcite replaces quartz, plagioclase and matrix material (eg. 17263). In metabasite, besides being a common vein mineral, calcite fills amygdules (eg. 17242) and sometimes replaces large portions of the more intensely veined samples (eg. 17257).

Plagioclase

Albitization of detrital plagioclase in sandstones is accompanied by alteration to sericite and epidote. Plagioclase

varies in composition from $An_{3.5} Ab_{95.3} Or_{1.2}$ to $An_{29.7} Ab_{69.5} Or_{0.8}$.

This variation in composition is due to the presence of both relic detrital and metamorphic grains.

Plagioclase in metabasite is altered to sericite, epidote, chlorite and sphene. Alteration of this type suggests albitization.

Sphene

Sphene occurs in both red and green metabasites and is more abundant in intensely sheared and veined samples (eg. 17288). Sphene ranges from light-brown to colourless in thin-section and most commonly occurs as anhedral grains of various sizes (eg. 17260, 17216). Sphene also occurs within calcite filled amygdules and veins (eg. 17257). Two small grains of fibrous sphene (average size 0.08mm by 0.05mm) were found in the groundmass of sample 17256; microprobe analyses (Table 4-1) showed both to be an Al-rich variety ($Al_2O_3 = 8.4\%$, FeO as Fe total = 1.8%).

Plagioclase in the metabasite sample 17255 often enclose a high Al-sphene ($Al_2O_3 = 8.3\%$, FeO as total Fe = 3.47%). Ti-magnetite in metabasite sample 17246 is partially altered to sphene with up to 4.3% Al_2O_3 and FeO (as total Fe) of 3.34%. Analyses of sphene are plotted on an Al-Ti-Fe diagram (Fig. 4-1) and compared with fields of sphenes from zeolite and pumpellyite-actinolite facies (ZPA) and from eclogites and granulites (EG). The Tararua Range sphenes show a range in compositions with the Al-poor sphenes falling close to the ZPA field. Kawachi *et al.* (1983) suggest that less (Al,Fe)-rich sphenes form at higher temperatures. This suggests that the Tararua Range sphenes were produced at relatively low temperatures.

Chlorite

Chlorite was observed in most rock types, being most abundant in

Table 4-1: Microprobe analyses of sphenes within metabasite from the
Tararua Range.

	1	17255 2	3	17246 4	5	17256 6	7
SiO ₂	31.94	31.78	32.23	29.50	32.34	30.74	31.79
Al ₂ O ₃	8.89	8.32	6.69	4.30	8.34	8.20	8.41
TiO ₂	24.71	25.30	27.79	31.00	23.81	24.30	23.50
*Fe ₂ O ₃	2.54	3.74	2.29	3.71	1.49	1.99	2.02
MgO	0.24	0.69	0.20				0.05
CaO	27.62	26.21	25.70	26.37	27.11	27.71	28.71
Na ₂ O				0.10	0.66		
Total	95.94	96.04	94.90	94.98	93.75	92.94	94.48

* Total Fe as Fe₂O₃.

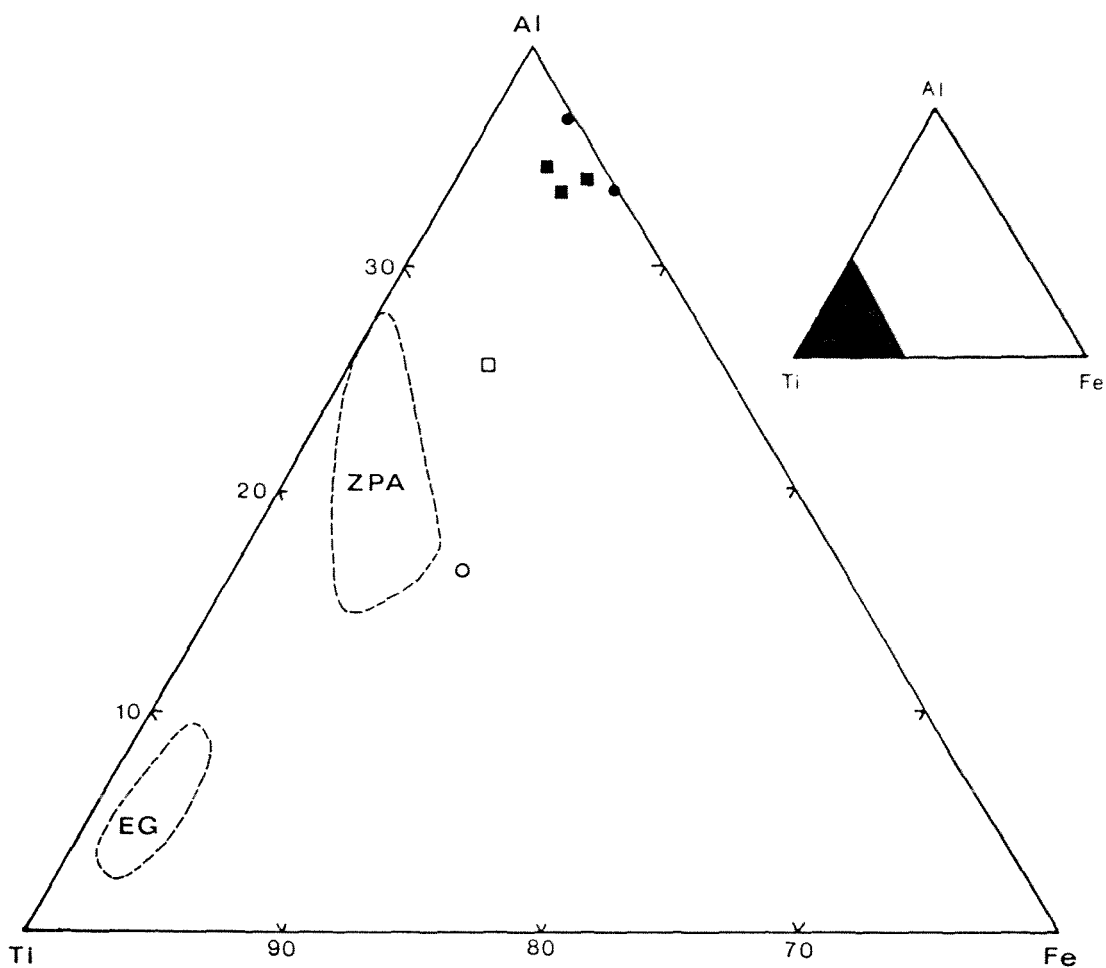


Figure 4-1: Al-Ti-Fe plot of analysed sphenes within metabasite from the Tararua Range.

Symbols

- sphene within plagioclase (Analysis 1 & 2, Table 4-1)
- sphene within Ti-magnetite (Analysis 4, Table 4-1)
- sphene within mesostasis (Analysis 3, Table 4-1)
- fibrous sphene within mesostasis (Analysis 5, 6 & 7, Table 4-1)

Fields

ZPA = sphenes from zeolite and pumpellyite-actinolite facies
(Boles & Coombs 1977; Coombs et al. 1976)

EG = sphenes from eclogites and granulites (Ernst & Dal Piaz 1978; Oliver 1976)

Table 4-2: Microprobe analyses of chlorites from the Tararua Range.

	METABASITE								
	17270			17255					
SiO ₂	28.90	30.44	25.86	27.40	27.41	28.11	26.23	27.22	
TiO ₂		0.23	0.08						
Al ₂ O ₃	15.03	14.51	14.17	16.25	16.13	14.37	15.48	15.77	
* FeO	28.85	26.06	26.99	27.89	27.68	31.41	29.65	27.95	
MnO	0.39	0.37	0.31	0.38	0.38	0.20	0.35	0.35	
MgO	13.15	13.90	12.09	13.48	13.37	11.95	12.74	11.81	
CaO	0.29	2.12	0.37	0.26	0.26	0.52	0.35	0.53	
K ₂ O				0.10	0.10				
Total	86.61	87.63	79.87	85.66	85.33	86.56	84.80	83.63	

	SANDSTONE		
	17211		
	green	red-brown	
SiO ₂	27.12	26.95	28.73
TiO ₂	0.07	0.65	1.28
Al ₂ O ₃	18.28	17.10	18.26
* FeO	26.48	28.16	29.50
MnO	0.33	0.27	0.30
MgO	13.28	11.89	8.62
CaO	0.05	0.10	0.12
K ₂ O	0.06	0.29	1.94
Total	85.67	85.41	88.75

* Total Fe as FeO

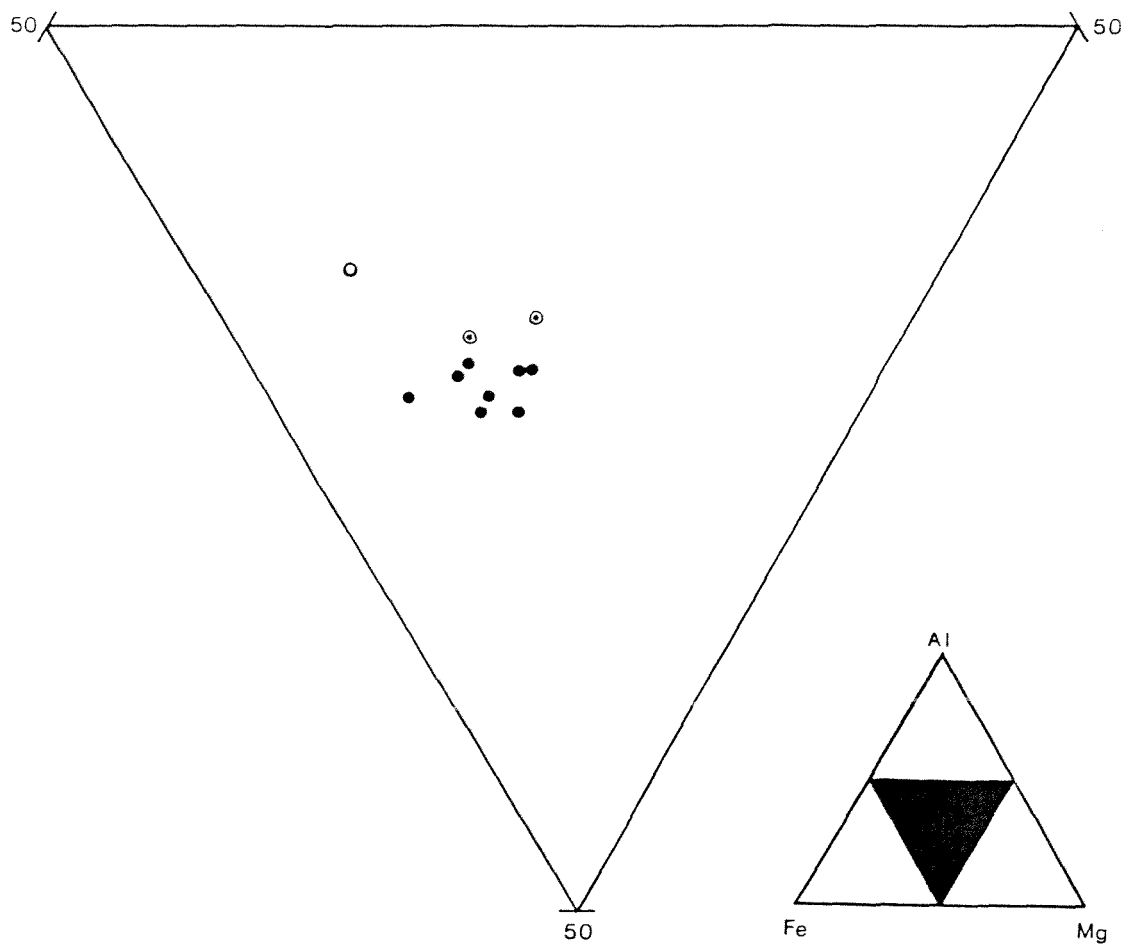


Figure 4-2: Al-Fe-Mg plot of analysed chlorites from the Tararua Range.

Symbols

- ⊙ green Ti-poor chlorite (sandstone 17211)
- red-brown chlorite (sandstone 17211)
- metabasite chlorite (17270,17255)

Data from Table 4-2.

metabasite. In the rocks of the sedimentary association chlorite occurred as an alteration product after detrital biotite (eg. 17209, 17218, 17221) and as a matrix constituent. Two light green chlorites (one being an altered portion of a biotite grain) were probed in sample 17210; both had low TiO_2 values relative to red-brown chlorite after biotite (Table 4-1). Both red-brown and pale green chlorites are pyrochlorites (Hey 1954).

In metabasite, chlorite has anomolous blue interference colours and occurs as a vein mineral (eg. 17258, 17249), as angular interstitial masses in the coarser grained metabasites (eg. 17260, 17262), in the groundmass of sheared and variolitic metabasites (eg. 17264, 17287) and as colloform masses in amygdules (eg. 17254, 17288). Chlorite is commonly associated with calcite in both veins and amygdules. Chlorite was also found associated with calcite veining in chert (eg. 17286) and coloured argillite (eg. 17258).

Analyses of metabasite chlorites (samples 17255 & 17290) are listed in Table 4-2; and are pyrochorite, diabantite and brunsvigite varieties (Hey 1954). All chlorite analyses are plotted on an Al-Fe-Mg diagram in Figure 4-3 which indicates that, for a given grade, host-rock composition is the major control of chlorite composition.

Pumpellyite

Pumpellyite was found in three specimens (17259, 17244, 17265) of intensely-sheared green metabasite.

Pumpellyite was observed in vein quartz as fine acicular grains (less than 0.09mm in length), pseudomorphing olivine and clinopyroxene (17244) and as finely crystalline aggregates (17259). The pumpellyite has strong dark green to light green pleochroism, indicating an Fe-rich variety (Coombs 1953). Several grains in sample 17259 showed colour

Table 4-3: Microprobe analyses of pumpellyite from the Tararua Range.

PUMPELLYITE 17265				
SiO ₂	37.19	36.21	36.02	36.42
Al ₂ O ₃	21.34	20.31	19.41	19.86
* FeO	9.77	11.10	11.39	11.71
MnO	0.24	0.18	0.15	0.25
MgO	1.92	1.60	1.77	1.75
CaO	21.82	22.13	22.00	22.08
	-----	-----	-----	-----
Total	92.28	91.53	90.74	92.07

* Total Fe as FeO

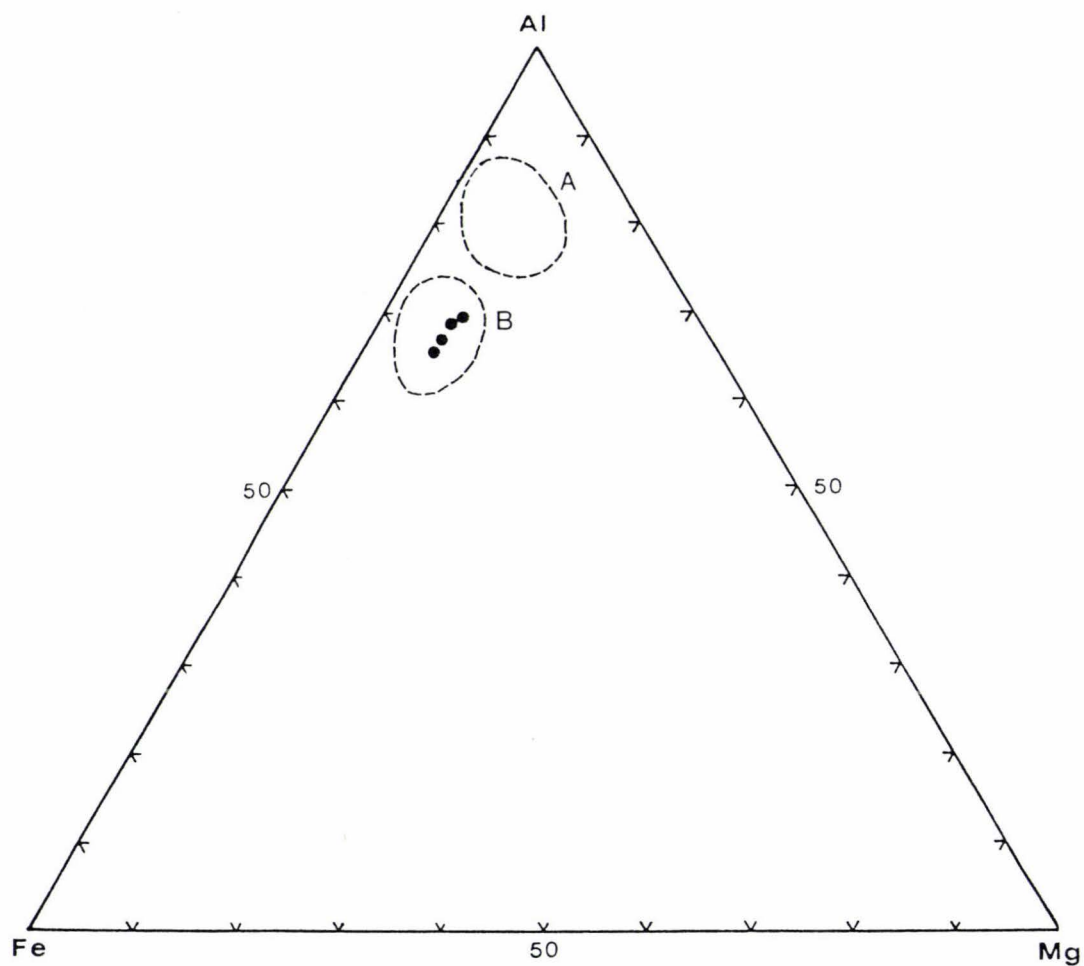


Figure 4-3: Al-Fe-Mg plot for analysed pumpellyites from the Tararua Range.

Fields (from Kawachi 1975)

- A. Upper Wakatipu Zone III
- B. Upper Wakatipu Zone I and II

Data from Table 4-3.

zoning indicating compositional zoning. The pumpellyite was probed in sample 17265 (Table 4-3) and found to be essentially homogeneous (ie. FeO as Fe total ranged from 9.77wt%-11.71wt%).

On an Al-Fe-Mg diagram (Fig. 4-3) the metabasite pumpellyite plots in the field of Kawachi's (1975) Upper Wakatipu Zones I and II which is characterized by Fe-rich pumpellyites that correspond closely in composition with those from other very low grade terranes (eg. prehnite-pumpellyite facies, Tanzawa Mountain, Japan; Seki et al. 1969). Pumpellyites of Kawachi's higher grade Zone III are more Al-rich. Generally, it has been observed that iron-rich pumpellyites occur in rocks of the zeolite and prehnite-pumpellyite facies and the aluminous varieties in the higher pressure pumpellyite-actinolite and blueschist facies (Coombs 1976). More recently, Offler et al. (1981) have shown a wide range in composition of pumpellyite in rocks of similar metamorphic grade, indicating that pumpellyite compositions should be used with caution when determining metamorphic conditions.

4.1 VEIN MINERAL SUMMARY

Quartz and calcite are by far the most abundant vein minerals with quartz + calcite as the most common vein mineral assemblage where quartz is typically the earlier phase (ie. calcite within quartz). Other minerals that occur as vein minerals are, sphene and chlorite, which both occur as late phases within calcite veins, and pumpellyite and chlorite, which occur within quartz veins. Chlorite also occurs as veinlets in both metabasite and chert. Two or three generations of vein minerals were observed in several samples. The most complex veining observed was that in sample 17286, a red chert; a brief summary of which is as follows: 1) quartz veining; 2) chlorite veining; 3) quartz + calcite veining (calcite within quartz); 4) quartz veining. In

intensely sheared samples, veins both cut and are cut by shear zones suggesting both occurred concurrently, at least in part.

METAMORPHIC GRADE

The highest minimum temperature of formation of the above mentioned minerals is that of pumpellyite, which is between 190°C and 200°C (Boles & Coombs 1977). Pumpellyite, which was only observed in metabasite is diagnostic of the Prehnite-Pumpellyite Facies of Coombs (1960).

CHAPTER FIVE

STRUCTURE

This chapter describes the structures observed in the study area and presents an interpretation of the deformational events which produced them. The description of the structures is divided into two sections. The first section describes mesoscopic structures observed in outcrop. The second section describes macroscopic structures that are too large to be observed in outcrop, but can be inferred to be present.

5.1 MESOSCOPIC STRUCTURE

5.1.1 Folds

Mesoscopic folds are not common in the field area, only being observed at nine locations (Table 5-1). Folds occur in well-preserved, alternating sandstone and argillite beds as well as disrupted units (Fig. 5-1). Folds commonly show thickening in the hinge region and thinning in the limbs. Axial surface orientations of folds in outcrop at G.R. S26D/ 1047 2288 indicate the presence of two fold generations. The basis for these generations, and the significance of the axial surface orientations is discussed in the section on geometric analysis below.

5.1.2 Faults

Faults at a low angle to bedding

Faults at a low angle to bedding are common throughout most of the field area. These faults cause offsets that are parallel or subparallel to bedding. The amount of offset produced by "low angle " faults ranges from a few centimetres to larger than outcrop scale. In outcrop, the intensity of low angle faulting can vary considerably. In many outcrops the low-angle faulting alone was intense enough to reduce the more competent sandstone beds to lozenge-shaped blocks and produce

Table 5-1: Mesoscopic fold data.

Reference number	Grid reference	Lithology folded: disruption*/bed thickness	Fold axis: azimuth/plunge	Axial surface: strike/dip	Interlimb angle	Fold type
1	S26D/ 1049 2293	1 / medium bedded	064/15	078/77N	open	antiform
2	S26D/ 1049 2293	1 / medium bedded	066/22	066/22NW	gentle	synform
3	S26D/ 1049 2293	1 / medium bedded	093/28	-	gentle	synform
4	S26D/ 1049 2293	1 / medium bedded	050/14	-	open	synform
5	S26D/ 1047 2288	1+2 / thin bedded	288/66	112/60SE	gentle	synformal anticline
6	S26D/ 1047 2288	2 / thin bedded	278/58	112/65SE	open	antiformal syncline
7	S26D/ 1047 2288	2 / thin bedded	050/35	048/85SE	close	antiformal syncline
8	S26D/ 1047 2288	2 / thin bedded	229/49	046/78SE	open	synformal anticline
9	S26D/ 1047 2288	2 / thin bedded	230/53	083/70S	open	antiformal syncline
10	S26D/ 1047 2288	1+2 / thin bedded	254/52	092/74S	gentle	antiformal syncline
11	S26C/ 0125 1590	2 / medium bedded	241/60	-	close	antiform
12	S26C/ 0130 1584	3 / thin bedded	051/72	-	close	antiform
13	S26C/ 0130 1584	3 / thin bedded	003/72	-	close	synform
14	S26C/ 0285 1629	1 / thin bedded	161/60	-	close	synform
15	S26C/ 0473 1873	2 / thin bedded	221/62	-	close	synform
16	S26C/ 0275 1615	2 / medium bedded	044/64	-	close	antiform
17	S26C/ 0366 1311	2 / thick bedded	153/38	-	open	syncline
18	S26D/ 1103 2230	1 / thin bedded	039/72	040/84NW	close	synform

* Disruption type, see section 5.2.2



a weakly-defined foliation within the less competent argillite. The juxtaposition of rocks of the sedimentary and volcanic associations often resulted from low-angle faults.

Even in outcrops where low-angle faults are relatively weakly-developed, surfaces between argillite and sandstone beds are commonly sheared and sandstone beds wedge out along anastomosing low-angle fault planes.

Faults at a high angle to bedding

Faults at a high angle to bedding also occur (Fig. 5-2a) throughout the field area. The amount of offsets along such faults were, in most cases indeterminable, as also was the sense of movement. However, dextral and sinistral offsets both occur, and measured offsets range from a few millimetres to several metres, although amounts well in excess of outcrop scale must occur also.

In many outcrops high angle faults offset low angle faults. However, the faults cannot be separated into early and late stages because the pattern is complex, suggesting more than one phase for each, or that both have occurred simultaneously. In outcrop, both types of faults appear to have been folded as well as being cut by "young" faults with crush and pug zones.

5.1.3 Cleavage

A weakly defined, spaced cleavage (Powell 1979) was observed in argillite at two locations, one in the Waiohine River (G.R. S26D/ 1048 2288) and one in the lower Tauherenikau Gorge (G.R. S26C/ 0277 1325). The possible cause of this cleavage is discussed below.

5.1.4 Lozenge fabric and mélanges

In outcrops where faulting is intense, faults at both high and low angles to bedding, have disrupted the bedding and produced a

Figure 5-2a: Thin bedded fine sandstone
and argillite with numerous faults at a
high angle to bedding.

Tauherenikau Gorge

pen 15 cm long

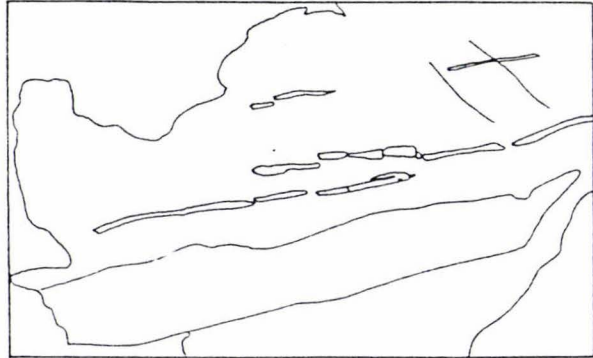
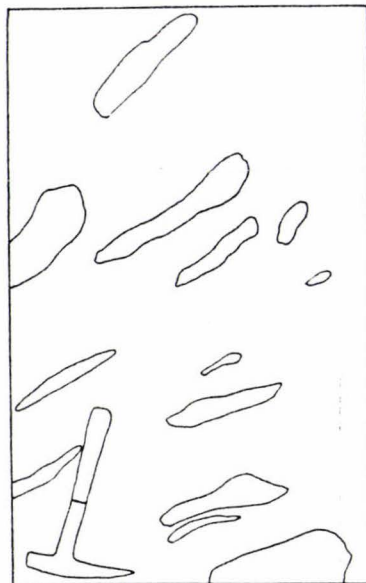
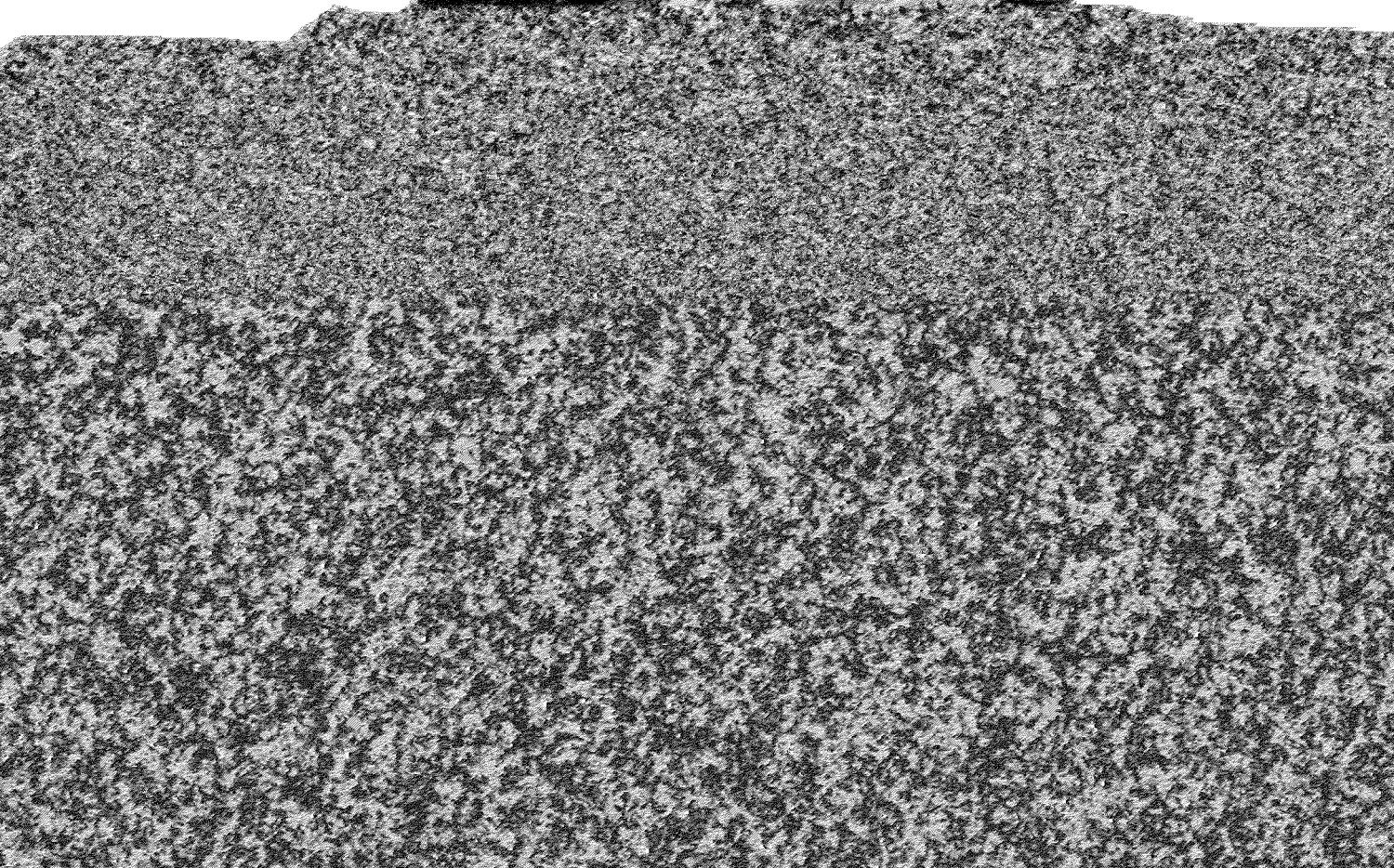
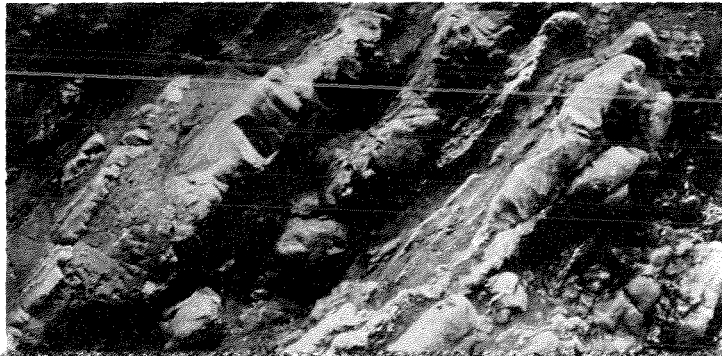
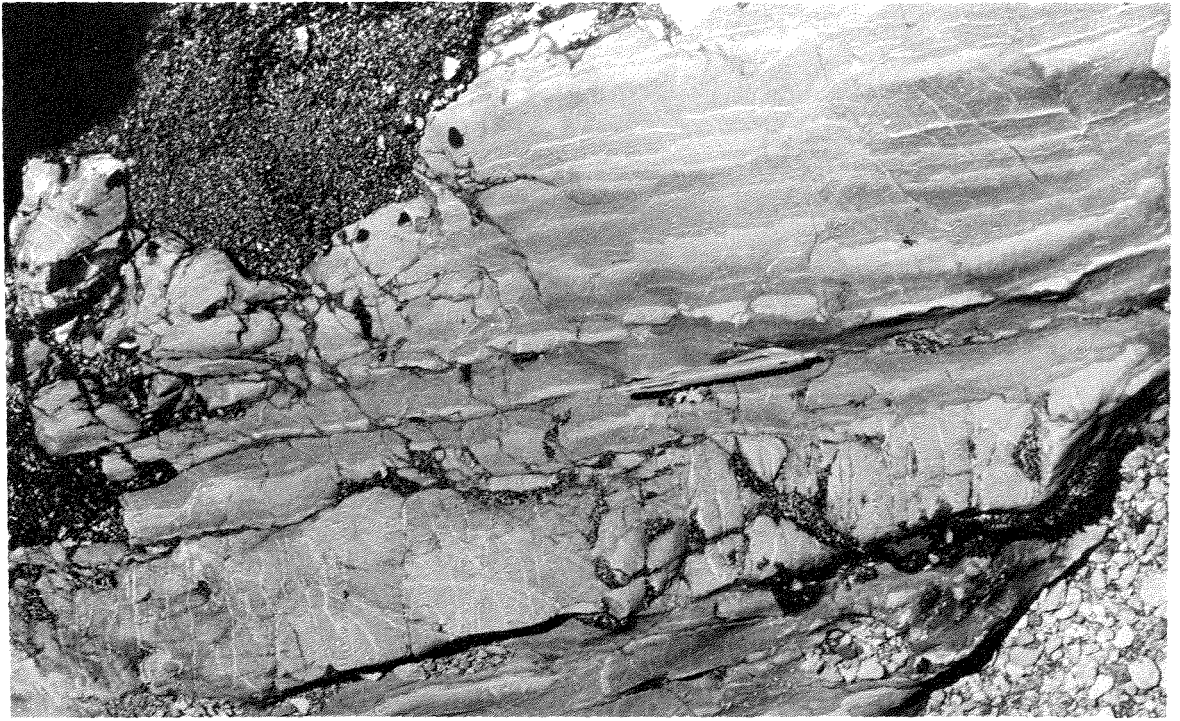


Figure 5-2b: Moderately disrupted thin
bedded sandstone and argillite.

Tauherenikau Gorge (see Fig. 5-8 for
location), geological hammer 31 cm long.





lozenge-fabric (Pettinga 1982). In the early stages of production of lozenge-fabric, high-angle faults (often as conjugate sets) offset the sandstone beds which are reduced to angular rhombic blocks (Fig. 5-2b). With increased bedding plane shear, these rhombic blocks become less angular (Fig. 3 & 4) and, in extreme cases, phacoid shaped (Fig. 5-5). A continuum occurs between well-preserved beds and outcrops that consist of rounded-sandstone phacoids in a sheared-argillite matrix. The degree to which beds are disrupted appears to be a function of the intensity of shearing coupled with the original lithology, that is, massive and thick-bedded sandstone units seem to be relatively resistant to disruption.

Units with different intensities of faulting and degree of lozenge-fabric development are often juxtaposed by steeply dipping faults (Fig. 5-6). Sometimes within highly-disrupted units, faults with a similar orientation to that of the shear foliation, juxtapose "packets" with slightly different shear foliation orientations. Even in outcrops that have suffered much faulting parallel to bedding, the shear foliation is essentially parallel to bedding. In units where bedding was not observed, the dip and strike of the faulted sandstone and argillite contacts were recorded. In outcrops where beds were completely disrupted the long axis of elongate phacoids was recorded. This information is used in the following section on geometric analysis.

In units of extreme disruption, lozenges and phacoids are commonly sandstone in composition although less common phacoids of the volcanic association were also observed. Phacoid sizes range from microscopic to blocks several hundred metres long and tens of metres wide (eg. metabasite block in upper Waiohine River; G.R. S26D/ 1050

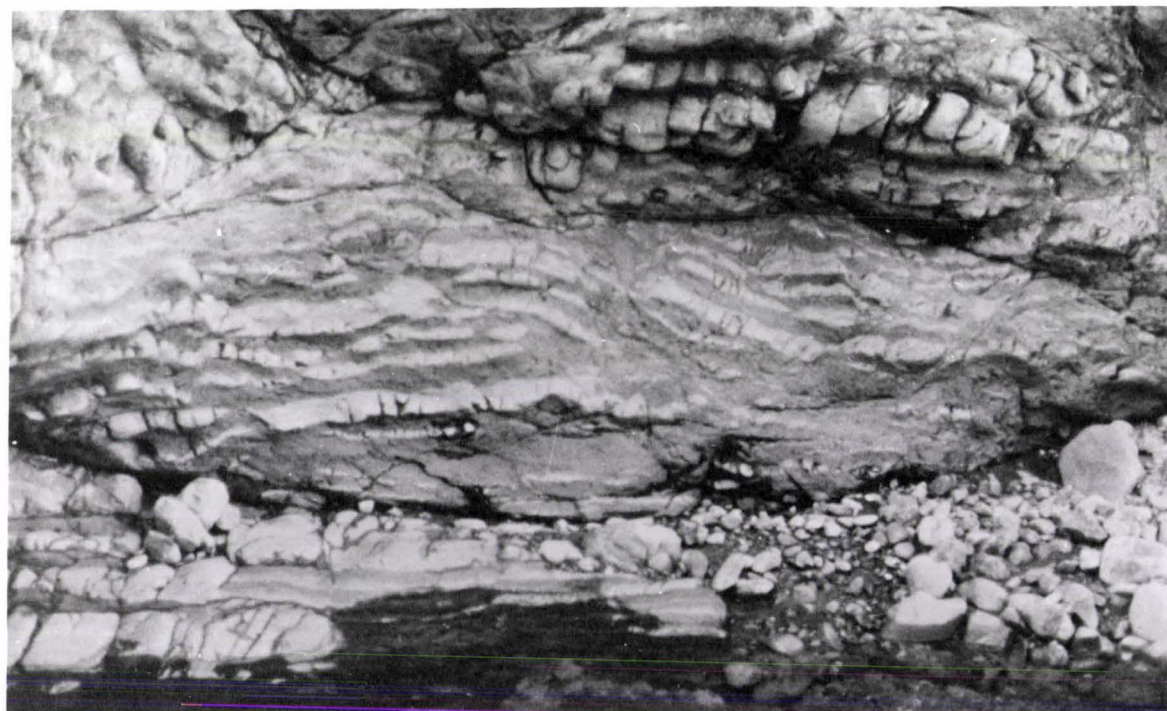


Figure 5-3a: Moderately disrupted medium bedded sandstone and argillite.

Tauherenikau Gorge (see Fig. 5-7 for location), field of view 6 metres across.

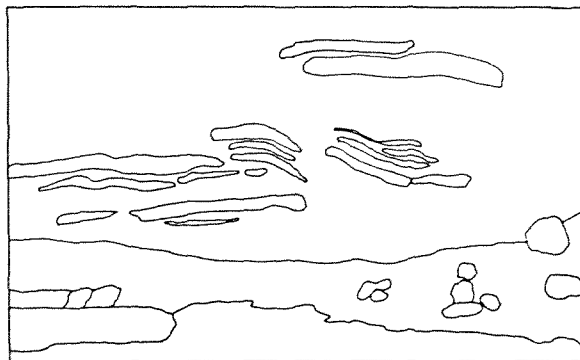


Figure 5-3b: Moderately disrupted thick bedded sandstone with minor argillite.

Tauherenikau Gorge (see Fig. 5-7 for location).

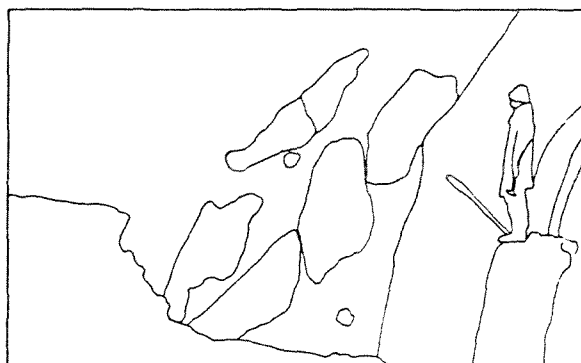


Figure 5-4a: Highly disrupted unit of sandstone (S) lozenges and phacoids and sheared black argillite.

Tauherenikau Gorge S26C/ 0273 1323,
geological hammer 31 cm long.

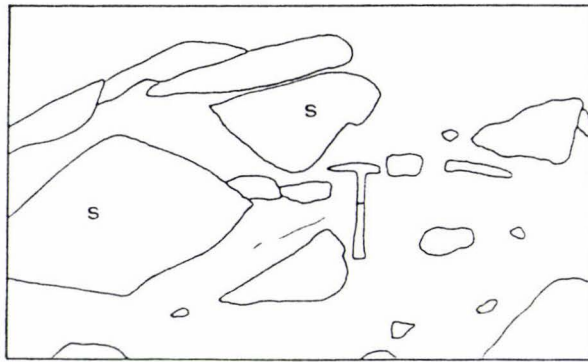
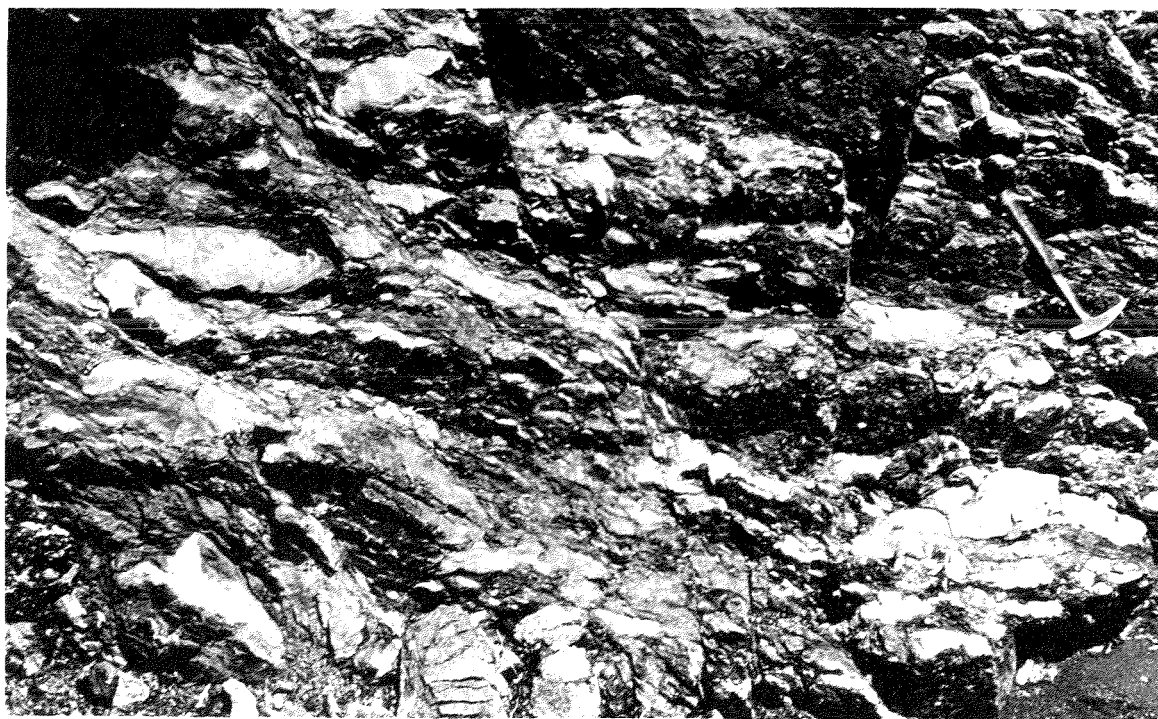


Figure 5-4b: Highly disrupted unit of elongate sandstone phacoids and sheared black argillite. Note faults (F) at a high angle to the shear foliation.

Waiohine River S26D/ 1057 2355,
geological hammer 31 cm long.





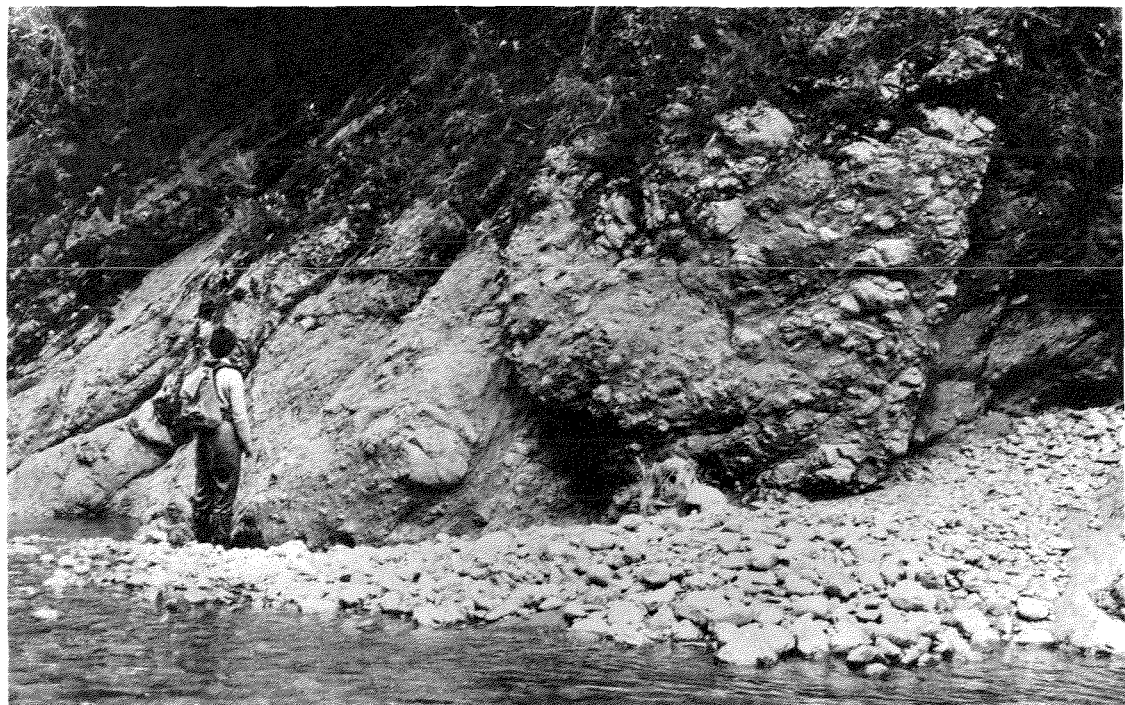


Figure 5-5a: Highly disrupted unit of sandstone phacoids and sheared black argillite.

Tauherenikau Gorge (see Fig. 5-8 for location), geological hammer 31 cm long.

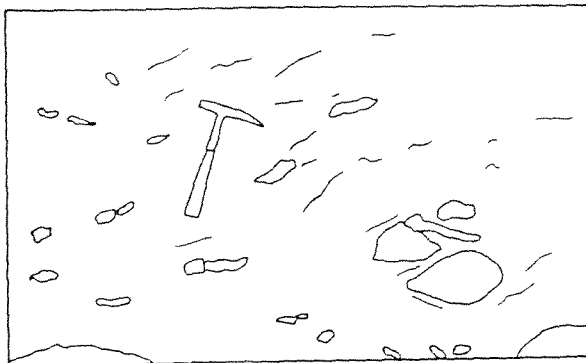


Figure 5-5b: Highly disrupted units in the Tauherenikau Gorge. Note fault (F) juxtaposes units with different phacoid sizes and matrix percentages (see Fig. 5-7 for location).

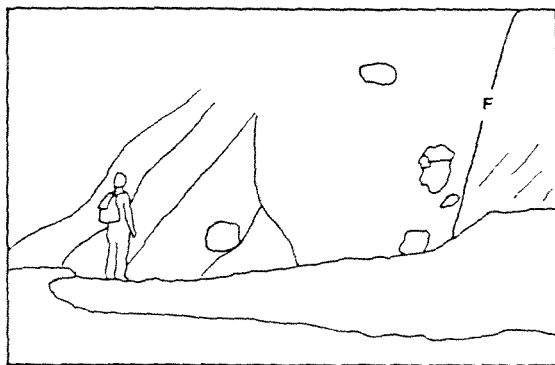


Figure 5-6a: Juxtaposition of a well preserved unit (S) and a highly disrupted unit, by a steeply dipping fault (F). Tauherenikau Gorge (see Fig. 5-7 for location)

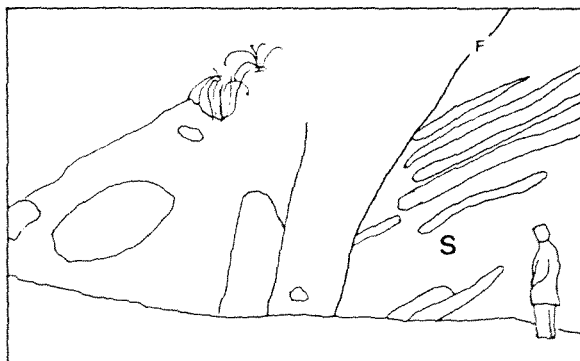
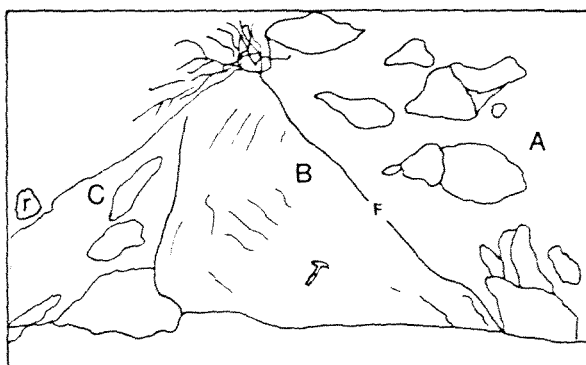
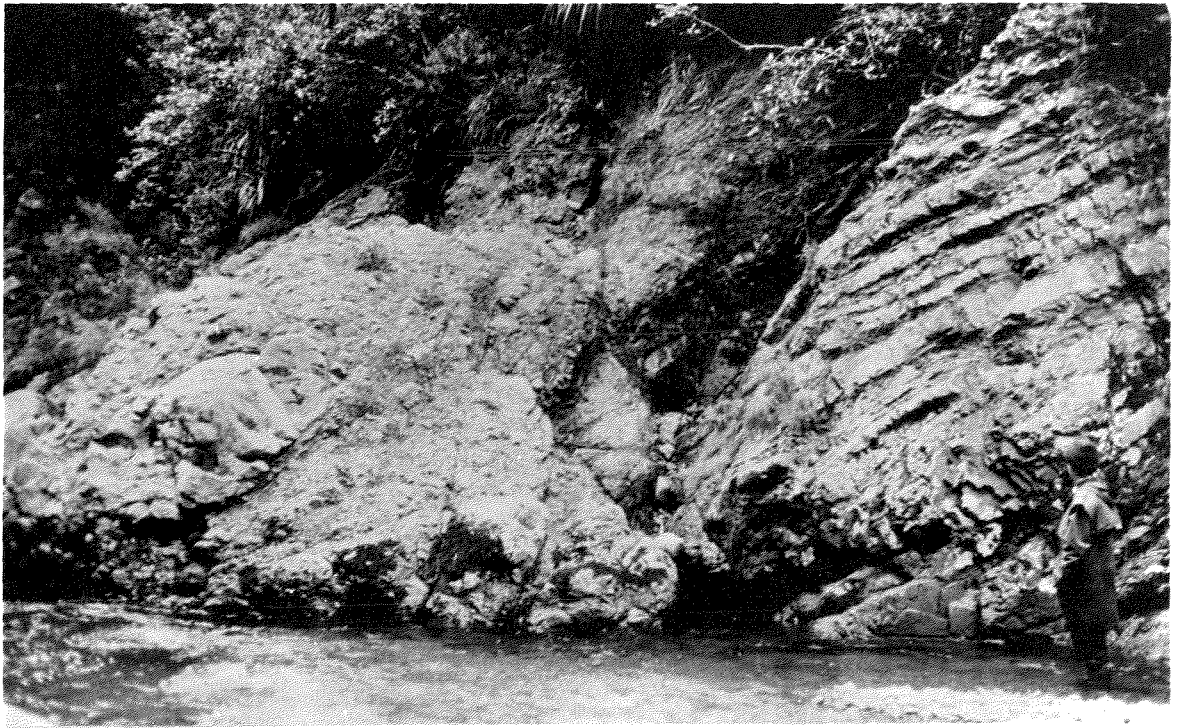


Figure 5-6b: Fault contact (F) between a highly disrupted unit (A) and a massive argillite unit (B). Unit C is an olistostrome and block R is the large microsparite block shown in Fig. 2-2b.

Tauherenikau Gorge (see Fig. 5-7 for location), geological hammer 31 cm long.





2320 which is at least 500m long by 80m wide).

The metabasite and associated deformed chaotic rock units at G.R. S26C/ 0283 1310 (at the confluence of "Campsite Creek" and the Tauherenikau River) have been mapped in some detail. This sequence is described below in order to illustrate the nature of such units that occur in the study area. Also included in this section is a detailed map of the olistostromes and mélanges at G.R. S26C/ 0255 1340 (Fig. 5-7).

Campsite Creek metabasite and associated units



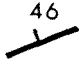
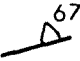

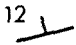
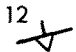


The sequence at Campsite Creek consists of three large metabasite slivers with interleaved units of intensely sheared and deformed sediments and volcanics. The various units show a dominant NE-SW trend, and contacts are generally faulted and dip steeply to the southeast. The following is a brief description, from south to north, of the units mapped in Figure 5-8:

Unit A consists of elongate lozenge-shaped sandstone clasts with variable but generally small amounts of sheared argillite matrix (average 25%). Remnants of bedding are discernible in several places. Clasts become more phacoid shaped and smaller towards unit B.

Unit B consists largely of sheared black argillite (70%) with minor amounts of moderately elongate phacoids of sandstone and green metabasite. Clasts show a crude alignment of long axes. The average clast size is 3cm by 4cm, and is much smaller than those observed in units A or C, the largest clast observed being 40cm by 25cm.

Unit C consists for the most part of lozenge to phacoid-shaped clasts of sandstone and sheared black argillite (30%). In a narrow zone close to the metabasite unit D, clasts and sheared

Figure 5-7: Detailed map of the olistostromes and mélanges at
G.R. S26C/ 0255 1340, Tauherenikau Gorge.

- KEY
-  Olistostrome with clasts of the sedimentary association
 -  Olistostrome with clasts of the sedimentary and volcanic associations
 -  Fault contact with dip
 -  Contact with dip
 -  Inferred or gradational contact
 -  Strike and dip of bedding
 -  Strike and dip of bedding with younging
 -  Strike and dip of shear foliation
 -  Strike and dip of shear foliation with younging

The variation in phacoid size and shape is shown diagrammatically

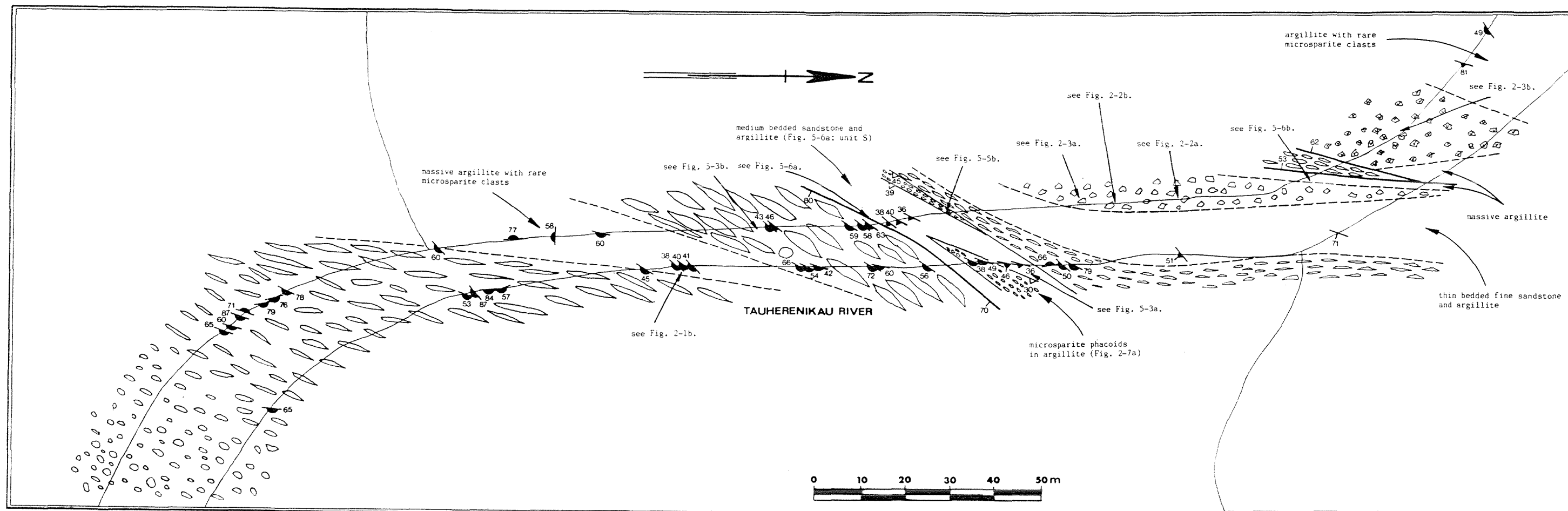


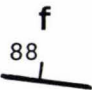



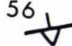





Figure 5-8: Map showing the metabasite and associated disrupted units at the confluence of "Campsite Creek" and the Tauherenikau River.

The variation in phacoid size and shape is shown diagrammatically.

KEY	
	Metabasite
	Coloured argillite
	Unit reference, see section 5.1.4
	Fault contact with dip
	inferred or gradational contact
	Strike and dip of bedding
	Strike and dip of bedding with younging
	Strike and dip of shear foliation
	Strike and dip of shear foliation with younging
	Strike and dip from phacoid

zones of green metabasite are common.

Unit D is massive red to blue-black amygdaloidal metabasite; the contact between units C and D is faulted and dips steeply to the southeast. A small angular sliver of sheared argillite with lozenges of fine sand has been faulted into this unit.

Unit E consists for the most part of equal amounts of elongate sandstone lozenges and sheared argillite. One 50cm thick sandstone bed was continuous for approximately 4 metres; such "beds" commonly show a pinch and swell type structure which is the result of offsets caused by faulting at a high angle to the shear foliation. It appears the originally undeformed unit had roughly equal amounts of sandstone and argillite, and the sandstone beds ranged in thickness from 2cm to 50cm.

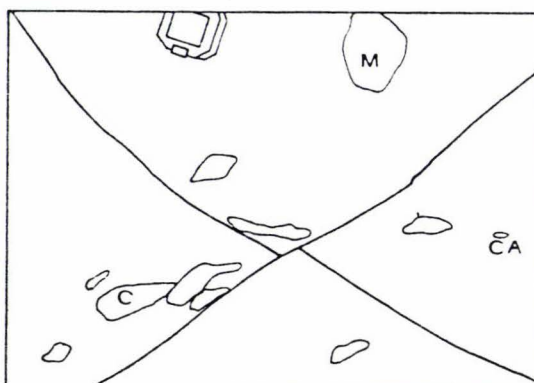
Unit F consists of lozenge and, less commonly, phacoid-shaped clasts of green metabasite (commonly amygdaloidal) and chert in a sheared, light to dark green argillite matrix (70 to 80%; Fig. 5-9). Clasts have an average size of 13cm by 7cm with long axis measurements that range from 2cm to 30cm. The fault contact between units E and F has a dip of 37° to the southeast.

Unit G is the largest of the three metabasite slivers and consists mainly of red amygdaloidal metabasite. Several possible metabasite pillows were noted in the central portion of this sliver; one pillow measured 60cm by 35cm by 35cm. Green metabasite occurs near the northern and southern margins. The northern margin consists of metre sized lozenges of red and green metabasite, the disruption of which becomes more intense towards the slivers margin. The F-G contact is a fault that dips to the southeast at 51°.

Unit H is a small sliver of intensely sheared and veined,



Figure 5-9: Highly disrupted unit of elongate lozenges and phacoids of green metabasite (M) and chert (C) within sheared green argillite (CA). Tauherenikau Gorge (see Fig. 5-8, unit F), Brunton compass 7 cm across.



massive fine grained sandstone that separates the metabasite units G and I. Both the northern and southern contact of this unit are faulted and dip steeply to the southeast.

Unit I consists of roughly equal amounts of red amygdaloidal metabasite and red argillite. Metabasite occurs as rounded and elongate clasts of various sizes which may possibly represent pillow lavas or be the result of disruption of once massive metabasite (Fig. 5-10a).

Unit J is separated from unit I by a fault that dips moderately steeply to the southeast. Unit J consists for the most part of sandstone clasts of various shapes set in sheared black argillite. A narrow zone of rocks close to unit I is intensely sheared and contains small slivers and phacoids of green metabasite (Fig. 5-10b). The eastern margin of this zone can be seen in Fig. 5-10a). Metabasite is not common in unit J outside this zone. Both clast size and shape vary considerably in this unit. In general clasts close to unit I are smaller and more rounded than those near the northern margin of the unit which are generally larger and more elongate. The variety of clast size and shape is shown diagrammatically in Figure 5-8. Four narrow, intensely-sheared slivers of red and green metabasite, chert and red and green argillite occur about 50 metres north of the I-J contact. Only one zone can be traced to the opposite bank of the river. In the portion most distal from the I-J contact, bedding is only moderately disrupted, and graded bedding can be discerned in some of the sandstones (Fig. 5-2b).

The following trends are noted in Unit J:

- 1) moving towards the I-J contact, metabasite clasts and slivers become more common;
- 2) moving away from the I-J contact, clasts become less rounded

Figure 5-10a: Faulted contact (F) between units I (I) and J (J). In unit I, metabasite blocks (M) can be seen within red argillite. Tauherenikau Gorge (see Fig. 5-7 for location).

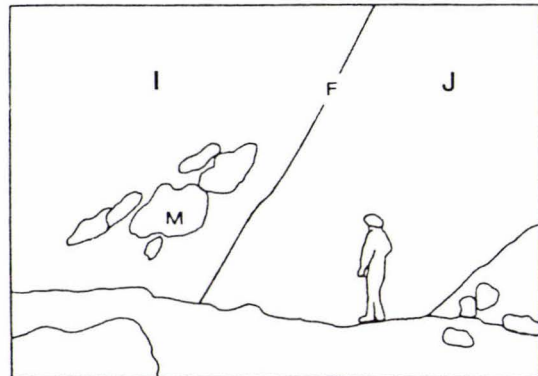
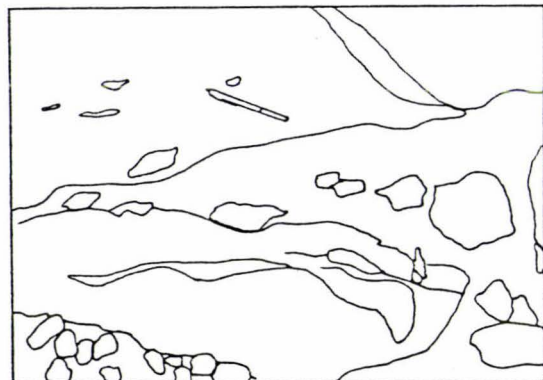


Figure 5-10b: Intensely sheared outcrop of metabasite(?), black argillite and sandstone. Unit J, Tauherenikau Gorge (see Fig. 5-7 for location), pen 15 cm long.





(ie. more lozenge shaped and elongate), with the most distant parts of Unit J consisting of only moderately disrupted sandstone and argillite units.

Comparison with other areas

In the field area, units that consist of phacoids and lozenges of both associations in a sheared matrix are here referred to as *mélanges* (see below Type Cii). *Mélange*, was defined by the 1980 Penrose conference (Silver & Beutner 1980) as "a mappable, internally fragmented and mixed rock body containing a pervasively deformed matrix". Using the terminology of Hsu (1968), *mélange* clasts of lithologies of the volcanic association would be referred to as "exotic" and those of the sedimentary association as "native".

Large parts of the field area consist of rock units that have a similar fabric to the *mélanges* mentioned above, but for the most part lack exotic clasts (see below, Type Ci). Hsu (1968) mapped similar units in the Franciscan of California, and referred to them as broken formation. Other authors (eg. Cowan 1974) have broadened the definition of *mélange* to include such units. In this study, rock units that show a *mélange*-like fabric are also referred to as *mélange*. The distribution of these units is described below.

Many examples of rock units with a similar fabric to *mélanges* in this study area are described from the Franciscan of California (eg. Hsu 1968; Cowan 1974 & 1978; Korsch 1982). Similar units have been described from other parts of the world, for example: Alaska (Connelly 1978), Japan (Suzuki & Hada 1979), Indonesia (Moore & Karig 1980) and Yugoslavia (Dimitrijevic & Dimitrijevic 1973).

5.2 MACROSCOPIC STRUCTURE

5.2.1 Macroscopic folds

Well preserved bedding occurs in Marchant Creek (G.R. S26C/ 0150 1575) and the Waiohine River (G.R. S26D/ 1060 2413) allowing facing reversals to be determined and macroscopic folds to be inferred. This apparent restriction of macroscopic folding to areas of well preserved bedding probably results from a general lack of facing evidence outside such areas.

In the lower Marchant Creek, the macroscopic folds are mainly tight to close with one being open. Fold axes generally plunge moderately or gently to the northeast. Three tight folds were overturned towards the east. Figure 5-11 shows a detailed map of the area and an interpretive cross-section for part of the sequence.

In the region of the Makaka Creek-Waiohine River confluence a tightly folded anticline is inferred to plunge moderately to the southwest.

5.2.2 Degree of disruption

During field mapping, it was possible to produce a map based on the intensity of disruption (Fig. 5-12) and outcrops were classified as one of three types, which represent arbitrary divisions and are stages in a structural continuum of deformation. These are:

Type A Beds are for the most part intact, although minor amounts of faulting both at a low angle and at a high angle to bedding may occur. Most facing evidence comes from rocks of this type.

Type B Moderate amounts of faulting at both low and at high angles to bedding cause disruption of the more competent sandstone beds. Faulting commonly produces a lozenge fabric (Pettinga 1982). Facing evidence generally cannot be determined as sandstone-argillite

Figure 5-11: Detailed map of the lower Marchant Creek with an
interpretative cross-section a-b.

Form lines are based on bedding and shear foliation orientations.

KEY


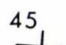
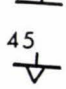






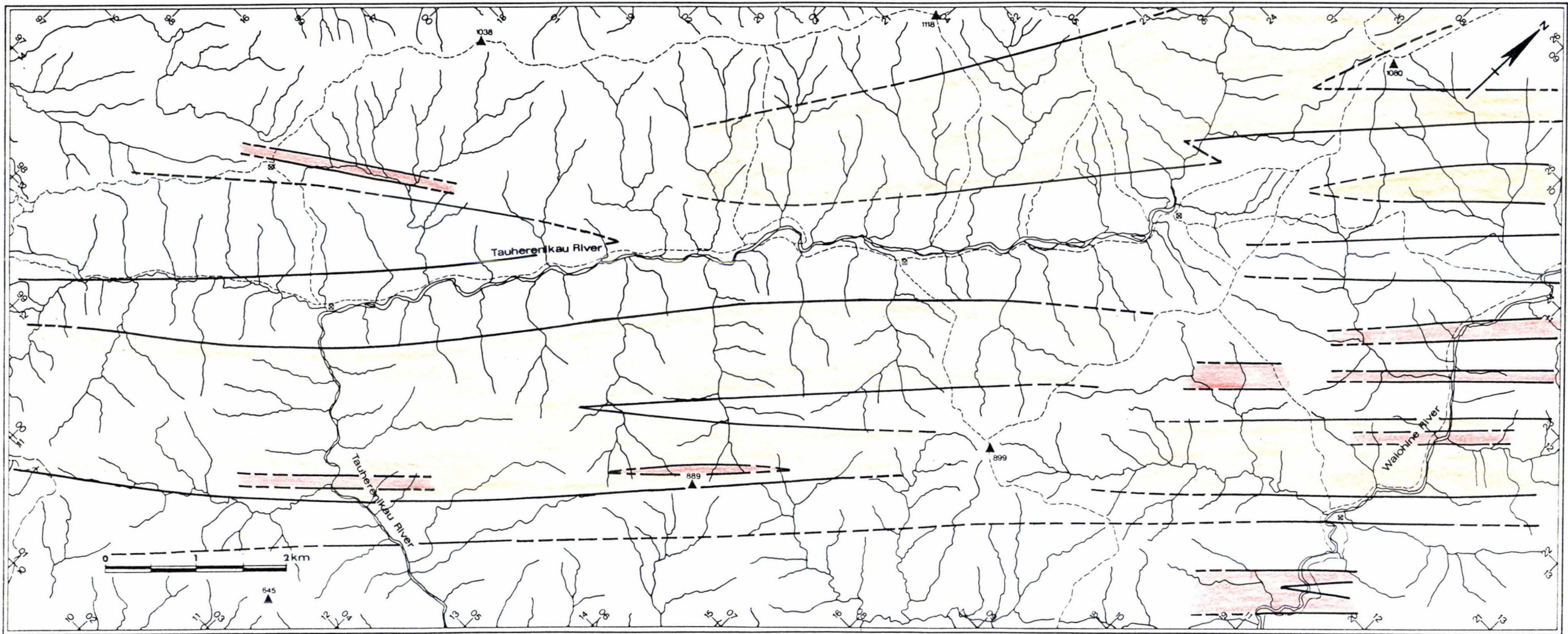
-  Form lines
-  Strike and dip of bedding
-  Strike and dip of bedding with younging
-  Strike and dip of shear foliation
-  Strike and dip of shear foliation with younging

Figure 5-12: Map showing the degree of disruption.

KEY

-  = A; well preserved bedding
-  = B; moderately disrupted
-  = Ci; highly disrupted (clasts only of the
sedimentary association)
-  = Cii; highly disrupted (clasts of both the volcanic
and sedimentary associations)



interfaces are faulted and argillite units are sheared.

Type C Bedding is only apparent from the alignment of phacoids. This type, often seen interleaved with type B, is subdivided into C(i) and C(ii) on the basis of the lithology present. Type C(i) contains clasts of only the sedimentary association whereas type C(ii) contains clasts of both the volcanic and sedimentary associations. In several outcrops along strike, transition from type B to type C(i) was observed.

Type C(i) is particularly well developed in the upper Tauherenikau River (G.R. S26C/ 0640 2340) and type C(ii) in the middle Tauherenikau River gorge (see section 5.1.4). The units shown in Figure 5-12 are named after the disruption type that dominates the geology of that area, that is, lesser amounts of other types may be present.

5.2.3 Geometric analysis

Based on both bedding and shear foliation orientations, the field area has been subdivided into eleven structurally-homogenous, geographically-continuous domains. Some areas have not been assigned to a structural domain due to lack of data caused by exceptionally poor exposure (see map in pocket). Most data are plotted on equal-angle stereographic projections (Wulff nets) although contoured diagrams are plotted on equal-area projections (Schmidt nets).

Based on field observations shear foliation is parallel or subparallel to bedding, and on a net (Fig. 5-13) showing both poles to bedding and shear foliation for domain 2, the two types of data have similar orientations. As the two types of orientation data are essentially the same, they are not differentiated on nets for individual domains. The areal distribution of structural domains is shown in Figure 5-14.

Within individual domains, the distribution of poles to bedding (So) and shear foliation plot along great circle girdles (Fig. 5-14). This indicates that So has been cylindrically folded and that beds were planar within each domain prior to this deformational event. However, the orientation of these great circle girdles are variable and on a synoptic net (Fig. 5-15) the poles to these girdles (the π axes for So, Ramsay 1967) lie along a great-circle girdle with an orientation of 044/SE/80. This implies that the rocks in the field area have undergone at least two fold events. If there had only been one fold event the axes should cluster around a point maximum.

The pattern displayed on the synoptic net (Fig. 5-15) may represent either:

Alternative 1: early folds that have been refolded. Here the

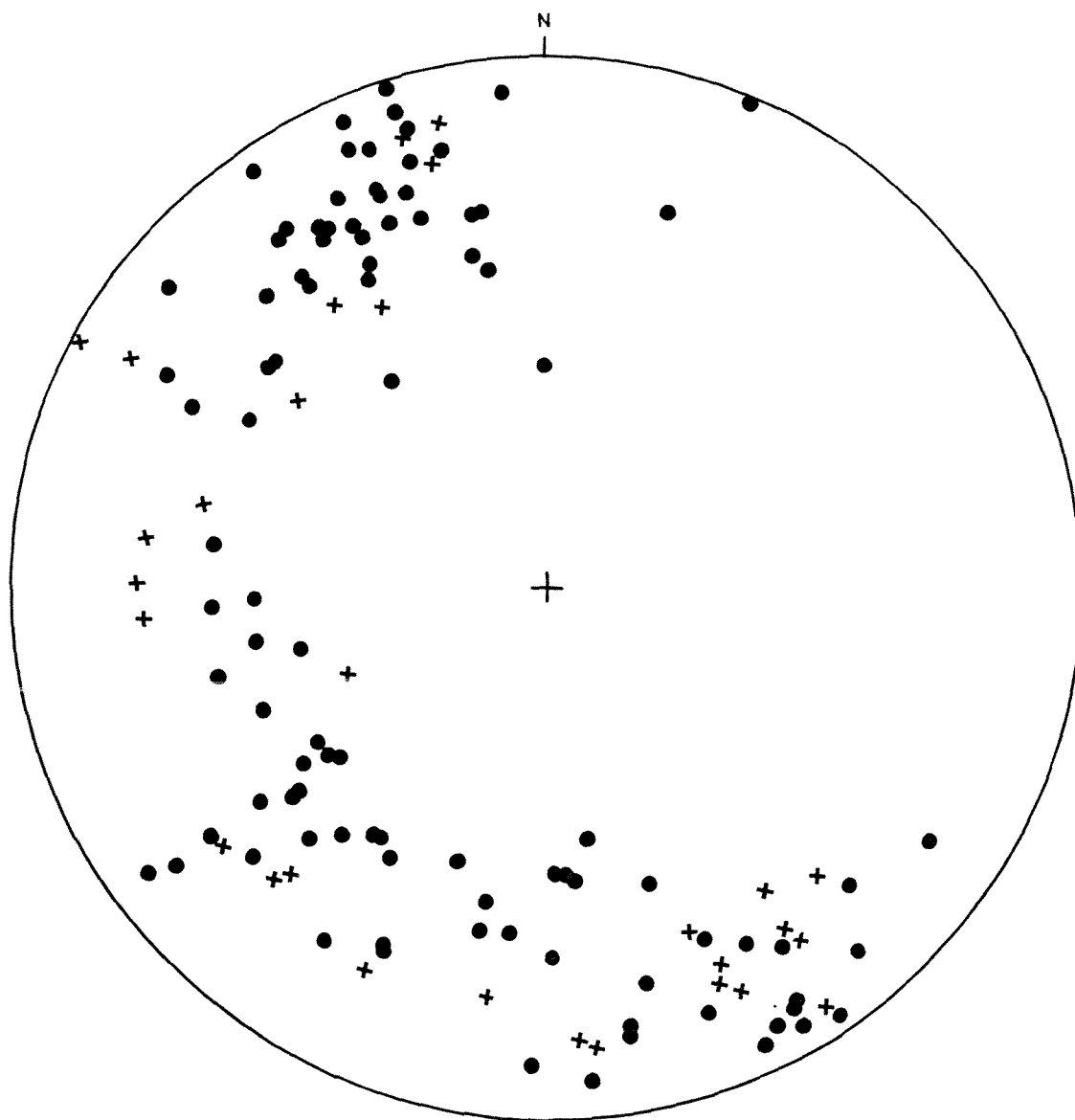


Figure 5-13: Comparison of bedding and shear foliation orientations from Domain 2.

● = pole to bedding
+ = pole to shear foliation

Figure 5-14: Map of the field area showing structural domains.

Poles to bedding and shear foliation have been plotted
for each domain (πS_0).

● = pole to S_0

○ = mesoscopic fold axis

□ = macroscopic fold axis

n = number of bedding and shear foliation orientations
plotted

C = contour interval (per 1 percent area)

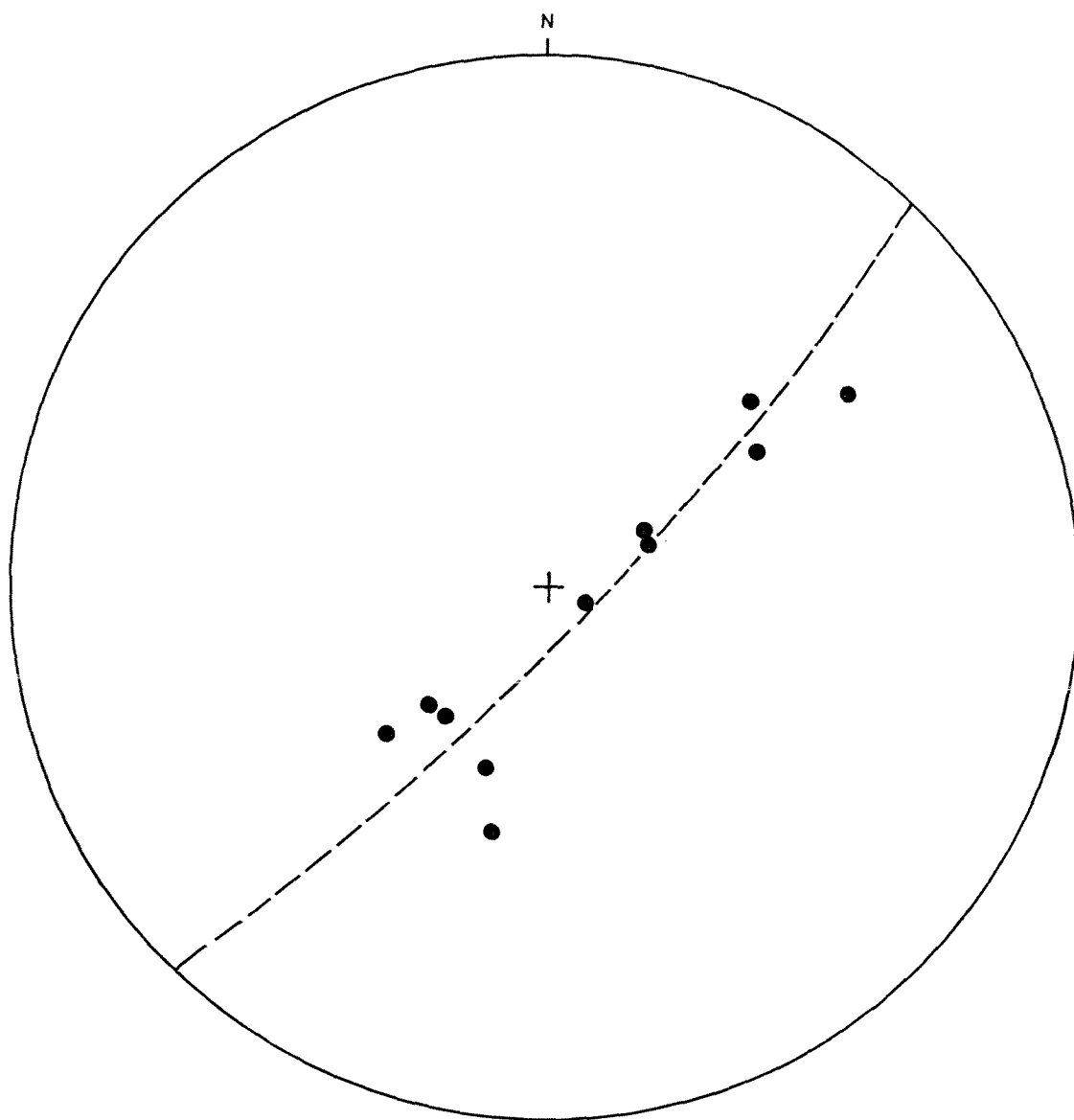


Figure 5-15: Synoptic net showing π axis (S_o) for each domain.

orientations of π So in each domain (Fig. 5-16a, area A and area B) define the early fold F1. The variation in the π axes defined by the great-circle girdles of π So for each domain, would be the result of F1 being refolded (which would change the orientation of F1). In this case, the synoptic net of π axes for each domain defines a plane in which the fold axes of F1 lie and is not related to the axial surface of either fold event.

Alternative 2: later folds that have refolded early folds. The orientations of π So in each domain (Fig. 5-16b, area A, area B and area C), represent the later fold event. Within individual domains, prior to the later fold event So was planar. That is, the late folds form in the limbs or in planar parts of the hinge zone of the early folds (Fig. 5-16b). Therefore the synoptic great-circle girdle of π axes for each domain defines the axial surface of the later fold event (F2).

The scatter of π axes (So) about the great circle girdle (Fig. 5-15) may be due to one or more of the following:

- 1). shear foliation was not strictly planar prior to the later fold event. Also, foliations are seen to anastomose;
- 2). folding may not be purely cylindrical;
- 3). beds within individual domains were not strictly planar prior to the later folding event;
- 4). minor, late warping or gentle folding.

Cleavage

The weakly-defined, spaced cleavage observed in two outcrops in the field area is essentially parallel to bedding, being less than 5° different in strike, which implies that the cleavage was produced during an isoclinal fold event. The average cleavage has an orientation 025/NW/88 (Fig. 5-17).

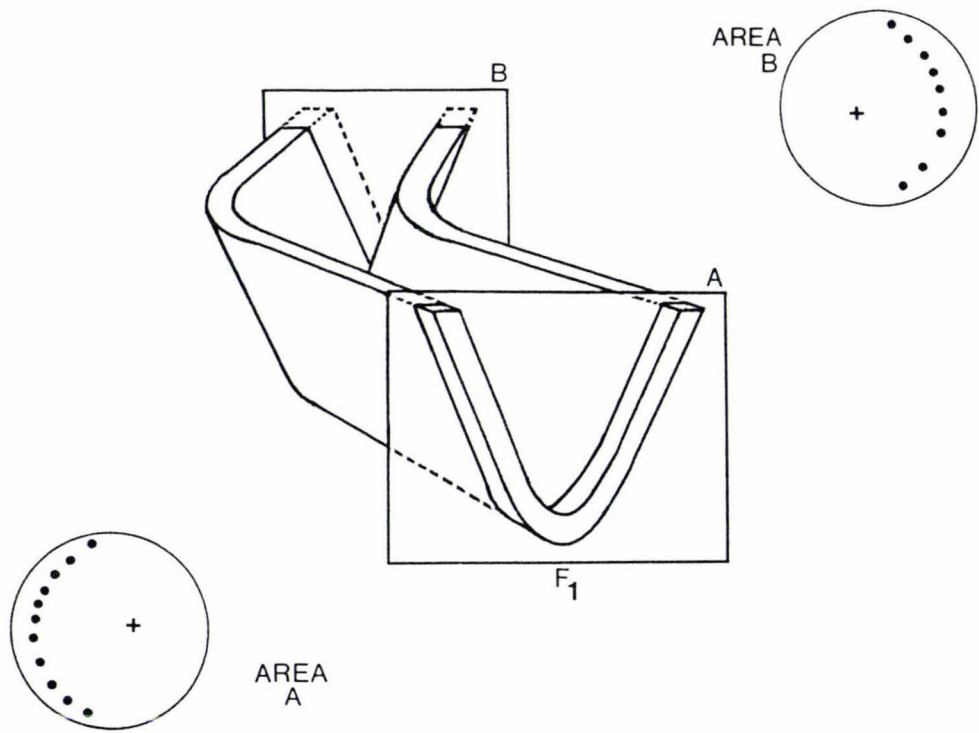
Figure 5-16a: Alternative 1: the pattern of π axes (So) is for an early fold system that has since been refolded. The orientations of π So in each domain eg. area A, area B, define the early fold F1

$$\bullet = \pi \text{ So}$$

Figure 5-16b: Alternative 2: later folds that have refolded early folds. The orientations of π So in each domain eg. area A, area B, area C, are for the F2 fold. The synoptic great-circle defined by F2 represents the axial surface of AS2.

$$\bullet = \pi \text{ So}$$

a



b

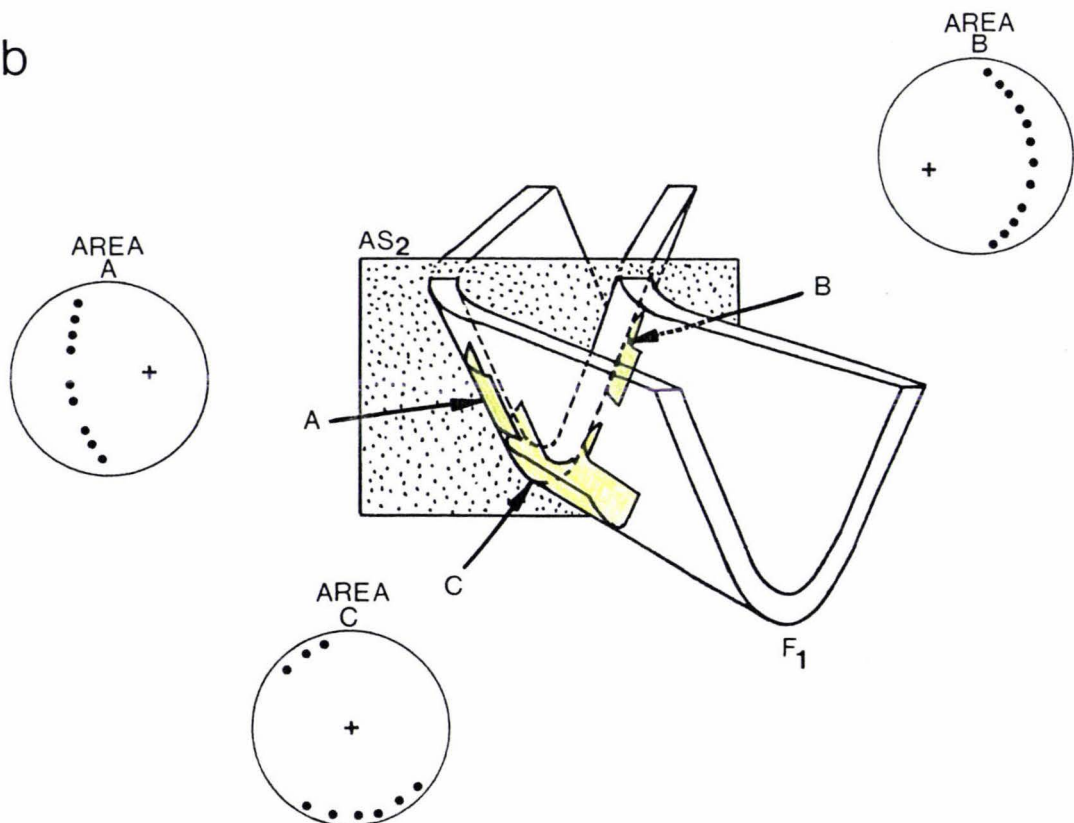


Figure 5-16

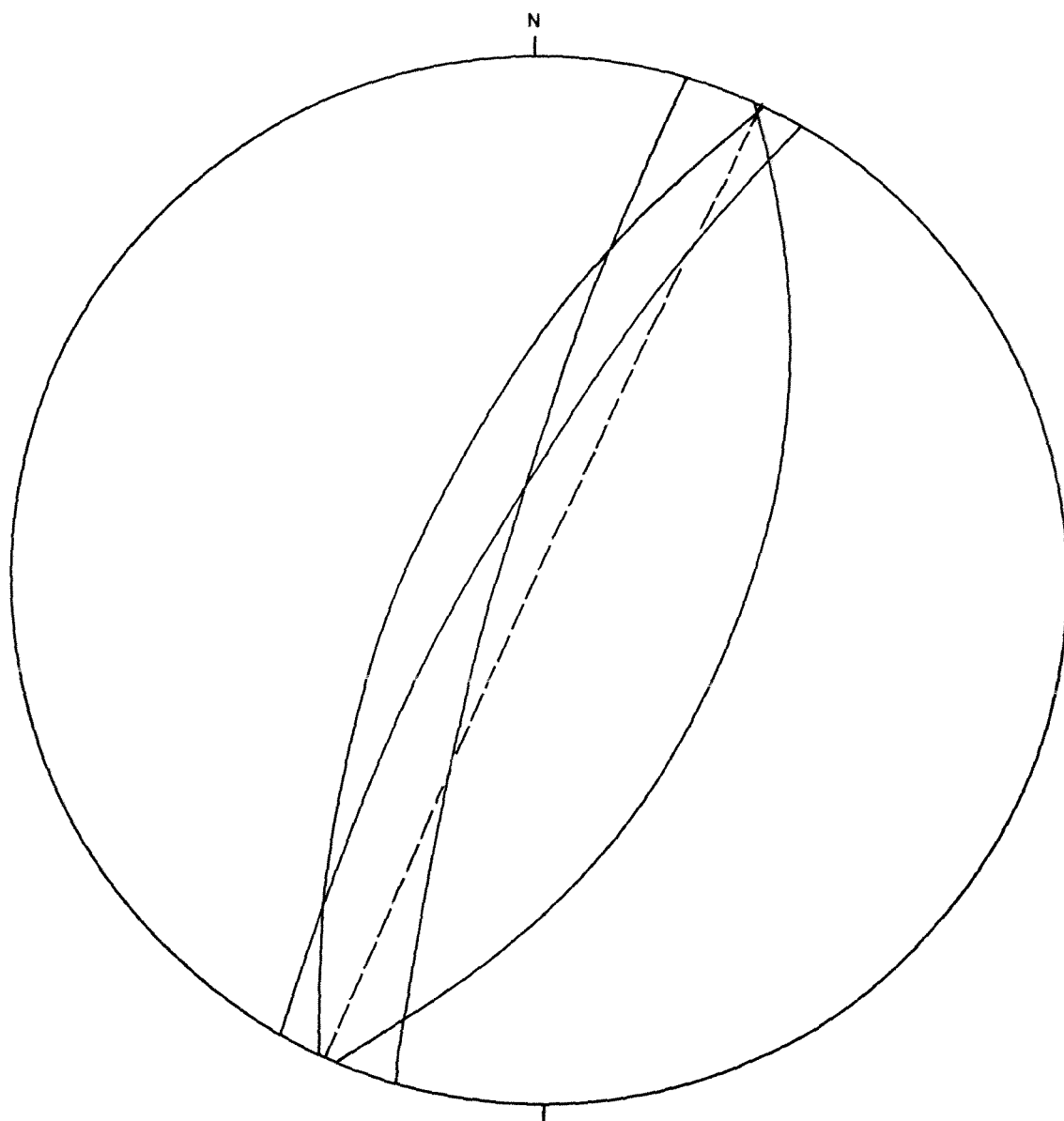


Figure 5-17: Cleavage traces from the Tauherenikau Gorge and the
Waiohine River.

Dashed great-circle girdle denotes the trace of the average cleavage.

As mesoscopic folds in the field area are close to open (see below), the cleavage probably developed during a different fold event than those which have been observed on the mesoscopic scale. There is no evidence that the isoclinal fold event is a late event (ie. overprinting relationships) and it is most likely an early fold event.

Mesoscopic folds

Axial surfaces of mesoscopic folds from one outcrop in the Waiohine River (G.R. S26D/ 1047 2288) show two different strike directions (Fig. 5-18). No overprinting relationships were apparent from these folds. The axial surface traces of two close to open folds strike northeast-southwest, while four open to gentle folds have axial surfaces that strike east-west and dip steeply to the south (Fig. 5-18). These two strike directions are interpreted to be the result of two different fold events. The relative timing of these two events can be inferred from the style and orientation of folds.

The open to close folds with axial surfaces that strike northeast-southwest have variable plunges. On the other hand, the east-west folds plunge steeply to the west and have open to gentle interlimb angles, which suggests that these folds were produced during a later fold event which possibly refolded the NE-SW striking folds. It is unlikely that the E-W gentle folds were produced during an early fold event, and then remained undeformed during a later deformation.

Three folds from other localities (two open to gentle folds at G.R. S26D/ 1049 2293, Table 5-1 numbers 1 & 2 and one close fold at G.R. S26D/ 1103 2230, Table 5-1 number 18) have axial surface traces that strike between 040 and 078 , and are interpreted here to be similar to the northeast-southwest orientated folds outlined above.

The great-circle girdle defined by π axes (Fig. 5-15) has a

Figure 5-18a: Axial surface orientations of mesoscopic folds from
Waiohine River (S26D/ 1047 2288).









-  = fold axis of fold with a NE-SW striking axial surface
-  = fold axis of fold with an E-W striking axial surface
-  = axial surface trace (NE-SW trending)
-  = axial surface trace (E-W trending)

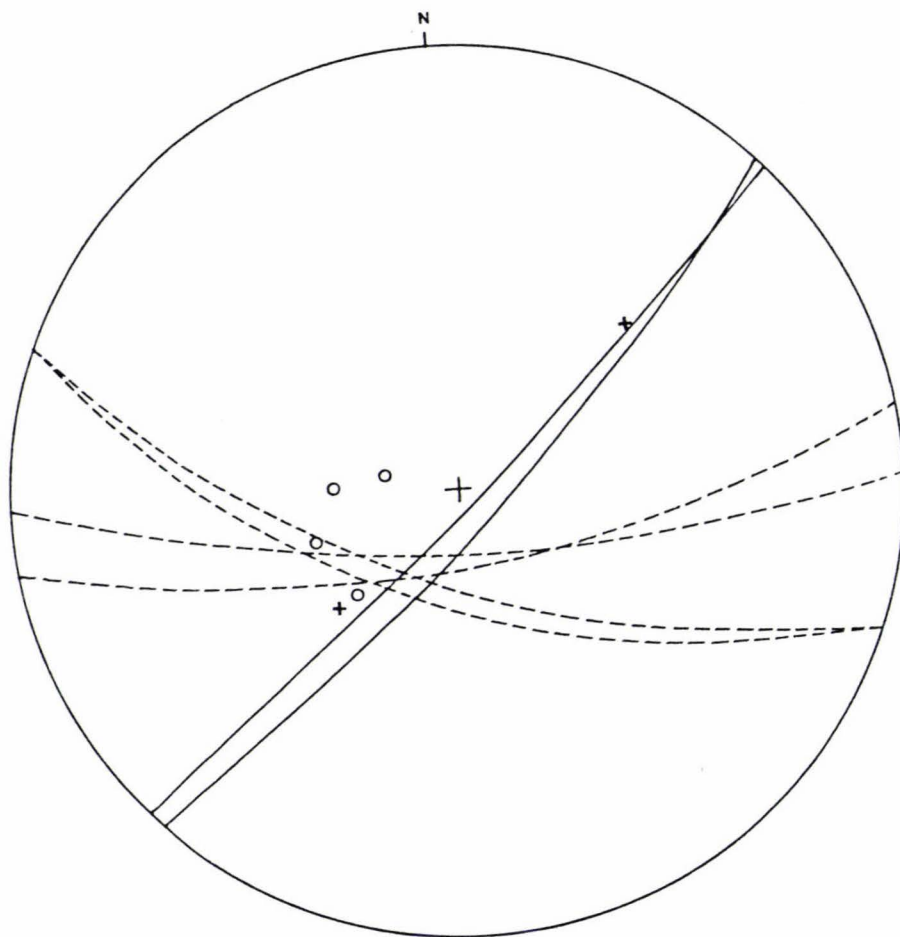
Figure 5-18b: Mesoscopic fold axis from the field area.

-  = fold axis of fold with an E-W striking axial surface
-  = fold axis of fold with a NE-SW striking axial surface

On the bases of style, other mesoscopic fold axes have been assigned to either the E-W or NE-SW trending folds.

-  = fold axis of fold inferred to have a E-W striking axial surface
-  = fold axis of fold inferred to have a NE-SW striking axial surface

a



b

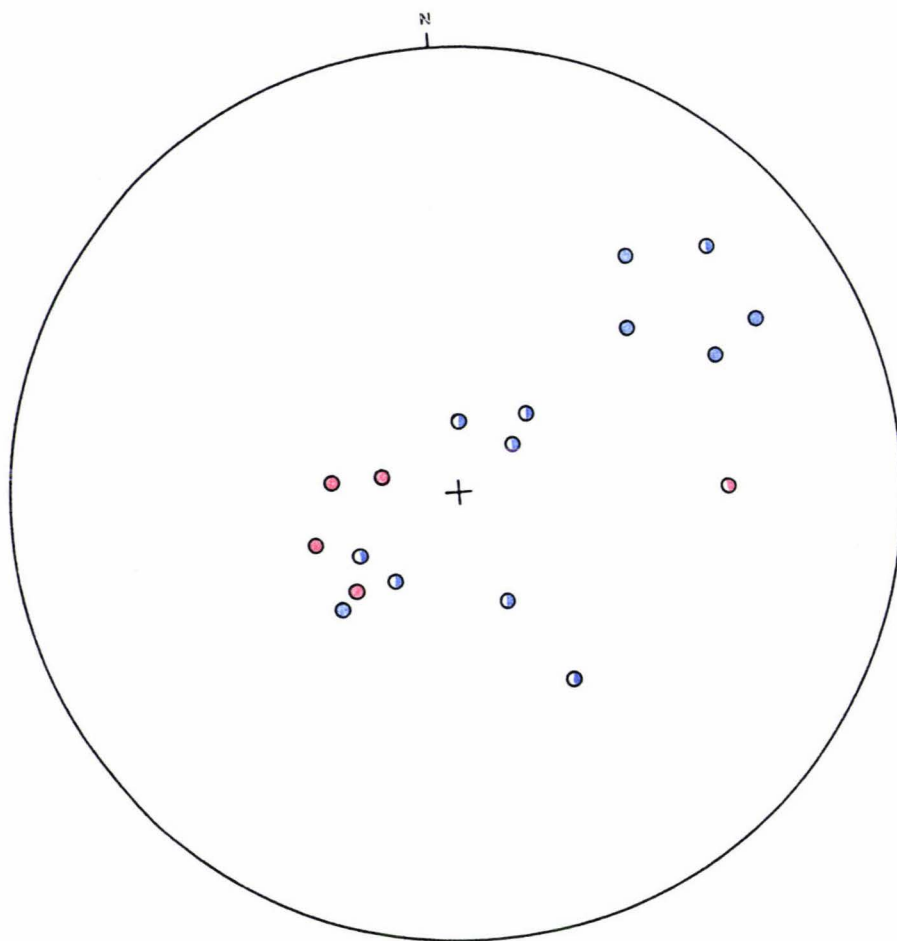


Figure 5-18

similar orientation to the axial surface traces of the NE-SW trending folds, which suggests that the π axes pattern may be reflecting the earlier fold event determined from mesoscopic folds. If this is the case, then the pattern of π axes (Fig. 5-15) is the result of alternative 2 described above.

Macroscopic folds

Macroscopic fold axes defined by the intersection of opposite limbs of inferred folds from lower Marchant Creek and the Waiohine River (see section 5.2.1; Fig. 5-11) lie along, or close to, the great-circle girdle defined by π axes (Fig. 5-15) and were most likely produced during the same deformation that is reflected by π axes (Fig. 5-19). The macroscopic folds can therefore be related to the NE-SW striking mesoscopic folds.

Faults at a high-angle to bedding

Poles to faults at a high-angle to bedding are plotted for individual domains in Figure 5-20. More than half the domains show a scattered pattern, but the rest appear to plot on great circle girdles (ie. domains 1,3,4,8). This raises the possibility that the faults at a high-angle to bedding (S_f) were originally planar and have been cylindrically folded. If this is so, then simultaneous cylindrical folding of two planar surfaces S_o and S_f may have occurred, in which case S_o and S_f should share the same axial surface (see Turner and Weiss 1963, pl30). The π axes of πS_o and πS_f for each of the domains 1, 4 and 8 lie along great circle girdles which are orientated northeast-southwest (Fig. 5-21). The great circle girdle for domain 3 is not shown as both π axes of πS_o and πS_f are almost the same. This indicates that both S_o and S_f may have been folded by the same event, and that it has a NE-SW axial surface.

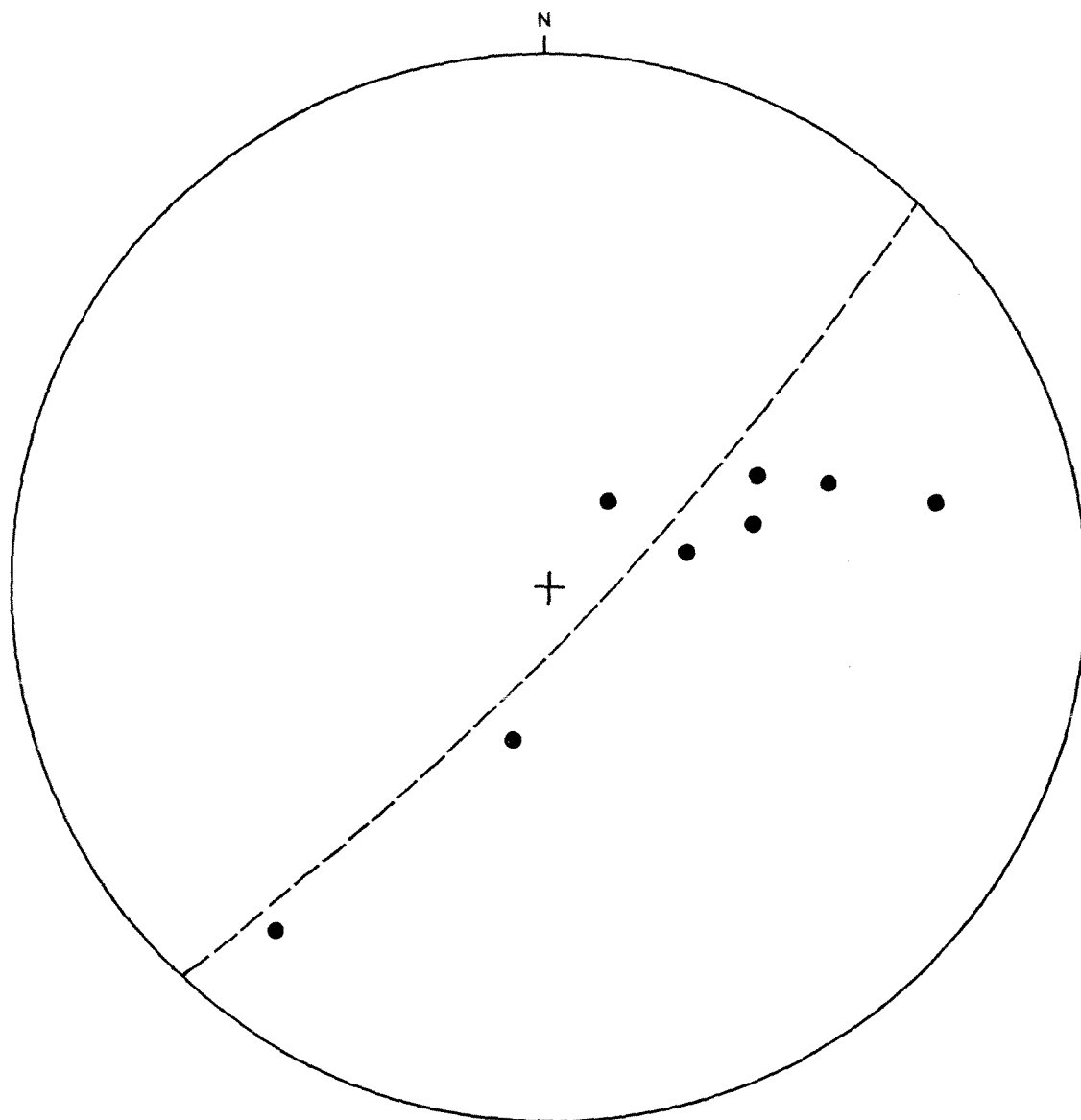


Figure 5-19: Macroscopic fold axes.

Dashed line denotes the great-circle girdle defined by π axes for each domain (Fig. 5-15).

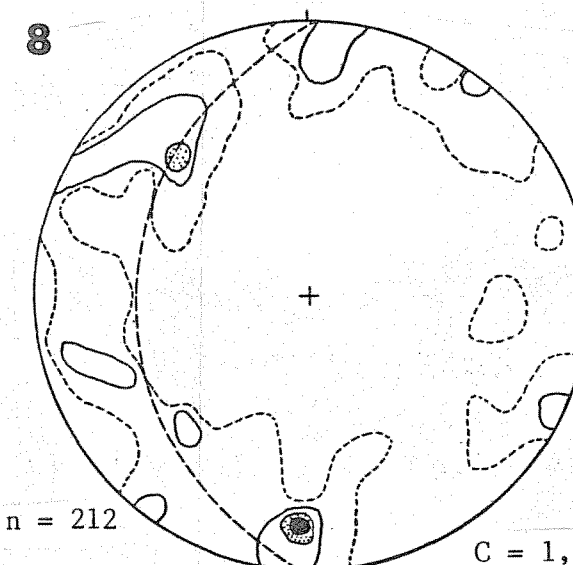
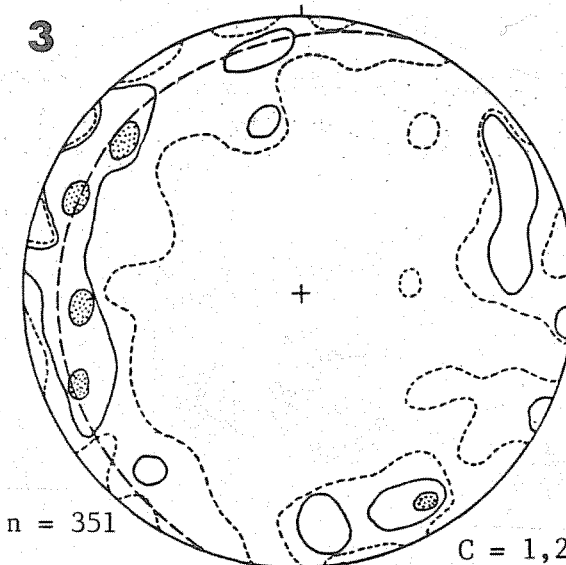
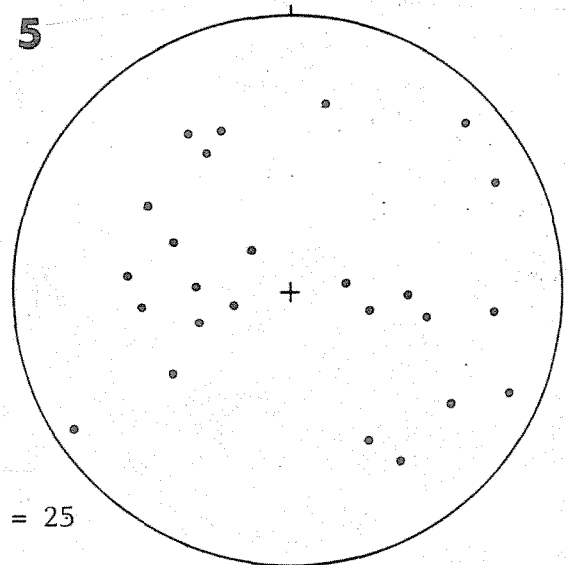
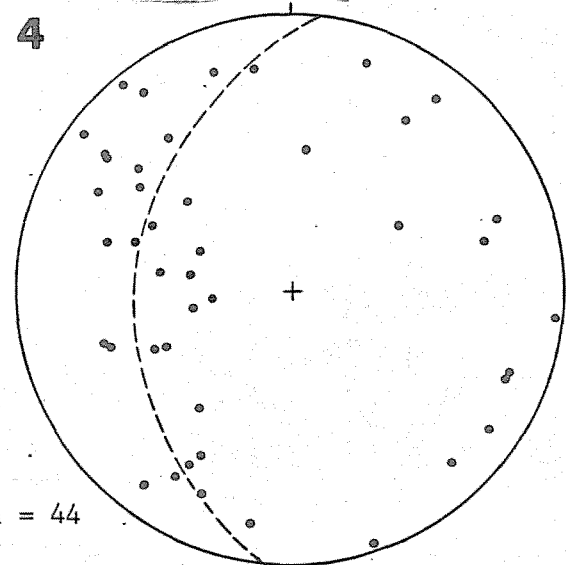
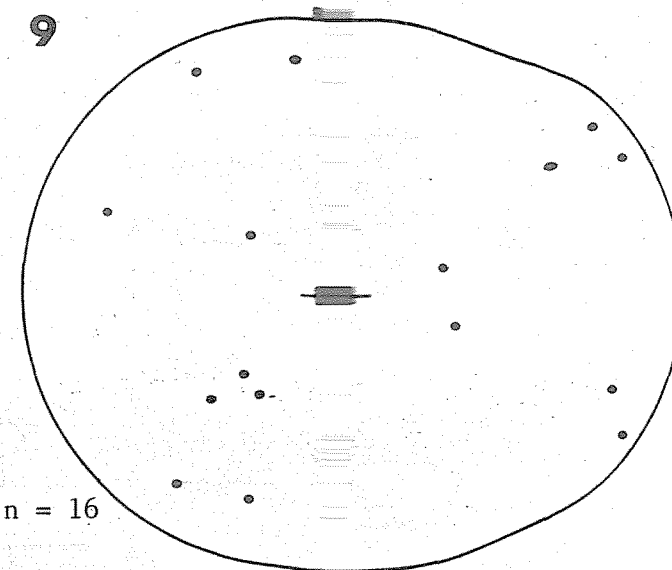
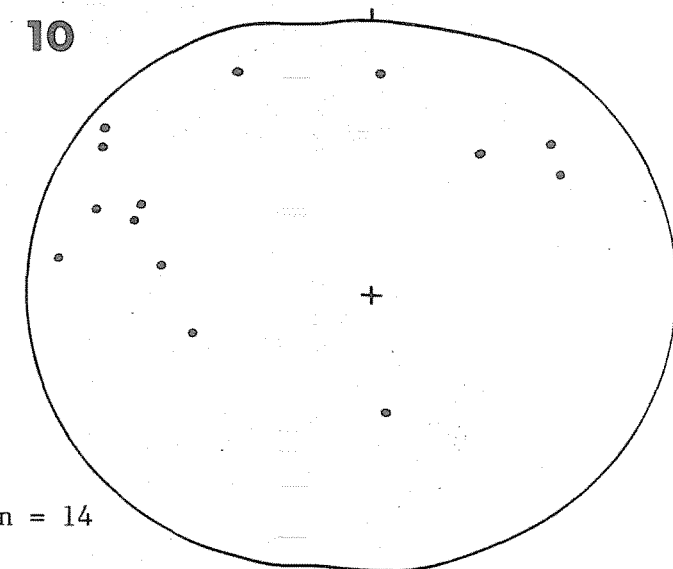
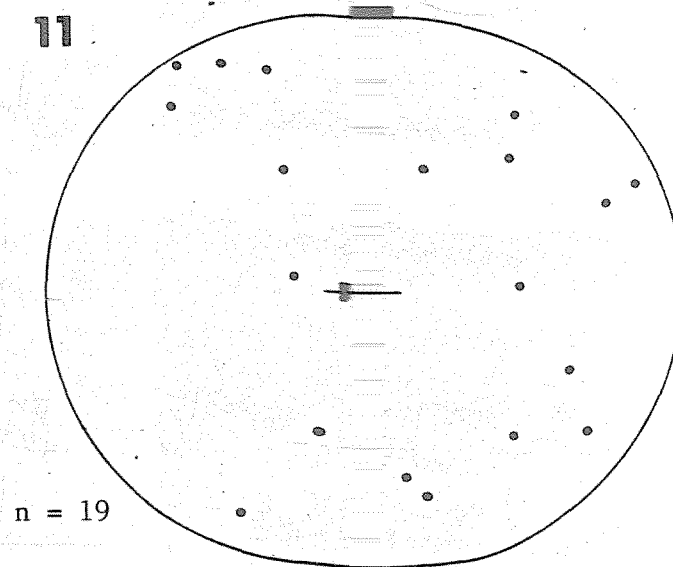
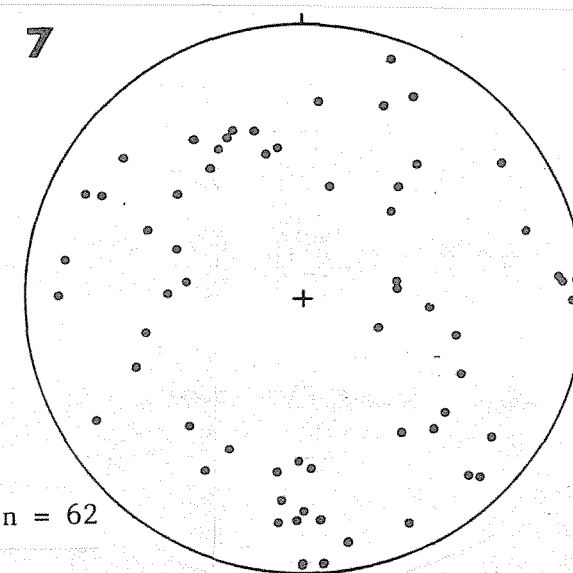
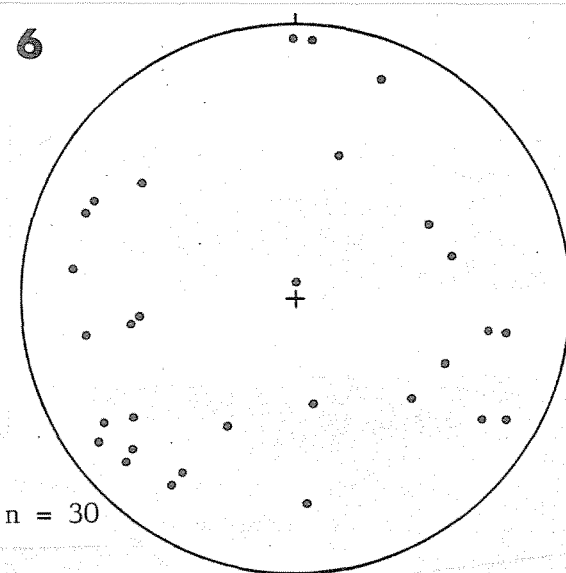
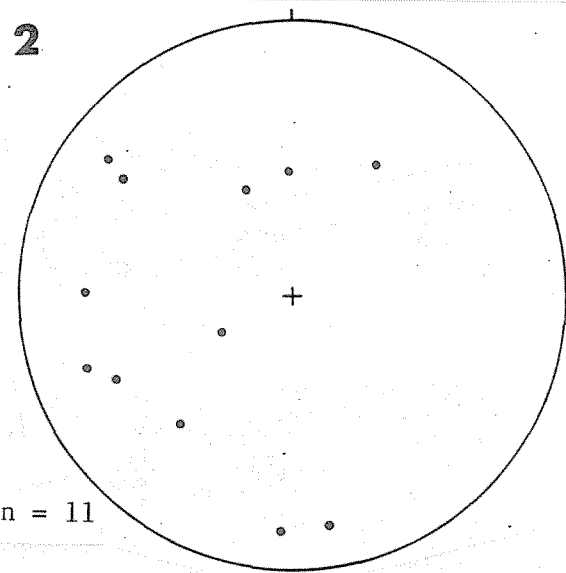
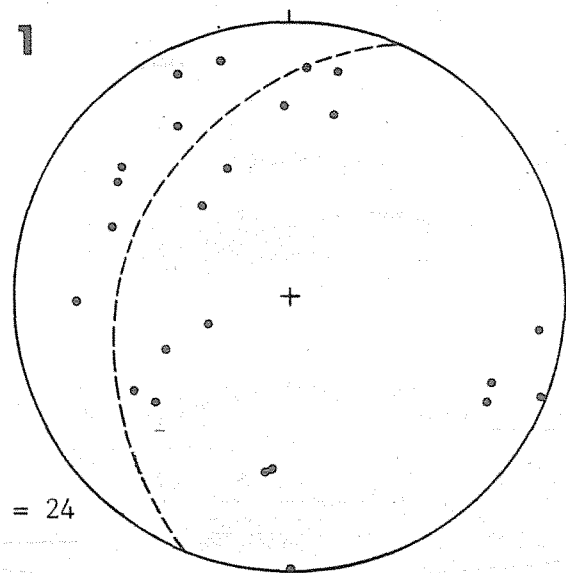
Figure 5-20: Map of the field area showing structural domains.

Poles to high-angle fault orientations have been plotted
for each domain (σ Sf).

● = pole to S_o

n = number of high-angle fault orientations plotted

C = contour interval (per 1 percent area)



C = 1,2,2.5

C = 1,2,3,4

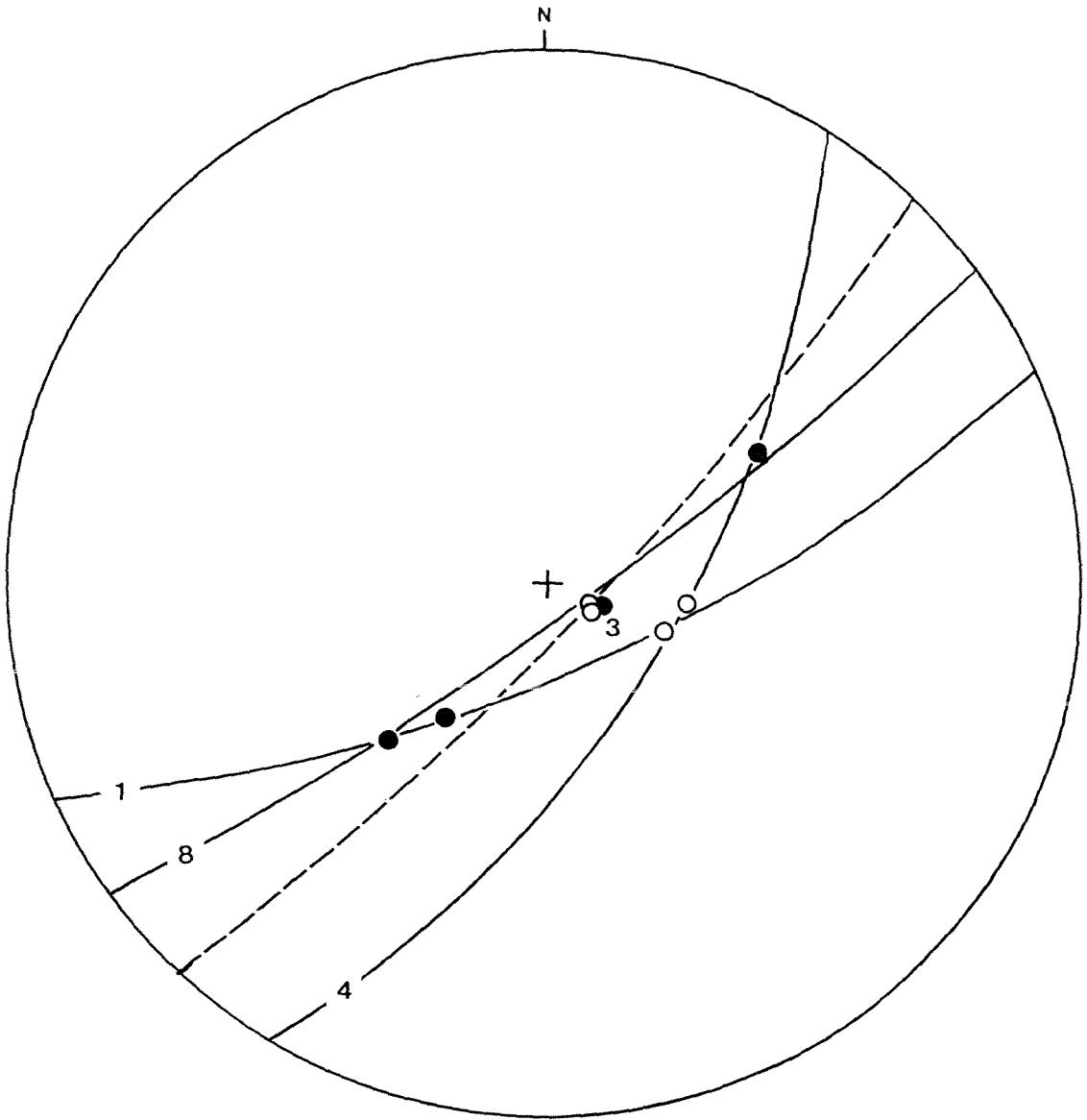


Figure 5-21: Net showing the great-circle girdles which contain the π axis of π So and π Sf for domains 1, 4 and 8. The π axis of π So and π Sf for domain 3 are also shown. Dashed line denotes the great-circle girdle defined by axes (So) for each domain (Fig. 5-15).

8 = domain number

○ = π axis of So

● = π axis of Sf

Summary

If the π axes pattern (Fig. 5-15) represents alternative 2 described above, the NE-SW fold event is refolding an already folded surface. The isoclinal fold event inferred from cleavage would be the earlier fold event, that is, prior to the NE-SW fold event.

Thus, three fold events are inferred:

F1: Isoclinal folding, with an axial plane slaty cleavage.

F2: NE-SW striking folds, with variable plunge. The fold event is reflected in the orientation of π axes (Fig. 5-15), mesoscopic folds (Fig. 5-18), and macroscopic folds (Fig. 5-19).

F3: E-W fold event evident from mesoscopic folds (Fig. 5-18).



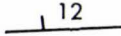

5.3 RECENT DEFORMATION

Many features of the geology and geomorphology of the field area are indicative of recent fault activity. Two major fault-related crush zones occur in the field area, one in the Tauherenikau Valley and another in the southern arm of Marchant Creek (Fig. 5-22).

The Tauherenikau crush zone is well exposed in river bank outcrops near the walkwire on the Tauherenikau Valley Track (G.R. S26C/0463 1853). Based on outcrops in this area, a width of 140 metres is estimated for the crush zone. In rocks close to the crush zone, several small faults with associated pug and minor crush zones were recorded. The orientations of these recent faults together with two other small young faults mapped are northeast-southwest (Fig. 5-23) and the dips are mainly eastward. The fault and associated crush zone in the Tauherenikau River, here referred to as the Tauherenikau Fault, appears to continue both to the northeast and southwest. On air photographs, the fault can be traced to the north over Cone Saddle across Totara Flats, and along Totara Creek. Lensen (1958) regards this fault trace, from a point near Cone Hut and north to be part of the Wellington Fault. To the south, the fault passes along the Smiths Creek valley where crush and pug zones occur. Near the headwaters of Smiths Creek, air photographs indicate that the fault splits into two. The two strands are possibly correlatives of faults 3 and 4 in the Rimutaka Railway Tunnel (Reed 1957b).

The Marchant Creek crush zone is, at the very least, as wide as the Tauherenikau fault crush zone. This crush zone appears to lie along a major air photograph lineament which is regarded as being part of the Wellington Fault (Lensen 1958). Several air photograph lineaments occur in a zone between the Marchant Creek crush zone and the Tauherenikau

Figure 5-22: Map showing air photograph lineaments, mapped occurrences of crush zones and recent faults.

KEY	
	Air photograph lineament
	Shutter ridge showing sense of movement
	Strike and dip of recent fault
	Crush zone (dashed line denotes inferred boundary)



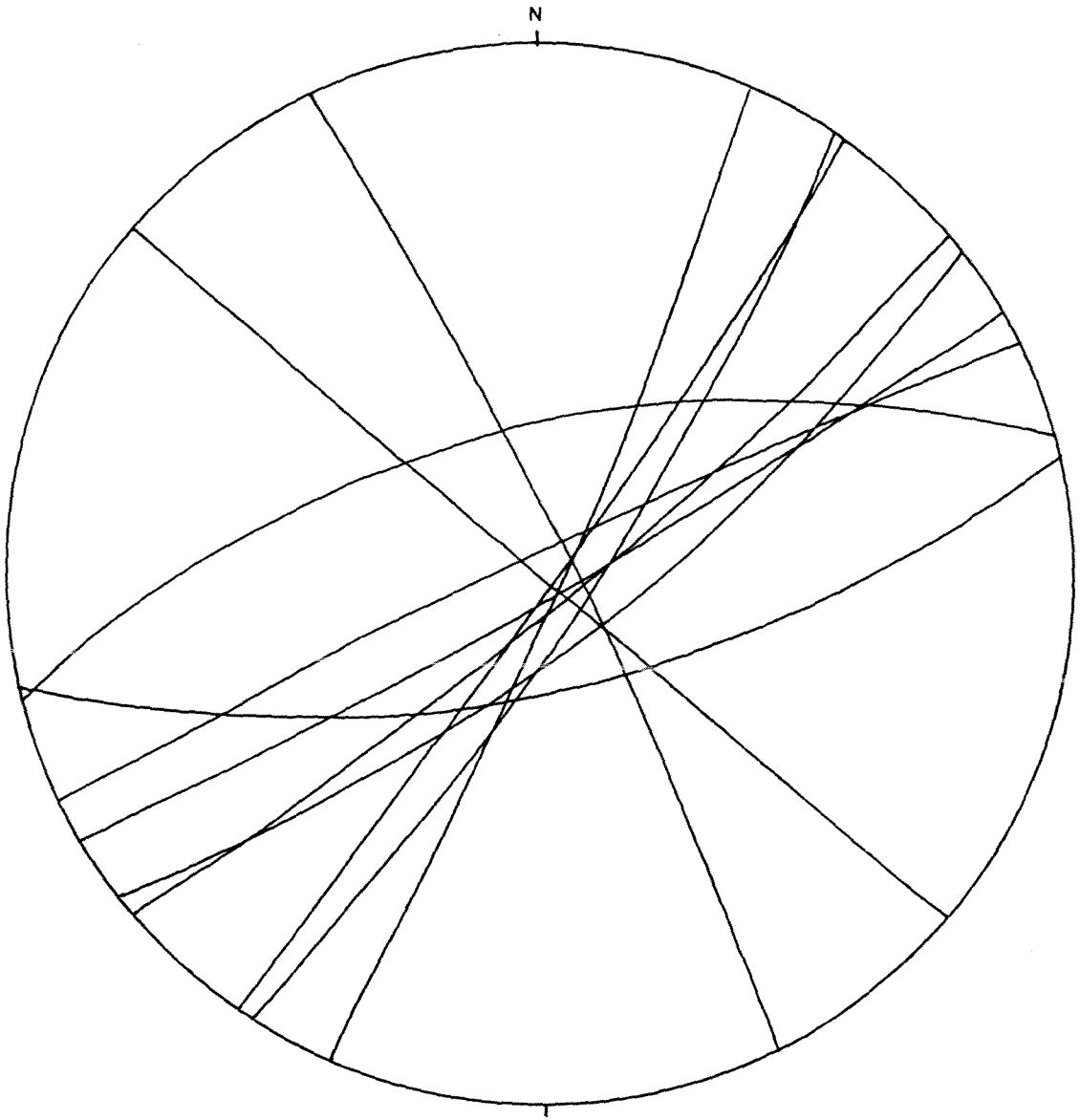


Figure 5-23: Recent faults plotted as planes on a Wulff net.

River. Each appears to represent a young fault. Along three of these traces shutter ridges indicate that the faulting is mainly dextral (Fig. 5-22).

The complex pattern of faulting in this part of the Tararua Range seems to be the result of a bend in the Wellington Fault, with a strike change of 35° between Farm Creek and Cone Saddle.

The Tauherenikau Fault appears to be part of a major, continuous fault that merges with the Wellington Fault rather than being a minor splay off the Wellington Fault. The Wellington Fault is regarded as a major strike-slip fault of regional importance (Lensen 1958) and is related to the Alpine Fault System in the South Island. A dextral offset of almost 480km is considered to have occurred along the Alpine Fault which is thought to have been active since at the Early Cretaceous (Wellman & Cooper 1971). Data from the Wellington fault approximately 30km north of Wellington City suggests the horizontal slip rate may be about 7mm/y (Berryman in prep).

To summarize, major dextral strike-slip faults and associated minor faults which are considered to show Holocene movement occur in the field area. Faulting is dextral along the Wellington and Tauherenikau Faults, both of which these dip steeply to the east.

5.4 SYNOPSIS OF STRUCTURE

The following structural history is proposed for the southern Tararua Range.

1. Pre-mélange structure

A deformational episode which occurred prior to the formation of the mélange is inferred because some phacoids contain veins which occur only within phacoids and do not extend into the surrounding matrix. These veins represent an extensional event and must have formed prior to the development of melange.

2. Early fold event

An early, isoclinal fold event (F1) is inferred from a weakly developed NNE striking cleavage. This fold event may have been produced prior to, during, or after mélange formation. Other workers (see below) have found that an isoclinal fold event is one of the earliest deformations recorded in rocks of the Torlesse Supergroup, occurring prior to, and during mélange formation. Therefore the isoclinal fold event identified in this study is thought to have occurred at a similar stage in the structural history.

3. Mélange formation

Low-angle and high-angle to bedding faults are common in most parts of the field area, disrupting and displacing bedding. Extreme amounts of this type of deformation has resulted in the formation of mélange.

Two post-mélange fold events are recognized, that is, two events are recognized that have folded the mélange and the associated disrupted units.

4. Post-mélange fold event 1

The first of two post-mélange fold events produced close to

gentle folds (F2) with subvertical axial surfaces that strike NE-SW.

5. Post-mélange fold event 2

The second post-mélange fold event (F3) has produced open to gentle folds with subvertical axial surfaces that strike east-west.

6. Recent faulting

Major NE trending strike-slip faults, with well developed crush and pug zones, occur in the field area as well as several smaller associated recent faults.

5.5 COMPARISON WITH OTHER WORKERS

The deformational history proposed here can be related to deformation seen in other areas of the Torlesse Supergroup. The correlation between deformation seen in this study and other areas is shown in Table 5-2.

Spörli (1978) proposed a structural history for the Torlesse of the North Island based on the observations of several studies (eg. Spörli & Bell 1976; Spörli & Barter 1973; Spörli et al. 1974). According to Spörli, three deformation phases can be recognised, these being:

D1) formation of melange and imbrication of strata, with fold axes trending across the now-dominant basement grain (northeast-southwest) and fold vergence predominantly toward the south;

D2) imbrication and further melange formation; strongly asymmetric folding on horizontal axes parallel to the present structural grain; folds verge to the east; beds in the Axial Ranges were rotated to vertical and overturned attitudes;

D3) open folding on steeply plunging axes; these folds show a close association with active faults.

Table 5-2: Comparison of deformation seen in other areas within the Torlesse Supergroup.

This study		Spörli 1978		Wellington Korsch 1984	Zircler Head MacKenzie 1983	Camp Bay Webster 1982	Otaki Forks Rattenbury 1983	SE Fanning Range Foley 1984	Esk Head Melange Botsford 1983
Recent faulting				Recent faulting	D4 Minor warps		Late faulting	Late faulting	Late faulting
E-W folding event open to gentle folds				Folding (F3) with E-W trending; axial surfaces			Minor buckling on limbs		Gentle flexing
NE folding event close to open folds		D3 Late steeply plunging folds NE trending		NE striking folds (F2), close to isoclinal.	D3 Open to tight folds plunge steeply to NE	D3 NE-SW trending folds, plunging NE, axial surfaces dip to NW	Steeply plunging folds	Folding with NE-SW trending axes	Steeply plunging NE-SW trending folds
Isoclinal folding, cleavage forming	Melange formation	D2 Asymmetric folds with subhorizontal axis. NE trending	Melange formation	Fragmentation and fracturing	D2 Tight to isoclinal gently plunging folds cleavage forming	D2 N-S trending isoclinal folding cleavage forming event	Open, moderately plunging folds	Melange formation	Melange formation
		D1 Steeply plunging folds, trending oblique to regional trend		Tight to isoclinal folding (F1)	D1 Gently plunging pre-cleavage folds	D1 Steeply plunging open folds with NW-SE trends	Isoclinal folds suggestive of deformation while soft		
Pre-melange fracturing and veining									
		D0 Soft sediment deformation				D0 Soft sediment deformation	Soft sediment deformation; clastic dykes etc.		

Spörli (1978) interprets D1 and D2 as being part of, or predating the Early Cretaceous Rangitata Orogeny while D3 occurred at least in part during Cenozoic time.

Other workers have determined similar sequences of deformation that can be related to that outlined by Spörli and this study (Table 5-2). A number of workers (Webster 1982; MacKenzie 1983; Rattenbury 1983; Foley 1984) have noted an early isoclinal fold event. By inference from the above workers the early isoclinal fold event determined in this study has been assigned a similar position in the deformation sequence.

All the workers listed in Table 5-2 have noted a late NE-SW fold event, suggesting this deformation occurred throughout the Torlesse Supergroup. Where melange formed (Spörli 1978; Botsford 1983; Foley 1984), the NE-SW folds formed after the melange.

Only a few workers (Rattenbury 1983; Korsch 1984) have distinguished a late fold event which might be comparable with the E-W fold event from this study. Korsch (1984) has evidence of such a late deformation in the Wellington area which post-dates the NE-SW fold event.

Hence, the deformational sequence proposed from my field area is similar to that of other areas of the Torlesse Supergroup.

CHAPTER SIX

DISCUSSION

The aim of this discussion is to relate the basement geology of the field area to that of the rest of the Torlesse Supergroup, and to discuss the implication of this study for models that have been proposed for the origin of the Supergroup. This is preceded by, a summary of the nature of the two associations in the southern Tararua Range.

6.1 SUMMARY OF THE SEDIMENTARY AND VOLCANIC ASSOCIATION

6.1.1 Sedimentary Association

The sedimentary association consists mainly of both bedded and massive sequences of sandstone and argillite which were deposited as turbidites in a mid- to outer- submarine fan environment. Due to the complexity of deformation and lack of paleocurrent indicators, little can be concluded as to the direction of sediment transport or the form of the turbidite fan system. The provenance of these sediments indicates that they were derived from an active continental margin magmatic arc that was heavily dissected and shedding sediment of mainly plutonic and metamorphic origin.

Associated with the turbidites are rare olistostromes, which at one location includes large blocks of previously-sheared sandstone and argillite. This implies that the source is in part older Torlesse rocks. The allochthonous sliver of lithic sandstone in the Waiohine River consists of mostly sedimentary clasts is thought to represent recycled older Torlesse fragments. Micrite is conformable within the turbidite sequence at several localities (Chapter 2, Fig. 2-1b). These sediments indicate that deposition was above the carbonate compensation depth.

6.1.2 Volcanic Association

The volcanic association consists mainly of metabasite and coloured argillite with minor amounts of chert and limestone.

Geochemical data indicate that the metabasites were erupted in an intraplate environment, and that the associated coloured argillites are of two types, namely:

- 1) sediments formed by the degradation of basalt;
- 2) pelagic sediments modified by metal-rich effluent either from hydrothermal systems associated with mid-ocean ridges or intraplate volcanism. The character of amygdules in the metabasites suggest extrusion in a shallow water environment, that is, less than 800 metres.

The cherts represent hemipelagic deposits and are part of a compositional continuum that exists with the coloured argillites of pelagic origin.

Limestone associated with coloured argillite contains bivalve shell fragments which suggests a relatively shallow water marine environment.

Hence, the rocks of the volcanic association indicate formation in an environment similar to present day mid-ocean islands (eg. Hawaii).

Within the study area, nowhere are rocks of the two associations conformable. Coupled with this, the nature of the two associations suggests that they were formed in separate environments. Any acceptable model proposed for the origin of the Torlesse Supergroup must explain adequately the origin and juxtaposition of the two associations.

6.2 MODELS FOR THE FORMATION OF THE TORLESSE SUPERGROUP

Models for the origin of the Torlesse Supergroup proposed since the advent of plate tectonics infer processes related to a convergent plate margin (eg. Landis & Bishop 1972; Coombs et al. 1976; Spörli 1978; Bradshaw et al. 1980; MacKinnon 1983; Korsch & Wellman in press). There is, however, little agreement as to the nature and the timing of the processes. These models include:

- 1) formation of a giant submarine fan system followed by addition to the Gondwana continental margin and subsequent deposition of younger sediments seaward of this (Bradshaw et al. 1980).
- 2) deposition and accretion at an unknown continental margin followed by rafting against the Gondwana continental margin (Coombs et al. 1976; Kamp 1980; Howell 1980).
- 3) deposition of turbidites in a trench at the Gondwana continental margin and subsequent strike-slip movement along that margin (MacKinnon 1983).
- 4) simultaneous deposition of turbidites and accretion at the Gondwana continental margin (Spörli 1978; Korsch & Wellman in press).

Bradshaw et al. (1980) divided the Torlesse Supergroup into four sub-terrane, namely:

- 1) Rakaia sub-terrane (Late Carboniferous to Late Triassic) which grades, by increasing metamorphism, into the Haast Schist.
- 2) Pahua sub-terrane, mainly Late Jurassic and Early Cretaceous sediments.
- 3) Esk Head sub-terrane, which forms a complex tectonic contact between the Rakaia and Pahua sub-terrane.
- 4) Hunua sub-terrane, Late Jurassic sediments and allochthonous Permian masses (included in the Waipapa Group by Spörli 1978).

In their model, Bradshaw et al. (1980) proposed that the Rakaia sediments were deposited in a giant submarine fan system, which was carried into contact with the Gondwana continental margin by plate convergence. During the Late Jurassic, the Puhua sediments, being derived from the older Rakaia sub-terrane, accumulated in a trench seaward of the Rakaia wedge. The Esk Head sub-terrane developed during the deposition of the Puhua sediments at the eastern margin of the Rakaia wedge. In this model convergence in the form of subduction is thought to have started during the Jurassic.

Coombs et al. (1976), Kamp (1980) and Howell (1980) consider that the Torlesse Supergroup formed at an unknown location to the east of the Gondwana continental margin. Coombs et al. suggest that the Torlesse Supergroup was rafted en mass into a subduction zone during the Jurassic, resulting in its juxtaposition with rocks of the Caples-Pelorous Group. Howell proposed that the Torlesse Supergroup formed somewhere to the east of the Gondwana continent as an accretionary prism at the margin of an unknown landmass. The Torlesse rocks were subsequently disconnected from the unknown landmass, and added to the Gondwana continental margin during the middle Cretaceous. Kamp (1980) suggested that the source of the Torlesse sediments was the Pacifica continent (Nur & Ben-Avraham 1977).

MacKinnon (1983) proposed that the rocks of the Torlesse Supergroup were deposited in a trench at the Gondwana continental margin, with the sediment being derived from an adjacent continental volcano-plutonic arc. Concurrently, the volcanoclastic rocks of the Hokonui Association were deposited in an island arc setting further along the margin. During the Early Jurassic, the Torlesse Supergroup and Hokonui Association were juxtaposed by strike-slip faults.

Subsequently, a new subduction zone may have formed, with the initial location of the subduction zone possibly being marked by the Esk Head Mélange.

Korsch and Wellman (in press) have proposed that the Torlesse Supergroup formed by the gradual accretion of turbidites deposited in a trench onto and oceanward of the Caples-Pelorous rocks. Similarly, Spörli (1978) views the Torlesse as being accreted to the rocks of the Caples-Pelorous group, but considers that the Torlesse sediments formed as a large submarine fan system which was then accreted. Both models infer a southerly source for the turbidites.

All the models outlined above infer subduction related convergence, which implies the likely development of an accretionary prism.

The most obvious features of the Torlesse Supergroup which support accretion are the mutually exclusive, eastward-younging, fossil zones (Speden 1976; Mackinnon 1983) within which the sediments predominantly face westward (Spörli 1978). This implies that the subduction zone was west-dipping.

6.2.1 Accretionary Prisms

The terminology used here follows that of Karig and Sharman (1975), the basic elements of which are shown in Fig. 6-1. Accretion of oceanic sediments and deeper oceanic crustal material onto the upper plate during subduction has been postulated by many workers (eg. Seely et al. 1974; Karig 1974; Karig & Sharman 1975; Moore & Karig 1976). Based on the geometric variations in young island arc systems, Karig and Sharman (1975) showed how subduction zones evolve and listed the factors that control their evolution.

The amount and relative proportion of sediments fed into the

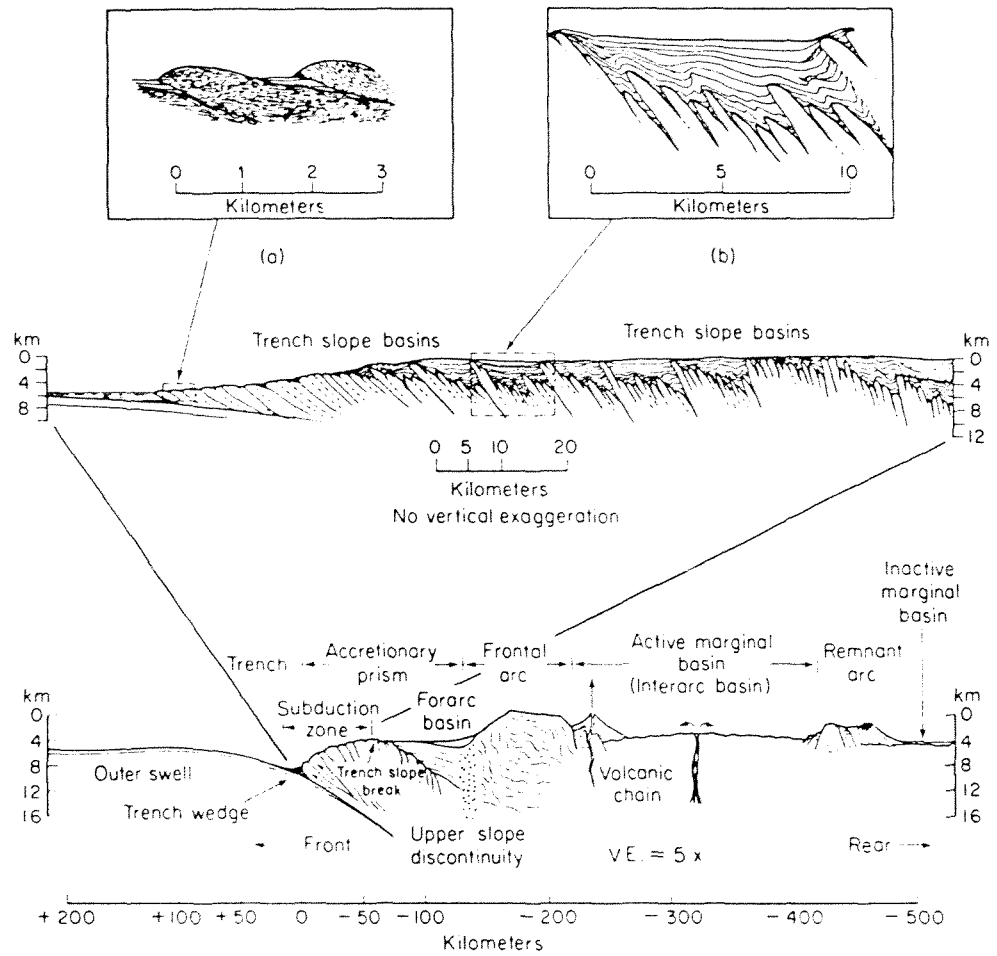


Figure 6-1: Cross-section of a typical island-arc system, showing tectonic units (after Karig & Sharman 1975 and Moore & Karig 1976).

subduction zone and to the upper-trench slope area determine the shape of an accretionary prism. Sediments fed into the trench slope area may be ponded by irregularities in the topography of the trench slope (Fig. 6-1) forming trench slope basins. The amount of sediment fed into the subduction zone is only partly related to the rate of subduction, that is, if there is little sediment on the subducting plate, even at high rates of subduction, the prism will grow relatively slowly.

The rate at which material is fed into a subduction zone is a function of the thickness of the sediment cover on the subducting plate and the rate of subduction acting perpendicular to the trench axis. In subduction zones where little sediment is arriving on the subducting plate, an accretionary prism that contains a relatively high proportion of seafloor material (ie. basalt, chert, pelagic sediment) will form (Karig & Sharman 1975). Melanges associated with the Semail Ophiolite, Northern Oman (Lippard et al. 1983), may be an example of such a regime. Where sediment supply to the subducting plate is substantial, the relative amount of ocean floor material incorporated into the accretionary prism is small (Karig & Sharman 1975). Some accretionary prisms show variation through time of the relative proportion of trench and seafloor material accreted. In the Southern Uplands Accretionary Complex (Leggett et al. 1982) accretion during the Ordovician included minor seafloor material, whereas by the Late Silurian a thick clastic pile was being accreted. Many accretionary prisms contain both clastic sediments and seafloor material, eg. Franciscan Complex, Nias Islands, Barbados, Aleutian arc system, Makran region of Iran and Pakistan.

Sediment incorporated into accretionary prisms is thought to undergo the following sequence of events (Karig & Sharman 1975; Moore

& Wheeler 1978; Fig 6-2):

1) During convergence, the sediment is initially dewatered and lithified. Folding may occur.

2) Sediment enters a "master" shear zone and undergoes initial decoupling from the downgoing plate. Shearing occurs.

3) Sediments are further sheared, with foliation developing in response to underthrusting as the sediment is incorporated into the accretionary prism.

4) With additional incorporation of material into the accretionary prism, older material undergoes landward tilting along with folding and shearing.

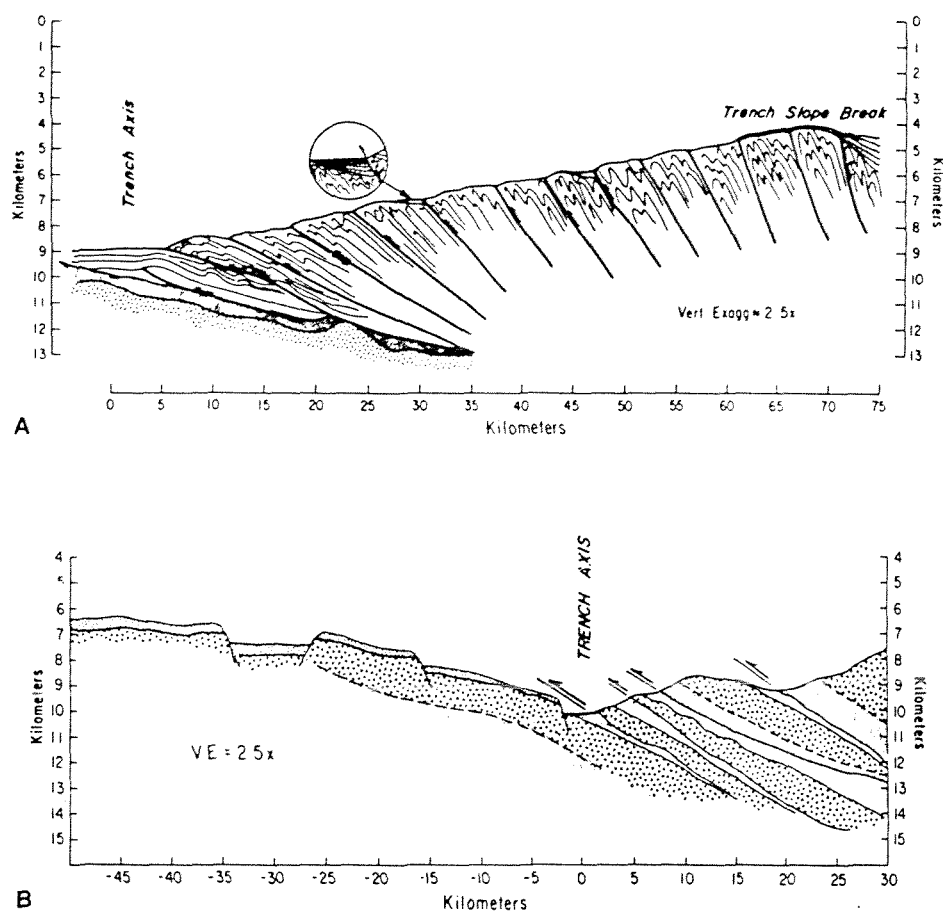
5) Sediments then undergo late faulting.

6.2.2 Mélange

Mélanges are a common feature of accretionary prisms, eg. Franciscan Complex of California (Hsu 1968; Cowan 1974, 1978; Korsch 1982), Alaska (Connelly 1978), Indonesia (Moore & Karig 1980), Japan (Suzukui & Hada 1979), Yugoslavia (Dimitrijevic & Dimitrijevic 1973). Mélange may be produced during fragmentation and shearing of material undergoing initial dislocation from the subducting plate and incorporation into the accretionary prism. It may also be produced to a lesser extent, along the imbricate packet boundaries in older parts of the accretionary prism. It is most likely that an accretionary prism would contain mélange.

6.3 DATA FROM THE FIELD AREA

Many features of the geology of the study area are comparable with those from accretionary prisms. The juxtaposition of rocks of the sedimentary and volcanic associations is explained by accretion of trench-fill deposits (sedimentary association) along with seafloor



A. Accretion of thick sediment cover or thick trench-wedge section. The upper turbidite section tends to be sheared off along the weak, high-porosity uppermost pelagic section and rides over the trench wedge, probably aided by high pore pressures. B. Accretion of thin pelagic sediment cover and oceanic crust. Slabs of the upper oceanic crust are intermittently sheared off when topographic irregularities enter the trench.

Figure 6-2: Speculative models of deformation of accreted material in a subduction zone (after Karig & Sharman 1975).

material (volcanic association), into a subduction zone. The lithic sandstone, mentioned above, may represent trench slope deposits that have subsequently been incorporated into the accretionary prism. The structural style described from the field area is similar to that outlined above for accretionary prisms with initial folding, subsequent fragmentation and shearing (leading to the development of *mélange*) and then later folding. Thus, data presented here from the southern Tararua Range supports an accretionary prism model for the development of the Torlesse Supergroup.

6.4 REGIONAL CORRELATIONS

Although no diagnostic fossils localities are known from the field area, fossil localities close to the study area can provide some age constraints. Late Triassic (Warepan) *Monotis* occur at Otaki Forks (Grant-Taylor & Waterhouse 1963) fourteen kilometres northwest of the field area. Limestone float containing Triassic conodonts was found in the Tauherenikau River near Tutuwai Hut (J. Begg pers. comm. 1984). Middle Jurassic radiolaria have been extracted from a chert, 1.5 kilometres east of the field area (Foley 1984). Thus rocks of the field area lie between rocks of Late Triassic and Mid-Jurassic age.

In the South Island, the Late Triassic *Monotis* zone (zone 4 of MacKinnon 1983) and the late Jurassic to Cretaceous zone (zone 5 of MacKinnon 1983) are separated by the Esk Head *Mélange* (Botsford 1983).

The Esk Head *Mélange*, up to 12 km wide and at least 60 km long, consists of packets of intensely deformed sediment and volcanics (*mélanges*), rafts of metabasite, chert and coloured argillite (seafloor material) along with packets of relatively undeformed sandstone and argillite. The *mélange* belt is gradational into Torlesse rocks on either side (Botsford 1983). *Monotis* zone fossils within the Esk

Head Mélange occur in seafloor material (ie. limestones) whereas zone 5 fossils occur within turbidites (Botsford 1983).

The Esk Head Mélange has been mapped in some detail by Botsford (1983), and from his map of an 8 km section across the belt, near Esk Head Station, I estimate the relative percentages of rock types to be:

- 1) Relatively undisrupted sandstone and argillite units - 46%;
- 2) Disrupted sediments and blocky mélange - 36%;
- 3) Volcanics and associated rocks types - 16%;
- 4) Polymict conglomerate - 2%.

The Esk Head Mélange is regarded as a tectonic mélange created in a westward-dipping subduction zone during the Early Cretaceous and possibly Late Jurassic (Botsford 1983). It is most likely the result of either or both of the following:

- 1) A change in the subduction regime, ie. a change in the rate of subduction, the obliqueness of subduction or the dip of the subducting plate;

- 2) A change in the nature of material coming into the subduction zone, ie. little terrigenous sedimentation would allow increased amounts of seafloor material to be incorporated into the accretionary prism, and possibly enhance mélange formation.

Many similarities exist between the Esk Head Mélange and my field area, namely:

- 1) A high percentage of seafloor material, relative to the "typical" areas of Torlesse rocks;
- 2) A high percentage of melange and associated disrupted units;
- 3) Both areas occur between rocks of fossil zones 4 and 5;
- 4) Olistostromes are intimately associated with tectonic mélange in both areas;

5) The occurrence of fine-grained calcareous sediments conformable within rocks of the sedimentary association.

On the basis of these similarities I suggest that rocks on the southern Tararua Range represent a northward continuation of the Esk Head Mélange belt.

The Pohangina Mélange described by Spörli & Bell (1976) from the southern Ruahine Range also shows many similarities to rocks of my field area and those of the Esk Head Mélange, as do rocks from the Manawatu Gorge and Rimutaka Range (pers. obs.). Fig. 6-3 outlines the possible continuation of the Esk Head Melange in the southern part of the North Island.

The following outcrop widths have been estimated for melanges shown in Fig. 6-3:

1) Esk Head Mélange, average width of 10 km.

2) Mélange in the Rimutaka Tunnel (Reed 1957b) and exposed on the Rimutaka Road, here referred to as the "Rimutaka Mélange", has an average width of 3.1 km.

3) Mélange in the Tauherenikau and Waiohine Rivers, here referred to as the "Tauherenikau Mélange" has an average width of 3 km.

4) The Pohangina Mélange (Spörli & Bell 1976) has an average width of 1.5 km.

A comparison of the widths of the Esk Head, Rimutaka, Tauherenikau and Pohangina Mélanges shows a trend of decreasing width northwards. It is interesting to note that this trend is also reflected by the fossil zones of the Torlesse Supergroup, which has been interpreted by Korsch & Wellman (in press), to reflect a southerly source for the terrigenous sediment.

In conclusion, rocks in the southern part of the Tararua Range

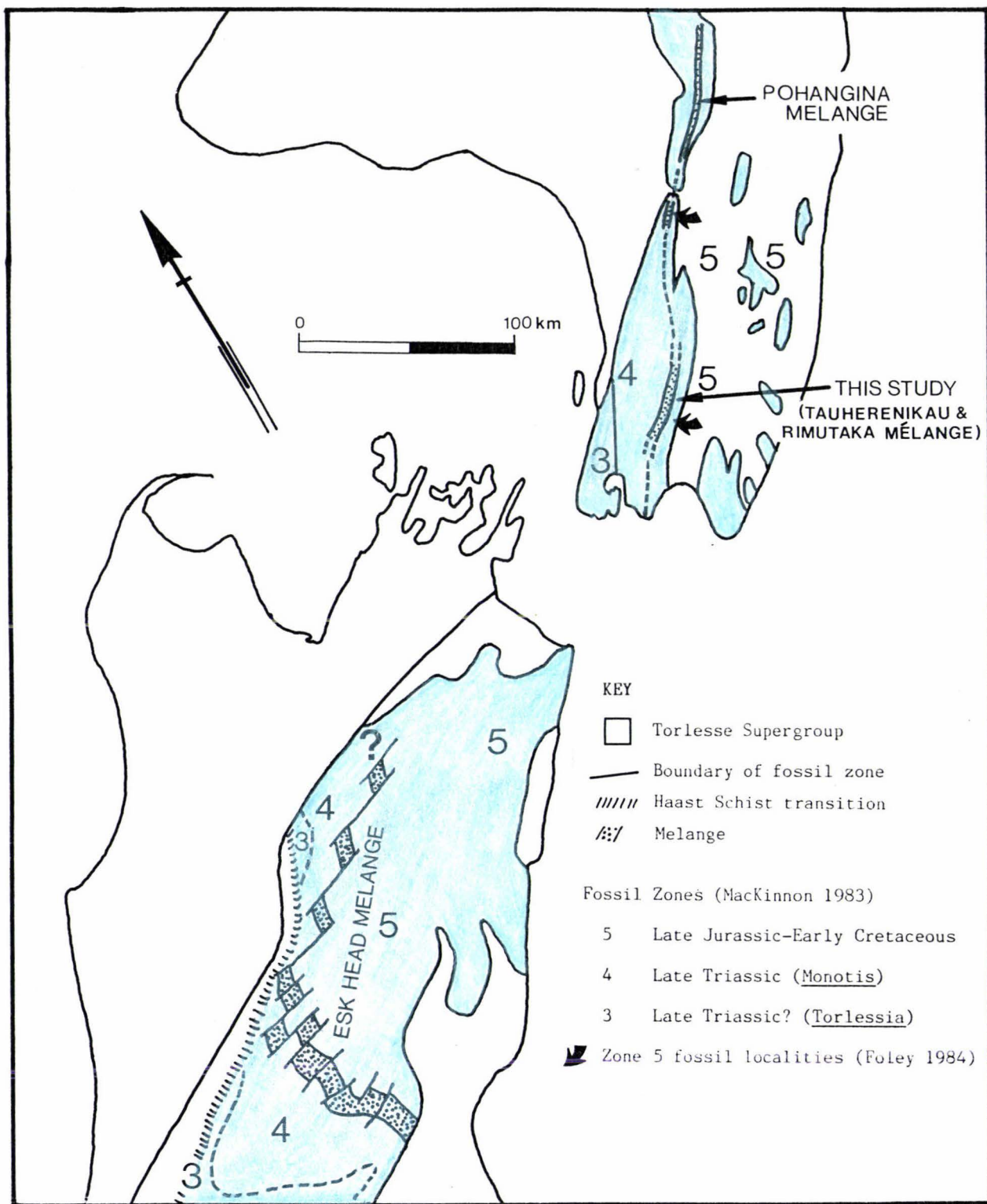


Figure 6-3: Map showing the Esk Head Mélange and possible North Island continuation (after Spörli & Bell 1976; Botsford 1983; MacKinnon 1983; Foley 1984).

represent a possible lateral equivalent of the Esk Head Mélange from the South Island.

REFERENCE LIST

- Andrews, P.B.; Speden, I.G.; Bradshaw, J.D. 1976: Lithological and palaeontological content of the Carboniferous-Jurassic Canterbury Suite, South Island, New Zealand. New Zealand journal of geology and geophysics 19: 791-819.
- Barnes, C.J. 1979: The structure and petrography of the Rimutaka greywackes and associated rocks. Unpublished B.Sc. (Hons) project, Geology department library, Victoria University of Wellington, 59 p.
- Bhatia, M.R. 1983: Plate tectonics and geochemical composition of sandstones. The journal of geology 91: 611-627.
- Boles, J.R.; Coombs, D.S. 1977: Zeolite facies alteration of sandstones in the Southland Syncline, New Zealand. American journal of science 277: 989-1012.
- Bostrom, K. 1970: Submarine volcanism as a source for iron. Earth and planetary science letters 9: 348-354.
- Bostrom, K.; Peterson, M.N.A.; Joensuu, O.; Fisher, D.E. 1969: Aluminium-poor ferromanganoan sediments on active spreading ridges. Journal of geophysical research 74: 3261-3270.
- Botsford, S. 1983: Structural geology of the Esk Head Mélange, South Island. Unpublished M.Sc. thesis, University of Canterbury. 249 p.
- Bouma, A.H. 1962: Sedimentology of some flysch deposits. Elsevier Amsterdam. 168 p.
- Bradshaw, J.D. 1973: Allochthonous Mesozoic fossil localities in mélange within the Torlesse rocks of North Canterbury. Journal of the royal society of New Zealand 3: 161-167.
- Bradshaw, J.D.; Adams, C.J.; Andrews, P.B. 1980: Carboniferous to Cretaceous on the Pacific margin of Gondwanaland: the Rangitata phase of New Zealand. In: Cresswell, M.M.; Vella, P. ed: Gondwana Five. A.A. Balkema Rotterdam: 217-221.
- Brodie, J.W. 1953: Stratigraphy and structure of the greywackes and argillites on the south-coast of Wellington Peninsula. New Zealand journal of science and technology 34: 205-226.
- Campbell, J.W.; Warren, G. 1965: Fossil localities of the Torlesse Group in the South Island. Transactions of the Royal Society of New Zealand geology 3: 99-137.
- Carter, R.M.; Hicks, M.D.; Norris, J.R.; Turnbull, I.M. 1978: Sedimentation patterns in an ancient arc-trench-ocean basin complex: Carboniferous to Jurassic Rangitata Orogen, New Zealand. In: Stanley, D.J.; Kelling, G. ed: Sedimentation in

- submarine canyons, fans and trenches. Dowden, Hutchinson, Ross Pennsylvania: 340-361.
- Connelly, W. 1978: Uyak Complex, Kodiak Islands, Alaska: A cretaceous subduction complex. Geological society of America bulletin 89: 755-769.
- Coombs, D.S.; Landis, C.A.; Norris, R.J.; Sinton, J.A.; Borns, D.J.; Craw, D. 1976: The Dun Mountain ophiolite belt, New Zealand, its tectonic setting, construction and origin, with special reference to the southern portion. American journal of science 276: 561- 603.
- Coombs, D.S. 1960: Lowergrade mineral facies in New Zealand. 21st international geological congress 13: 339-351.
- Cooper, R.A. 1975: New Zealand and southeast Australia in the early Paleozoic. New Zealand journal of geology and geophysics 18: 1-20.
- Cowan, D.S. 1974: Deformation and metamorphism of the Franciscan subduction zone complex northwest of Pacheco Pass, California. Geological society of America bulletin 85: 1623-1634.
- Cowan, D.S. 1978: Origin of blueschist-bearing chaotic rocks in the Franciscan Complex, San Simeon, California. Geological Society of America Bulletin 89:1415- 1423.
- Cranny, P.J. 1979: Structure and sedimentology of Lower Mesozoic rocks at Titahi Bay. Unpublished B.Sc.(Hons) project, Geology dept. library, Victoria University of Wellington, 33 p.
- Cressman, E.T. 1962: Nondetrital siliceous sediments. United States geological survey professional paper 440-T.
- Crook, K.A.W. 1974: Lithogenesis and geotectonics: the significance of compositional variations in flysch arenites (greywackes). Society of economic paleontologists and mineralogists special publication 19: 304-310.
- Dickinson, W.R. 1970: Interpreting detrital modes of greywacke and arkose. Journal of sedimentary petrology 40: 695- 707.
- Dickinson, W.R. 1982: Compositions of sandstone in Circum-Pacific subduction complexes and forearc basins. American association of petroleum geology bulletin 66: 121-137.
- Dickinson, W.R.; Suczek, C.A. 1979: Plate tectonics and sandstone compositions. American association of petroleum geologists bulletin 63: 2164-2182.
- Dickinson, W.R.; Ingersoll, R.V.; Cowan, D.S.; Helmold, K.P.; Suczek, C.A. 1982: Provenance of Franciscan greywackes in coastal California. Geological society of America bulletin 93: 95-107.

- Dimitrijevic, M.D.; Dimitrijevic, M.N. 1973: Olistostrome Mélange in the Yugoslavian Dinarides and Late Mesozoic plate tectonics. Journal of geology 81: 328-340.
- Ernst, W.G.; Dal Piaz, G.V. 1978: Mineral parageneses of eclogitic rocks and related mafic schists of the Piemonte ophiolitic nappe, Brevil-St. Jacques area, Italian western Alps. American mineralogist 63: 621-640.
- Foley, L.A. 1984. The geology of basement rocks in the southeastern Tararua Range, North Island, New Zealand. Unpublished M.Sc. thesis, Victoria University of Wellington 156 p.
- Grant-Taylor, T.L.; Waterhouse, J.B. 1963: Monotite from the Tararua Range, Wellington. New Zealand journal of geology and geophysics 6: 623-627.
- Grapes, R. Palmer, K. 1984: Magma type and tectonic setting of metabasites, Southern Alps, New Zealand, using immobile elements. New Zealand journal of geology and geophysics 27: 21-25.
- Hey, M.H. 1954: A new review of chlorites. Mineralogical magazine 30: 277-292.
- Howell, D.G. 1980: Mesozoic accretion of exotic terranes along the New Zealand segment of Gondwanaland. Geology 8: 487-491.
- Hsu, K.J. 1968: Principles of mélanges and their bearing on the Franciscan-Knoxville paradox. Geological society of America bulletin 79: 1063-1074.
- Ingersoll, R.V.; Suczek, C.A. 1979: Petrology and provenance of Neogene sand from Nicobar and Bengal fans, D.S.D. P. sites 211 and 218. Journal of sedimentary petrology 49: 1217-1228.
- Jenkyns, H.C.; Hardy, R.G. 1976: Basal iron-titanium rich sediments from Hole 315A (Line Islands, central Pacific). In: Initial reports of the deep sea drilling project 33: 833-836.
- Kamp, P.J.J. 1980. Pacifica and New Zealand: Proposed eastern elements in Gondwanaland's history. Nature 288: 659-664.
- Karig, D.E. 1974: Evolution of arc systems in the western Pacific. Annual review of earth and planetary sciences 2: 51-75.
- Karig, D.E.; Sharman, G.F. 1975: Subduction and accretion in trenches. Geological society of America bulletin 86: 377-389.
- Kawachi, Y. 1975: Pumpellyite-actinolite and contiguous facies metamorphism in part of Upper Wakitipu district, New Zealand. New Zealand journal of geology and geophysics 18: 401-441.
- Kawachi, Y. Grapes, R.H.; Coombs, D.S.; Dowse, M. 1983: Mineralogy and petrology of a piemontite-bearing schist, western Otago.

- New Zealand. Journal metamorphic geology 1: 353-372.
- Keall, P.C. 1980: The structure and stratigraphy of the Torlesse Supergroup near Owango Stream, Rimutaka Range, Wairarapa. Unpublished B.Sc.(Hons) project, Geology dept. library, Victoria University of Wellington, 39 p.
- Kingma, J.T. 1967: Sheet 12, Wellington (1st ed) "Geological map of New Zealand 1:2,500,00". D.S.I.R., Wellington.
- Korsch, R.J. 1982: Structure of Franciscan complex in the Stanley Mountain Window, southern coast ranges, California. American journal of science 282: 1406-1437.
- Korsch, R.J. 1984: Geological aspects of the Torlesse Complex, south coast of Wellington. New Zealand geological society miscellaneous series 31B: 67-90.
- Korsch, R.J.; Wellman, H.W. in press: The geological evolution of New Zealand and the New Zealand region. In: Nairn, A.E.M., Stehi, F.G. ed: The ocean basins and margins, volume 7A. The Pacific ocean. Plenum Press New York.
- Landis, C.A.; Bishop, D.G. 1972: Plate tectonics and regional stratigraphic-metamorphic relations in the southern part of the New Zealand geosyncline. Geological society of America bulletin 83: 2267-2284.
- Landis, C.A.; Coombs, D.S. 1967: Metamorphic belts and orogenesis in southern New Zealand: Tectonophysics 4: 501-518.
- Lauder, W.R. 1962: Notes on the greywackes near Wellington City. New Zealand journal of geology and geophysics 5: 626-629.
- Legget, J.K.; McKerrow, W.S.; Casey, D.M. 1982: The anatomy of a Lower Palaeozoic accretionary forearc: the Southern Uplands of Scotland. In: Legget, J.K. ed: Trench-Forearc geology. London geological society special publication 10: 495-520.
- Lippard, S.J.; Graham, G.M.; Smewing, J.D.; Searle, M.P. 1983: Mélanges associated with the Semail Ophiolite in the Northern Oman Mountains Allocthon, southwest Arabia. In: McCall, G.J.H. ed: Ophiolitic and related melanges. Hutchinson Ross publishing company, Stroudsbury. 300-309.
- MacKenzie, A-F.T. 1983: The structure and stratigraphy of the greywacke-suite Sinclair Head, Wellington. Unpublished B.Sc. (Hons) project, Geology dept. library, Victoria University of Wellington 72 p.
- MacKinnon, T.C. 1983: Origin of the Torlesse terrane and coeval rocks, South Island, New Zealand. Geological society of America bulletin 94: 967-985.
- Malahaff, A.; McMurtry, G.M.; Wiltshire, J.C.; Yeh, H.W. 1982: Geology and

- chemistry of hydrothermal deposits from active submarine volcano Loihi, Hawaii. Nature 298: 234-239.
- McKay, A. 1888a: On mineral deposits in the Tararua and Ruahine mountains. New Zealand geological survey report, geology exploration 1887-1888 19: 1-6.
- McKay, A. 1888b: On the Tauherenikau and Waiohine valleys, Tararua Range. New Zealand geological survey report, geology exploration 1887-1888 19: 37-48.
- Middleton, G.V.; Hampton, M.A. 1973: Sedimentary gravity flows: mechanics of flow and deposition. In. Turbidites and deep water sedimentation SEPM Pacific short course, Anaheim: 1-38.
- Moore, G.F.; Karig, D.E. 1980: Structural geology of Nias Island, Indonesia: implications for subduction zone tectonics. American journal of science 280: 193-223.
- Moore, J.C. 1975: Selective subduction. Geology 3: 530-532.
- Moore, J.C.; Wheeler, R.L. 1978: Structural fabric of a mélangé Kodiak Islands, Alaska. American journal of science 278: 739-765.
- Moore, J.G. 1965: Petrology of deep-sea basalt near Hawaii. American journal of science 263: 40-52.
- Mutti, E.; Ricci-Lucchi, F. 1972: Le torbiditi dell'Appennino settentrionale: introduzione all'analisi di facies. Memorie della società geologica Italiana 11: 161-199. Translated by Nielson, T.H. 1975: Turbidites of the northern Appennines: Introduction to facies analysis. International geology review 20: 125-165.
- Nisbet, E.G.; Pearce, J.A. 1977: Clinopyroxene compositions in mafic lavas from different tectonic settings. Contributions to mineralogy and petrology 63: 149-160.
- Nur, A.; Ben-Averaham, Z. 1977: Lost Pacifica continent. Nature 270: 41-43.
- Offler, R.; Baker, C.K.; Gamble, J. 1981: Pumpellyites in two low grade metamorphic terranes north of Newcastle, NSW Australia. Contributions to mineralogy and petrology 76: 171-176.
- Oliver, G.J.H. 1976: The high grade metamorphic rocks of Doubtful Sound, Fiordland, New Zealand: a study of lower crust. Unpublished Ph.D. thesis, University of Otago.
- Pearce, J.A.; Cann, J.R. 1973: Tectonic setting of basic volcanic rocks determined using trace element analyses. Earth and planetary science letters 19: 290-300.
- Pearce, J.A.; Norry, M.J. 1979: Petrogenetic implications of Ti, Zr, Y and Nb variations in volcanic rocks. Contributions to

mineralogy and petrology 69: 33-47.

- Pettijohn, F.J. 1963: Chemical composition of sandstone excluding carbonate and volcanic sands. United States geological survey professional paper 440-T, 21 p.
- Pettinga, J. 1982: Upper Cenozoic structural history, coastal Southern Hawkes Bay, New Zealand. New Zealand journal of geology and geophysics 25: 149-191.
- Powell, C.McA. 1979: A morphological classification of rock cleavage. Tectonophysics 58: 21-34.
- Ramsay, J.G. 1967: Folding and fracturing of rocks. McGraw Hill, New York, 568 p.
- Rattenbury, M.S. 1983: Geology of Otaki Forks, Tararua Range. Unpublished M.Sc.(Hons) thesis, University of Auckland 109 p.
- Reed, J.J. 1957a: Petrology of the lower Mesozoic rocks of the Wellington district. New Zealand geological survey bulletin 57, 60 p.
- Reed, J.J. 1957b: Fault zones in part of the Rimutaka Range. New Zealand journal of science and technology 38: 686-687.
- Roser, B.P. 1983: Comparative studies of copper and manganese mineralisation in the Torlesse, Waipapa and Haast Schist Terranes, New Zealand. Unpublished Ph.D. thesis, Victoria University of Wellington 491 p.
- Rowe, G.H. 1980: Applied geology of Wellington rocks for aggregate and concrete. Unpublished Ph.D. thesis, Victoria University of Wellington 397 p.
- Rupke, N.A. 1978: Deep clastic seas. In: Reading, H.G. ed: Sedimentary environments and facies. Blackwell, Oxford:
- Seely, D.E. 1974: Evolution of arc systems in the western Pacific. Annual review of earth and planetary science 2: 51-75.
- Seki, Y.; Oki, Y.; Matsuda, T.; Mikami, K.; Okumura, K. 1969: Metamorphism in the Tanzawa Mountains, Central Japan. Journal of the Japaneses association of mineralogists, petrologists and economic geologists 61: 1-25.
- Shervais, J.W. 1982: Ti-V plots and the petrogenesis of modern and ophiolitic lavas. Earth and planetary science letters 59: 101-118.
- Silver, E.A.; Beutner, E.C. 1980: Penrose conference report- mélanges: Geology 8: 32-34.
- Speden, I.G. 1976: Fossil localities in the Torlesse rocks of the North Island, New Zealand. Journal of the royal society of New Zealand 6: 73-91

- Spörli, K.B. 1978: Mesozoic tectonics, North Island, New Zealand. Geological society of America bulletin 89: 415-425.
- Spörli, K.B.; Barter, T.P. 1973: Geological reconnaissance in the Torlesse Supergroup of the Kaimanawa Range along the lower reaches of the Waipakihi River, North Island, New Zealand. Journal of the royal society of New Zealand 3: 363-380.
- Spörli, K.B.; Stanaway, K.J.; Ramsay, W.R.H. 1974: Geology of the Torlesse Supergroup in the southern Liebig and Burnett Ranges, Canterbury, New Zealand. Journal of the royal society of New Zealand 4: 177-192.
- Spörli, K.B.; Bell, A.B. 1976: Torlesse mélange and coherent sequences, eastern Ruahine Range, North Island, New Zealand. New Zealand journal of geology and geophysics 19: 427-447.
- Suggate, R.P. 1961: Rock-stratigraphic names for the South Island schists and undifferentiated sediments of the New Zealand geosyncline. New Zealand journal of geology and geophysics 4: 392-399.
- Suggate, R.P.; Stevens, G.R.; Te Punga, M.T. 1978: The geology of New Zealand. Government printer, Wellington, 2 vols, 820 p.
- Suzuki, T.; Hada, S. 1979: Cretaceous tectonic mélange of the Shimanto Belt in Shikoku, Japan. Journal of the geological society of Japan 85: 467-478.
- Taylor, S.R. 1965: The application of trace element data to problems in petrology. Physics and chemistry of the earth 6: 133-213.
- Turner, F.J.; Weiss, L.E. 1963: Structural analyses of metamorphic tectonites. McGraw-Hill Book Company, New York, 545 p.
- Van der Plais, L.; Tobi, A.C. 1965: A chart for determining the reliability of point counting results. American journal of science 263: 87-90.
- Webby, B.D. 1959a: Sedimentation of the alternating greywacke and argillite strata in the Porirua district. New Zealand journal of geology and geophysics 2: 461-478.
- Webby, B.D. 1959b: The structure of the Lower Mesozoic rocks in the Porirua district. New Zealand journal of geology and geophysics 2: 538-540.
- Webster, M.A. 1982: The structure and sedimentology of greywacke-suite rocks at Camp Bay, Eastbourne. Unpublished B.Sc.(Hons) project, Geology dept. library, Victoria University of Wellington, 64 p.
- Wellman, H.W. 1952: The Permian-Jurassic stratified rocks. In: Teichert, C. ed: Symposium sur les series de Gondwana.

Proceedings of 19th international geological congress
13-24.

- Wellman, H.W.; Willet, R.W. 1942: The geology of the west coast from Abut Head to Milford Sound. Part 1. Transactions of the royal society of New Zealand 71: 282-306.
- Wellman, P.; Cooper, A.F. 1971: Potassium-argon ages of some New Zealand lamprophyre dikes near the Alpine Fault. New Zealand journal of geology and geophysics 14: 341-350.

APPENDIX I

MAPS AND AERIAL PHOTOGRAPHS

Topographic maps and aerial photographs used in this study are:

Topographic maps scale 1:25,000

N.Z.M.S 260 S26/C

N.Z.M.S 260 S26/D

Aerial photographs scale approximately 1:50,000

SN 5309 F/1

SN 5309 F/2

SN 5309 F/3

SN 5309 F/4

SN 5309 F/5

SN 5309 F/6

SN 5309 F/7

APPENDIX II

POINT COUNT METHODS

Point-counting procedures

Thin-sections of fifteen sandstones were point-counted noting grain compositions. Sections were counted using a Swift automatic point-counter. Within each thin-section, five hundred points were initially counted. As the percentage of lithic rock fragments is low, a further one hundred and fifty counts of lithic rock fragments were made.

Theoretical reliability of compositional values obtained is within 4.5% of true values at the 95% confidence level (Van der Plais & Tobi 1965).

Grain-size determination technique

The grain size of sandstones which were point counted for modal analysis, was obtained by measuring the apparent long axis of one hundred grains using a graduated micrometre eyepiece. A Swift automatic stage was used to determine which grains were measured.

APPENDIX III

SAMPLES

Samples are housed in the petrology collection, Geology Department, Victoria University of Wellington. Rock samples are housed as well as specimens that are listed under "Sample type" where:

T = Thin section

P = Powder

M = Electron microprobe section

V.U.W Number	Field Number	Sample type	Grid reference		Short description
17209	TO.2	T	S26C/9985	1337	Fine grained sandstone
17210	TO.16	T	S26C/0214	1391	Fine grained sandstone
17211	TO.19	T.M	S26C/0232	1360	Fine grained sandstone
17212	TO.31	T	S26C/0027	1517	Fine grained sheared sandstone
17213	TO.39	T	S26C/0200	1543	Fine grained sandstone
17214	TO.46	T	S26C/0245	1557	Fine grained calcite cemented sandstone
17215	TO.53	T	S26D/1110	2190	Fine grained sandstone
17216	TO.55	T	S26D/1097	2078	Fine grained veined sandstone
17217	TO.60	T	S26D/1061	2280	Fine grained sandstone
17218	TO.62	T	S26D/1080	2258	Fine grained sandstone
17219	TO.77	T	S26C/0585	1870	Fine grained sandstone
17220	TO.89B	T	S26C/0938	2065	Fine grained sandstone
17221	TO.91	T	S26C/0921	2249	Fine grained sandstone
17222	TO.108	T	S26C/0478	1577	Fine grained sandstone
17223	TO.58	T	S26D/1055	2350	Lithic sandstone
17224	TO.3	P	S26C/0035	1378	Black argillite
17225	TO.10	P	S26C/0278	1323	Fine grained sandstone
17226	TO.26	P	S26C/0309	1308	Medium grained sandstone
17227	TO.93	P	S26D/1045	2240	Fine grained sandstone
17228	TO.115	P	S26C/0278	1324	Medium grained sandstone
17229	TO.116	P	S26C/0278	1324	Black argillite
17230	TO.131	P	S26C/0148	1570	Fine grained sandstone
17231	TO.132	T.P	S26C/0148	1570	Fine grained sandstone
17232	TO.134	P	S26C/0190	1545	Black argillite
17233	TO.135	P	S26C/0190	1545	Black argillite
17234	TO.136	P	S26C/0190	1545	Black argillite
17235	TO.137	T.P	S26C/0190	1545	Fine grained sandstone
17236	TO.138	P	S26C/0190	1542	Very fine grained sandstone
17237	TO.139	P	S26C/0192	1542	Black argillite
17238	TO.140	P	S26C/0193	1542	Black argillite
17239	TO.133	T.P	S26C/0203	1539	Red argillite
17240	TO.130	T.P	S26C/0115	1600	Sheared green metabasite
17241	TO.122	T.P	S26C/0025	1122	Red amygdaloidal metabasite
17242	TO.109	T.P	S26C/0468	1577	Red variolitic amygdaloidal metabasite
17243	TO.104	T.P	S26C/0818	2385	Green variolitic metabasite
17244	TO.78	T.P	S26C/0690	2263	Green variolitic metabasite
17245	TO.59	T.P	S26D/1045	2305	Green variolitic metabasite & selvage
17246	TO.54	T.P.M	S26D/1133	2153	Subophitic green metabasite
17247	TO.52	T.P	S26D/1110	2208	Red chert
17248	TO.49	T.P	S26D/1128	1988	Subophitic sheared metabasite
17249	TO.44	T.P	S26C/0325	1700	Selvage material

V.U.W Number	Field Number	Sample type	Grid reference		Short description
17250	TO.43	T.P	S26C/0325	1700	Intensely veined selvage material
17251	TO.36	T.P	S26C/0092	1588	Red argillite
17252	TO.25	T.P	S26C/0285	1305	Red variolitic amygdaloidal metabasite
17253	TO.18	T.P	S26C/0228	1360	Red argillite
17254	TO.7	T.P	S26C/0282	1314	Red variolitic amygdaloidal metabasite
17255	TO.5	T.P.M	S26C/0283	1313	Green variolitic metabasite
17256	LF.103	T.M	S26C/0280	1305	Red subophitic metabasite
17257	TO.20	T	S26C/0523	1910	Red variolitic amygdaloidal metabasite
17258	TO.32	T	S26C/0033	1546	Intensely veined red metabasite
17259	TO.37	T	S26C/0100	1593	Intensely sheared green metabasite
17260	TO.42	T	S26C/0345	1723	Subophitic red metabasite
17261	TO.117	T	S26C/0253	1342	From large block of microsparite
17262	TO.85	T	S26C/0510	2022	Very weathered green metabasite
17263	TO.90	T	S26D/1028	2045	Medium grained sandstone
17264	TO.99	T	S26C/0789	2463	Red variolitic metabasite
17265	TO.100	T.M	S26C/0837	2483	Sheared green metabasite
17266	TO.64	T	S26D/1103	2235	Calcareous concretion, radiolaria ghosts
17267	TO.4	T	S26C/0081	1408	Calcareous siltstone
17268	TO.11	T	S26C/0255	1337	Microsparite lens
17269	TO.12	T	S26C/0255	1340	Microsparite clast
17270	WF.4	T.M	S26D/1133	2153	Green subophitic metabasite
17271	LF.292	P	S26D/1090	1952	Red chert
17272	TO.114	T	S26C/0255	1340	Microsparite clast
17273	TO.33	T	S26C/0074	1578	Red argillite
17274	TO.65	T	S26D/1103	2235	Red variolitic metabasite
17275	TO.89A	T	S26C/0915	2095	Basaltic red argillite
17276	TO.88	T	S26C/0915	2094	Limestone
17277	TO.92	T	S26C/0979	2222	Intensely veined red argillite
17278	TO.94	T	S26D/1047	2241	Red metabasite
17279	TO.96	T	S26C/0795	2318	Chert float
17280	TO.103	T	S26C/0802	2412	Intensely veined green metabasite
17281	TO.119	T	S26C/0254	1347	Olistostrome
17282	TO.9	T	S26C/0280	1323	Sheared red argillite
17283	TO.76		S26C/0630	1843	Medium grained sandstone
17284	TO.79	T	S26C/0695	2222	Intensely sheared, altered metabasite
17285	TO.FL1	T	S26C/0400	1308	Red amygdaloidal metabasite
17286	TO.15	T	S26C/0270	1402	Complexly veined red chert
17287	TO.101	T	S26C/0958	2463	Green sheared metabasite
17288	TO.105	T	S26C/0863	2362	Red sheared subophitic metabasite
17289	TO.8	T	S26C/0280	1322	Red chert, sponge? spicules & radiolaria
17290	TO.22	T	S26C/0470	1865	Silicified altered green argillite
17291	TO.28	T	S26C/0317	1315	Highly sheared silty limestone
17292	TO.21	T	S26C/0470	1867	Intensely sheared argillite
17293	TO.48	T.P	S26D/1130	1966	Medium grained sandstone
17294	TO.6	T	S26C/0283	1313	Red basaltic argillite
17295	TO.13	T	S26C/0160	1415	Sheared metabasite
17296	TO.14		S26C/0160	1415	Green? metabasite
17297	TO.17		S26C/0228	1360	Red? metabasite
17298	TO.129		S26C/0080	1743	Red? metabasite
17299	TO.27	T	S26C/0312	1313	Limestone
17300	TO.29	T	S26C/0317	1314	Melange matrix
17301	TO.24	T	S26C/0434	1845	Red argillite
17302	TO.34	T	S26C/0082	1583	Green argillite

V.U.W Number	Field Number	Sample type	Grid reference	Short description
17303	TO.47	T	S26D/1090 2053	Medium grained sandstone
17304	TO.50		S26D/1102 1995	Red metabasite?
17305	TO.51		S26D/1100 2002	Red argillite?
17306	TO.57		S26D/1058 2350	Red argillite?
17307	TO.61	T	S26D/1073 2263	Red metabasite & selvage
17308	TO.63		S26D/1088 2244	Red argillite?
17309	TO.68		S26C/0760 1849	Black argillite
17310	TO.72		S26C/0690 1910	Red argillite
17311	TO.73		S26C/0673 1958	Red and green metabasite
17312	TO.74		S26C/0668 1968	Green metabasite
17313	TO.81		S26C/0700 2200	Red argillite?
17314	TO.82		S26C/0723 2182	Green argillite
17315	TO.83	T	S26C/0392 2144	Medium grained sandstone
17316	TO.84	T	S26C/0480 2045	Medium grained sandstone
17317	TO.86	T	S26C/0945 2124	Red argillite
17318	TO.87	T	S26C/0910 2102	Red metabasite?
17319	TO.95	T	S26D/1045 2245	Sheared green argillite
17320	TO.97	T	S26C/0795 2318	Mélange
17321	TO.106	T	S26C/0600 1647	Medium grained sandstone
17322	TO.107	T	S26C/0542 1578	Fine grained green metabasite
17323	TO.111		S26C/0378 1657	Red argillite
17324	TO.112	T	S26C/0375 1665	Red variolitic metabasite
17325	TO.113	T	S26C/0370 1670	Sheared altered metabasite?
17326	TO.118		S26C/0254 1347	Red metabasite?
17327	TO.120	T	S26C/0070 1052	Gritty sandstone
17328	TO.121	T	S26C/0040 1100	Mélange
17329	TO.123	T	S26C/0022 1186	Mélange
17330	TO.124	T	S26C/0022 1211	Mélange
17331	TO.125	T	S26C/0005 1252	Red argillite
17332	TO.127	T	S26C/9982 1252	Medium grained sandstone
17333	FL.2		S26D/1056 2050	Sandstone & carbonaceous clasts
17334	LF.104	T	S26C/0332 1223	Sheared variolitic metabasite

APPENDIX IV

FELDSPAR STAIN

Fifteen thin-sections of fine grained sandstone were etched with hydrofluoric acid to aid the identification of alkali feldspars for point-counting purposes. The staining procedure is outlined below:

- 1) HF acid was placed in a shallow dish;
- 2) Thin-sections were placed over the shallow dish for 90 seconds allowing the HF acid fumes to etch the rock surface;
- 3) Thin-sections were submerged in a sodium cobaltinitrite solution for 30 seconds;
- 4) Washed in tap water.

This procedure stains alkali feldspars yellow.

APPENDIX V

CARBONATE STAIN

Thin sections of calcareous siltstone, microsparite and limestone were stained to aid carbonate identification. For staining thin-sections the following steps were taken:

- 1) Thin-sections were etched in a dilute (1.5%) HCl acid solution for 10-15 seconds;
- 2) Immersed in a solution of alizarin red S and potassium ferricyanide for 75 seconds;
- 3) Thin-sections were washed in distilled water and then air dried.

The carbonate stain aids differentiation of calcite, ferroan calcite, ferroan dolomite and dolomite. Alizarin red S distinguishes calcite from dolomite, staining the former pink, while potassium ferricyanide stains Fe-rich carbonates blue.

APPENDIX VI

GEOCHEMICAL ANALYTICAL METHODS

X-Ray fluorescence analysis

Major and trace elements were obtained by X-ray fluorescence analysis (XRF) using the Siemens SRS-1 spectrometer of the Analytical Facility, Victoria University of Wellington.

Samples were prepared by hydraulically crushing the rock samples. Any "chips" with veining or weathered surfaces were discarded, and the clean "chips" were then ground in a tungsten carbide "Tema" swing mill for two minutes, producing a fine powder.

Major elements were determined from fused glass discs while trace elements were determined from pressed powder pellets. Analytical procedure is further outlined in Roser (1983).

Electron-microprobe analysis

Electron-microprobe analysis were made using the computer controlled Jeol 733 Superprobe of the Analytical Facility, Victoria University of Wellington. Microprobe mounts were carbon-coated.

APPENDIX VII
CLINOPYROXENE COMPOSITIONS

17246								
SiO ₂	51.35	49.17	51.17	48.34	49.33	50.65	50.12	50.70
Al ₂ O	1.81	3.65	1.90	4.19	3.50	2.25	2.86	1.62
TiO ₂	1.01	1.73	1.04	2.20	1.66	1.13	1.33	0.92
*FeO	8.71	8.30	8.79	9.20	9.35	7.78	9.59	9.41
MnO	0.26	0.13	0.28	0.26	0.23	0.22	0.27	0.29
MgO	15.37	14.28	15.45	14.02	14.17	15.40	14.94	15.62
CaO	20.99	21.28	20.75	20.74	21.11	20.37	19.24	19.54
Na ₂ O	0.25	0.36	0.31	0.39	0.38	0.29	0.43	0.21
	-----	-----	-----	-----	-----	-----	-----	-----
Total	99.75	98.90	99.69	99.34	99.73	98.09	98.78	98.31

17255						
SiO ₂	51.39	50.14	50.98	50.79	50.72	50.14
Al ₂ O ₃	2.87	3.51	2.92	2.62	2.73	2.97
TiO ₂	0.86	1.14	0.97	0.91	1.14	0.91
*FeO	6.87	8.04	7.02	7.59	8.72	7.06
MnO	0.13	0.18	0.20	0.20	0.23	0.14
MgO	16.33	15.50	16.13	15.88	15.64	16.23
CaO	20.34	20.56	20.56	21.26	20.36	20.21
Na ₂ O	0.30	0.35	0.28	0.26	0.23	0.27
Cr ₂ O ₃	0.43		0.44	0.22		0.51
	-----	-----	-----	-----	-----	-----
Total	99.52	99.42	99.50	99.73	99.77	98.44

17256						
SiO ₂	43.85	44.93	42.79	46.29	45.58	44.72
Al ₂ O ₃	6.53	6.13	7.93	5.43	5.84	6.18
TiO ₂	4.65	3.80	4.97	2.92	3.55	3.52
*FeO	9.90	9.49	10.30	9.94	9.45	10.18
MnO	0.19	0.21	0.15	0.15	0.25	0.25
MgO	11.15	11.47	10.65	11.78	11.77	11.19
CaO	22.33	22.40	21.77	21.88	21.92	21.56
Na ₂ O	0.55	0.57	0.59	0.59	0.56	0.58
	-----	-----	-----	-----	-----	-----
Total	99.15	99.00	99.15	98.98	98.92	98.18

17270							
SiO ₂	49.83	51.02	50.36	49.39	50.52	48.97	51.08
Al ₂ O ₃	3.02	1.47	2.76	3.35	2.04	3.84	1.81
TiO ₂	1.46	0.62	1.28	1.70	0.97	1.63	1.10
*FeO	8.18	10.90	10.83	10.07	9.54	8.46	9.34
MnO	0.16	0.34	0.23	0.30	0.28	0.11	0.27
MgO	14.78	15.26	14.05	14.20	15.37	13.73	15.63
CaO	21.47	18.91	20.31	20.54	19.58	21.23	19.77
Na ₂ O	0.36	0.30	0.36	0.40	0.28	0.43	0.29
Total	99.26	98.82	100.18	99.95	98.58	98.40	99.29

* Total Fe as FeO

APPENDIX VIII

GEOCHEMICAL ANALYSES

Analyses of interpillow material (17250,17241)
and sheared metabasite (17240).

	17250	17249	17240
SiO ₂	44.27	50.66	47.60
TiO ₂	2.13	1.16	3.23
Al ₂ O ₃	13.20	15.91	13.50
Fe ₂ O ₃	3.31	7.92	4.27
FeO	7.57	2.95	5.82
MnO	0.21	0.11	0.13
MgO	9.40	4.06	5.23
CaO	8.83	5.85	7.08
Na ₂ O	2.97	6.39	5.98
K ₂ O	0.39	0.15	0.16
P ₂ O ₅	0.24	0.09	0.53
Loss	7.11	4.49	6.18
	-----	-----	-----
Total	99.63	99.74	99.71
Fe ₂ O ₃ T	11.72	11.20	10.74

Trace elements (ppm)

Ba	101	33	69
Ce	42	22	57
Cr	440	308	262
Cu	72	106	49
Ga	18	15	17
La	11	5	21
Nb	20	<2	34
Ni	204	82	148
Pb	2	<2	<2
Rb	6	4	2
Sc	33	36	28
Sr	202	154	184
Th	2	<2	2
U	<2	<2	<2
V	269	245	283
Y	28	29	37
Zn	112	134	107
Zr	163	73	281

